



THESIS

(:333)

This is to certify that the

dissertation entitled

C-Clamp Porphyrins: Models for

H-Bonded Heme Active Site

presented by

Ying Liang

has been accepted towards fulfillment of the requirements for

Ph.D degree in Chemistry

09/19/95 Date__

LIBRARY Michigan State University

PLACE IN RETURN BOX to remove this checkout from your record.

TO AVOID FINES return on or before date due.

DATE DUE	DATE DUE	DATE DUE

MSU is An Affirmative Action/Equal Opportunity Institution

C. p. C.

C-CLAMP PORPHYRINS: MODELS FOR H-BONDED HEME ACTIVE SITE

By

Ying Liang

A DISSERTATION

Submitted to
Michigan State University
in partial fulfillment of the requirements
for the degree of

DOCTOR OF PHILOSOPHY

Department of Chemistry

ABSTRACT

C-Clamp Porphyrins: Models for H-Bonded Heme Active Site

By

Ying Liang

Heme proteins play many critical roles in biological systems such as O₂ binding, activation and reduction. H-bonding to the heme-bound O₂ is an important factor in affecting their activities. Synthetic model compounds previously have established the positive effect of H-bonding in increasing O₂ affinity. However, it has not been possible to examine how much the influence on heme-substrate reactions are brought about by structural and steric perturbations of the proton donor. In an effort of providing better understanding on the influence of H-bonding effect on heme proteins, C-clamp porphyrins and derivatives have been designed and synthesized. Among these compounds, the Naphthalene Kemp's Acid Porphyrin (NKAP), is equipped with a carboxylic acid hovering over the porphyrin center through a naphthalene spacer linked with a Kemp's triacid. This intramolecular acid proton is in close distance (4-5Å) to the porphyrin center to achieve effective H-bonding according to the X-ray single crystal analysis.

This naphthalene C-clamp porphyrin and its zinc complexes are capable of recognizing small neutral molecules such as water or methanol through multiple H-bonding network, which is evidenced by X-ray crystal

structure and UV-vis and NMR studies. The extended Anthracene Kemp's Acid Porphyrin (AKAP) has a similar ability to recognize even larger substrates such as purine, imidizole and triazoles. We have analyzed the contribution of each individual H-bond and predicted that NKAP is the best host for mono atomic ligands.

Oxygen binding to Co^{II}NKAP exhibits such a high affinity constant that breaks all record reported so far in literature. In comparison with Naphthoic Acid Porphyrin (NAP), the ΔS of O₂ binding in Co^{II}NKAP is relatively small suggesting a higher degree of freedom of motion. It is interpreted that the NKAP system allows the H-bond occur at the proximal oxygen (O1) or the O=O π -bond instead of the distal oxygen (O2) only. Further evidence from ¹⁵N NMR on (CN)₂FePorphyrins supports our interpretation.

Additionally, we have investigated the H-bonding effect on oxo-metal porphyrins. Ferryl (Fe=O) species is an important intermediate of heme proteins and the H-bonding effect on ferryl heme in various enzymes remains to be established. Stable V=O (vanadyl) porphyrins are used as a model, and the H-bonding effect on the 5- and 6-coordinated vanadyl porphyrin causes V=O vibration shift from 4 to 20 cm⁻¹. Also, H-bonding is found to be an important factor in directing the orientation of vanadyl oxygen. Both "cis" and "trans" isomers have been identified for vanadyl Naphthalene Kemp's Amide Porphyrin (NKAmideP) and NAP(VO).

Finally, H-bonding on CO heme complexes is shown to be not important. However, H-bonding to the coordinated methanol or water ligand trans to the metal-bound CO shifts the $\nu_{C=O}$ in a predictable manner.



ACKNOWLEDGMENTS

I would like to express my deepest respect and gratitude to my research advisor and mentor, Dr. C.K. Chang, for his guidance, inspiration and support during the course of this work. I refer myself exceptionally lucky of being his graduate student. I thank him for accepting me to his research group which has provided me great opportunities to learn the most outstanding researches at MSU. His excellent research expertise and enthusiasm have inspired and always will inspire me.

I would like to thank Dr. Jackson for serving as the second reader in my research committee. Drs. Pinnavaia, McCracken and Babcock are appreciated for being my research committee members and for their helpful discussions.

I want to thank Dr. S.-M. Peng at National Taiwan University for solving all the X-ray single crystal structures I presented in this dissertation. Without the help of the X-ray structure, I cannot explore a lot important aspects of the systems I studied.

Dr. Rui Huang is appreciated for teaching me of running the benchtop GC-MS spectrometer and I thank Drs. Long Lee and Kermit for their help in NMR techniques.

Also, I am grateful to the past and present group member in Dr. Chang's group, especially for their helpful discussions and friendship.

Among them are: Dr. N. Bag, Dr. E. Schmidt, Dr. W. Wu, Dr. W. Lee, Dr. A. M. Gladys, Mr. J. P. Kirby, Ms. D. M. Conrad-Vlasak, Ms. E. Guerin, Ms. I. M. Morrison, Dr. S. Lee, Dr. S.-S. Chern, Dr. M. Sato, Mr. C. Shinner, Mr. B. Guo, Mr. Y. Deng...

Friendship from Carolyn Hsu, Zoe Pikramenou, Gregory R. Cook, Scott J. Stoudt, K. Paulvannan and lot of graduate students and postdocs is always appreciated. I will never forget their understanding, supports and helpful discussions. Thank you, all my friends, for sharing my tears and happiness at MSU.

I'd like to thank my best friends, Zhixia Wu, Xinhua Yu, Yiliang Liu, Jiahwa Yeh, Qing Yang, Feng Tian, Xiaoming Chen, Weishih Wu, Hongjun Yan and Weiqing, who spent a lot of wonderful moments with Tie Lan and me. Their friendship made my life and study at MSU an enjoyable one.

At last, but not the least, I want to thank my husband, Tie Lan, for his encouragement, support and understanding during my Ph.D. studies. I am looking forward to our better lives together with the coming baby next March.

TABLE OF CONTENTS

CHAPTER Page
LIST OF FIGURESxii
LIST OF TABLESxviii
ABBREVIATIONxxi
CHAPTER I Introduction
Introduction1
References29
CHAPTER II Synthesis and Characterization of C-
clamp Porphyrin
A. Introduction32
B. Synthesis33

	1. Tetrapyrrole Pathway	33
	2. Dipyrrole Pathway by McDonald Condensation	37
C.	Variant Temperature NMR	49
D.	Experimental	52
E.	References	72
CH	HAPTER III Hydrogen Bonding in Molecular Recognition: Inclusion Complex and Substrate Recognition by C-Clamp Porphyrins	
A.	Introduction	74
В.	Experimental	76
	1. Crystal Structure Analysis	76
	2. Determination of Binding Constants	76
	a) NMR Method	76
	b) UV-Vis Method	77
	c) DSC Method	77
C.	Result and Discussion	77
	1. Structure of Receptors and Their Znic Complexes	77
	2. Substrate Binding Studies	91
	a) Substrate Binding of Metal-free Systems	91

	b) Substrate Binding of Zinc Porphyrins	100
	3. Discussion	106
D.	Conclusion	108
E.	References	109
CH	HAPTER IV Conformational Control of Intramolecular Hydrogen Bonding in Heme Models: Maximal Co(II)-O ₂ Binding in Naphthalene Kemp's Acid Porphyrin	
A.	Introduction	111
В.	Experimental	112
	1. Cobalt Insertion	112
	2. O ₂ Binding Studies	113
	3. Iron Insertion	116
	4. ¹⁵ N NMR Studies	117
C.	Result and Discussion	117
	1. Oxygen Binding	117
	2. Further Information from ¹⁵ N NMR	122
D.	Conclusion	125
E.	References	126

CHAPTER V Structural and Vibrational Character of H-Bonded Vanadyl Porphyrins. Models of H-Bonded Ferryl Heme

Α.	Introduction	129
В.	Experimental	131
	1. Reagent	131
	2. VO Insertion	131
	a) NKAP(VO)	131
	b) NKAmideP(VO), NAP(VO) and OEP(VO)	132
	3. Instrumentation	132
	a) Spectroscopy	132
	b) X-Ray Determination	134
C.	Result and Discussion	136
	1. H-Bonding for 5-Ligated VO-porphyrins	136
	2. H-Bonding for 6-Ligated VO-porphyrins	140
	3. X-Ray Single Crystal Structure of NKAP(VO) and NAP(VO)	146
	4. Orientation of the VO Dictated by H-Bonding	156
D.	Conclusion	159
E.	References	162

CHAPTER VI Structural and Vibrational Properties of RuCO and FeCO C-clamp Porphyrin and Derivative

Α.	Introduction166
В.	Experimental167
	1. Preparation of RuCOporphyrins167
	2. Preparation of FeCOporphyrins168
	3. Instrumentation169
	a) Spectroscopy169
	b) X-Ray Determination169
C.	Result and Discussion
	1. X-Ray Single Crystal STructures of RuCONKAP(MeOH)
	and RuCONKAmideP(MeOH)171
	2. IR studies of RuCOporphyrins181
	3. IR studies of FeCOporphyrins181
	4. Trans Ligands Effect in Affecting CO Vibration in M-
	COporphyrins185
D.	Conclusion
E.	References

LIST OF FIGURES

FIGU	RE Page
I-1.	Structure of the β subunit of hemoglobin. (M. F. Perutz,
	Nature, 1970, 228, 726)3
I-2.	(a) Structure of Fe(II) protoporphyrin IX4
	(b) Histidines near the oxygen bound heme active site4
I-3.	Cytochrome c oxidase8
I-4.	Proposed catalytic cycle for oxygen reduction by
	cytochrome c oxidase10
I-5.	The reduction pathway proposed by Caughey11
I-6.	Some heme enzymes capable of reducing O ₂ to water13
I-7.	Schematic representation of the cytochrome c peroxidase
	heterolytic cleavage of the RO1-O2H bond14
I-8.	"Push-pull" for O-O bond cleavage of Fe-bound
	cytochrome P450 (left) and horseradish peroxidase (right)16
I-9.	Anthracene diporphyrins17
I-10.	Some structures of porphyrin models for studies of

	H-bonding effects19
	a) basket handle porphyrin-through ether linkage;
	b) basket-handle porphyrin-through amide linkage;
	c) picket-fence porphyrin;
	d) substituted picket-fence porphyrin.
I-11.	Naphthalene porphyrin model compounds22
I-12.	Essential components of the C-clamp porphyrins23
I-13.	Structure of series of anthracene Kemp's porphyrins25
I-14.	Co-O ₂ complexes of naphthalene Kemp's isomer and
	anthracene Kemp's acid porphyrin (AKAP)26
II-1.	Target compound NKAP34
II-2.	Two synthetic approaches to naphthalene linked porphyrin35
II-3.	Synthetic route to 2-carboxybenzyl porphyrin and
	proposed synthetic pathway to naphthalene ester porphyrin
II-4.	Synthesis of corrole, failed attempts to make porphyrin38
II-5.	MS and UV-vis spectra of corrole39
II-6.	(a) The equilibrium between 8-formyl-1-naphthoic acid

	and its lactone form	41
	(b) The equilibrium between 8-formyl-1-naphthoic ester	
	and its lactone form.ester	41
II-7.	Synthesis of naphthalene mesylate porphyrin	42
II-8.	Synthesis of NKAP	44
II-9.	Naphthalene Kemp's isomer porphyrin	45
II-10.	¹ H NMR of NKAP and NKEsterP	46
II-11.	Synthesis of NKEsterP and NKAmideP	48
II-12.	Variant Temperature NMR of NKAP	50
II-13.	¹ H NMR spectrum of 2	61
II-14.	¹ H NMR spectrum of 3	62
II-15.	¹ H NMR spectrum of 4	63
II-16.	¹ H NMR spectrum of 5	64
II-17.	¹ H NMR spectrum of 6	65
II-18.	¹ H NMR spectrum of 8	66
II-19.	IR spectrum of 8	67
II-20.	¹ H NMR spectrum of 9	68
II-21.	¹ H NMR spectrum of NKAP	69

II-22.	¹ H NMR spectrum of 10 70
II-23.	¹ H NMR spectrum of 11 71
III-1	(a) ORTEP plot and labeling scheme for NKAP-H ₂ O78
	(b) Side view of the X-ray structure showing H-bonds.
	The distance between the water oxygen and the
	porphyrin center is 2.31(4) Å79
	(c) Another view showing distortions around the
	C20-C33 connetor79
III-2	(a) ORTEP plot and labeling scheme for ZnNKAP-MeOH80
	(b) Side view of the X-ray structure of ZnNKAP-MeOH81
	(c) Side view from another angle showing the porphyrin outward bending
III-3	¹ H NMR Titration of H ₂ O into NKAP. [NKAP] = 3 mM ,
	[H ₂ O] in a: 0.000; b: 0.022; c: 0.037; d: 0.047 M
	93
III-4	DSC measurement of NKAP-H ₂ O complex94
III-5	¹ H NMR of Imidazole titration of AKAP. [AKAP]
	= 0.00276M, [Im] in a: 0.0000; b: 0.0082; c: 0.0272;

	d: 0.3264 M95
III-6	Schematic structure of AKAP-imidazole and plot of
	the anthryl methylene protons as a function of
	concentration of imidazole in CDCl ₃ 97
III-7	Schematic structure of AKAP-Purine and plot of
	the anthryl methylene protons as a function of
	concentration of purine98
III-8	¹ H NMR titration of methanol to ZnNKAP.
	[ZnNKAP] = 0.014 M, [MeOH] in a: 0.000;
	b: 0.013; c: 0.032; d: 0.064; e: 0.132; f: 0.395 M
	101
III-9	(a) ZnAKAP-1,2,4-triazole. (b) ZnAKAP-1,2,3-triazole105
III-10	(a) Calculated structure of syn acid monohydrates107
	(b) Partial X-ray single crystal structure of NKAP-H ₂ O107
IV-1.	Typical O ₂ titration spectra of Co(II)porphyrins114
IV-2.	Van't Hoff plot of 1/T vs Ln(1/P _{1/2})118
IV-3.	The equation of reversible O ₂ binding and the
	definition of P _{1/2} 121
IV-4.	Side-view of NKAP-H ₂ O complex124
V-1. '	VO insertion to NKAP

V-2.	IR Spectrum of NKAP(VO). The Sample was layered
	on NaCl plate138
V-3.	IR Spectra of NKAmideP(VO): (a) Major Product;
	(b) Minor Product. The Sample was layered on NaCl
	plate141
V-4.	The optical spectra of NKAmideP(VO) in (a)
	CH ₂ Cl ₂ ; (b) pyridine; (c) 1-methyl-imidazole143
V-5.	(a) ORTEP structure of NKAmideP(VO)153
	(b) Sideview of NKAmideP(VO)155
V-6.	(a) X-Ray crystal structure of NAP(VO)157
	(b) Unit cell structure of NAP(VO)158
VI-1	ORTEP structure of RuCONKAP(MeOH)179
VI-2	ORTEP structure of RuCONKAmideP(MeOH)180

LIST OF TABLES

TABLE		Page	
III-1	Crystallographic Data of NKAP and ZnNKAP	.82	
III-2	Atomic Parameters x, y, z and Biso for NKAP and		
	ZnNKAP with E.S.Ds. Refer to the Last Digit Printed		
		83	
III-3	Selected Bond Distances (Å) and Angles (deg) and Their		
	Estimated Standard Deviations for NKAP and ZnNKAP	.89	
III-4	Association Constants (M-1) of AKAP and NKAP with		
	Substrates	99	
III-5	Association Constants of Zn-porphyrins with MeOH		
	and Triazoles10	04	
IV-1.	O ₂ Binding Parameters to Co(II)porphyrins1	19	
IV-2.	15N NMR Chemical shift of Fe(CN)2porphyrins1	23	
V-1	Crystallographic Data for NKAmideP(VO) and NAP(VO)1	35	
V-2	IR Data of Vanadyl Porphyrins1	37	
V-3	The Optical Absorption Spectral Data of Several		
	Vanadyl Porphyrins14	45	

V-4	Atomic Parameters x, y, z and B _{iso} for NAP(VO)
	with E.S.Ds. refer to the last digit printed147
V-5	Atomic Parameters x, y, z and Beq for NKAmideP(VO)
	with E.S.Ds. refer to the last digit printed149
V-6	Selected Bond Distances (Å) and Angles (deg) and Their
	Estimated Standard Deviations for NKAmideP(VO) and
	NAP(VO)152
V-7	Structural Data of several vanadyl compounds160
VI-1	Crystallographic Data of RuCONKAP(MeOH) and
	RuCONK-AmideP(MeOH)170
VI-2	Atomic Parameters x, y, z and B _{iso} for
	RuCONKAP(MeOH) with E.S.Ds refer to the last
	digit printed172
VI-3	Atomic Parameters x, y, z and B _{iso} for
	RuCONKAmideP(MeOH) with E.S.Ds refer to
	the last digit printed175
VI-4	Selected Bond Distance (Å) and Angles (deg) and
	Their Estimated Standard Deviations for
	RuCONKAP(MeOH) and RuCONK-AmideP(MeOH)
	178
VI-5	Bond Distance (Å) and Angle (deg) Comparison

	of Selected Carbonylated Metalloporphyrins	182
VI-6	C-O Vibrations for RuCOporphyrins	183
VI-7	C-O Vibrations for FeCOporphyrins	184

ABBREVIATIONS

OEP Octaethylporphyrin

TPP meso-Tetraphenylporphyrin

DeutP 2,7,12,18-tetramethyl-13,17-dipropionicacidporphyrin

ETP Etioporphyrin

"Picket-fence" Porphyrin

meso-tetrakis($\alpha,\alpha,\alpha,\alpha$ -o-pivalamidophenyl)porphyrin

PovPivP "Small Pocket" = 5,10,15((1,3,5-benzenetriyltri-

acetyl)tris(α,α,α -o-aminophenyl))-20-(α -o-

pivalamidophenyl)porphyrin

NAP "Naphthoic Acid Porphyrin" = 5-(8-Hydroxycarbonyl-

1-naphthyl)-2,8,13,17-tetraethyl-3,7,12,18-

tetramethylporphyrin

NKAP "Naphthalene Kemp's Acid Porphyrin" = 5-{8-[endo-

7-(Hydroxycarbonyl)-1,5,7-trimethyl-2,4-dioxo-3-azobicyclo[3,3,1]non-3-yl]-methyl-1-naphthyl}-2,8,13,17-tetraethyl-3,7,12,18-tetramethylporphyrin

NKEsterP "Naphthalene Kemp's Ester Porphyrin" = 5-{8-[endo-

7-(Methoxycarbonyl)-1,5,7-trimethyl-2,4-dioxo-3-azobicyclo[3,3,1]non-3-yl]-methyl-1-naphthyl}-2,8,13,17-tetraethyl-3,7,12,18-tetramethylporphyrin

NKAmideP "Naphthalene Kemp's Amide Porphyrin" = 5-{8-

[endo-7-(Aminocarbonyl)-1,5,7-trimethyl-2,4-dioxo-3-azobicyclo[3,3,1]non-3-yl]-methyl-1-naphthyl}-2,8,13,17-tetraethyl-3,7,12,18-tetramethylporphyrin

AKAP "Anthracene Kemp's Acid Porphyrin" = 5-{8-[endo-7-

(Hydroxycarbonyl)-1,5,7-trimethyl-2,4-dioxo-3-azobicyclo[3,3,1]non-3-yl]-methyl-1-anthryl}-

2,8,13,17-tetraethyl-3,7,12,18-tetramethylporphyrin

"Anthracene Kemp's Ester Porphyrin" = 5-{8-[endo-**AKEsterP**

> 7-(Methoxycarbonyl)-1,5,7-trimethyl-2,4-dioxo-3azobicyclo[3,3,1]non-3-yl]-methyl-1-anthryl}-

> 2,8,13,17-tetraethyl-3,7,12,18-tetramethylporphyrin

"Anthracene Kemp's Alcohol Porphyrin" = 5-{8-AKOHP

> [endo-7-(Hydroxymethyl)-1,5,7-trimethyl-2,4-dioxo-3-azobicyclo[3,3,1]non-3-yl]-methyl-1-anthryl}-

> 2,8,13,17-tetraethyl-3,7,12,18-tetramethylporphyrin

1,5-Diazabicyclo[4.3.0]non-5-ene **DBN**

Pyridine ру

1-Methylimidazole 1-MeIm

Differential Scanning Calorimetry DSC

Fourier Transformed Infra Red FT-IR

FAB-MS Fast Atom Bombardment Mass Spectroscopy

CHAPTER I

Introduction

Hemes and heme proteins play many critical roles in biological systems. They are vital components of essentially every cell of nearly all living organisms. Even though their active sites all contain heme (iron porphyrin), their functions are quite diverse. To name a few of their functions in life processes, they include:

- Hemoglobin and myoglobin: transport and storage of O₂ in higher animals;¹
- Cytochrome c oxidase: the last enzyme in the respiratory chain for O₂ activation and reduction;²
- Cytochrome a.b.c.d.e.f and o: electron transport in the respiratory chains of organisms as diverse as bacteria, yeasts, plants and animals, and in photosynthetic cells from those of the simplest photosynthetic bacteria to those of higher plants;³

Cytochrome *P450*: synthesis, modification and/or degradation of fatty acid, steroid and adrenal hormones, anesthetics, polycyclic aromatic hydrocarbons and other xenobiotics. By doing so, it detoxifies poisonous compounds in living organisms;⁴

Peroxidases, catalases: activation and metabolism of hydrogen peroxide.⁵

The many functions of heme proteins depend on the properties and the micro-environments of their active sites. Among the heme proteins, a variety of axial ligations, oxidation states, and spin states of the central metal ion are stabilized by the particular protein environments created within the heme pockets of these proteins.

Among all the heme proteins, hemoglobin has been the most extensively studied system. It was the first protein crystallized, the first protein recognized for its physiological purpose of O₂ and CO₂ transport, the first to have its amino acid sequence determined, and one of the first proteins whose tertiary and quartenary structure was determined by X-ray crystallography. Hemoglobin (MW 64,500) is a tetrameric protein, having four subunits, two α and two β , chains with 141 and 146 amino acid residues, respectively. Each subunit (Figure I-1) has one iron(II) protoporphyrin IX complex as the active site (Figure I-2). The four-chain structure of hemoglobin is directly related to the way it behaves in fulfilling its biological role. The interactions between the subunits are known as allosterism and they determine the cooperative binding of O₂. Myoglobin is a monomeric protein of 160 amino acid residues (MW 17,800) and one heme molecule. It is found in the skeletal muscles and stores dioxygen, transported to it by hemoglobin, for use in the mitochondria.

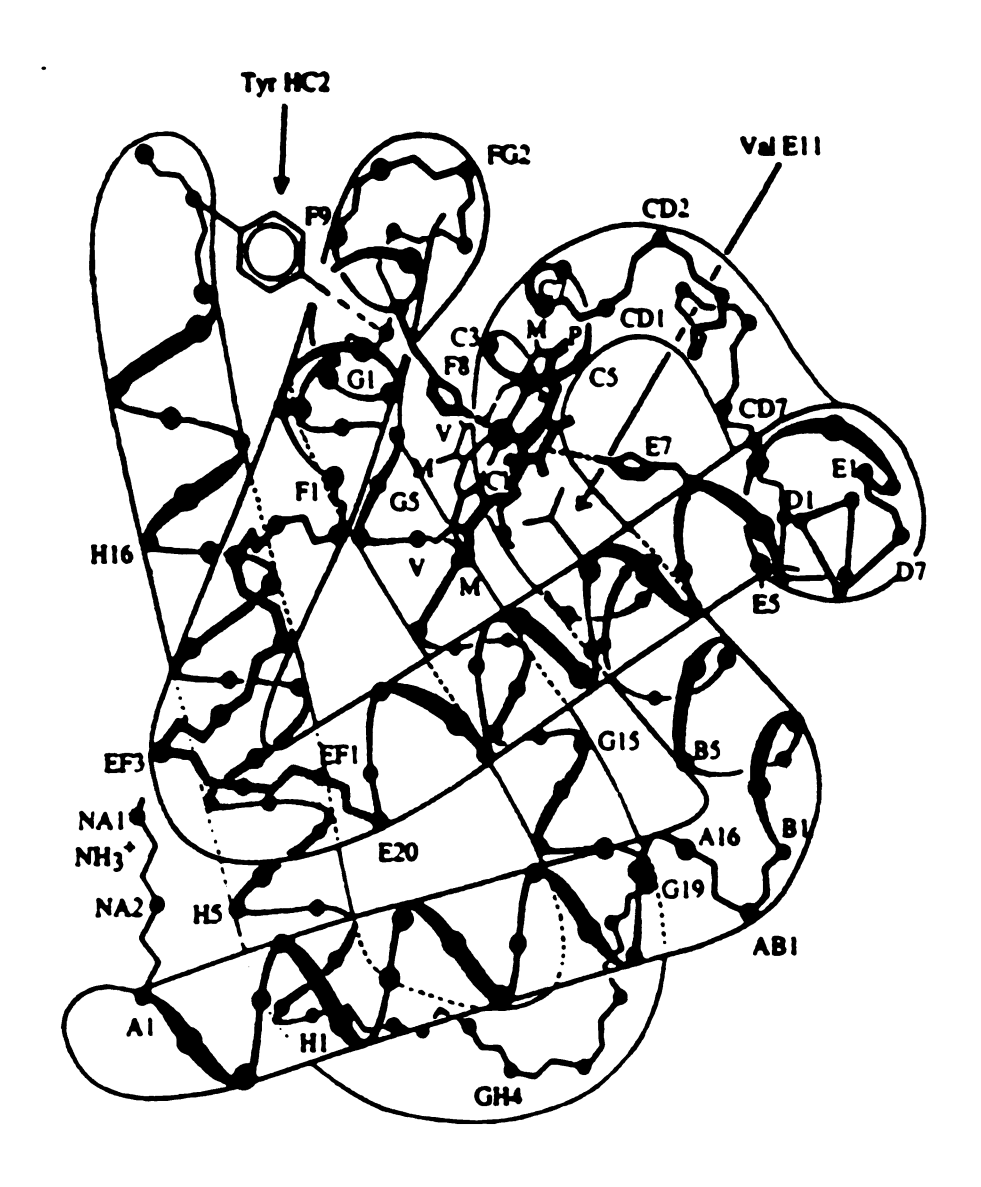


Figure I-1. Structure of the β subunit of hemoglobin. (M. F. Perutz, Nature, 1970, 228, 726)

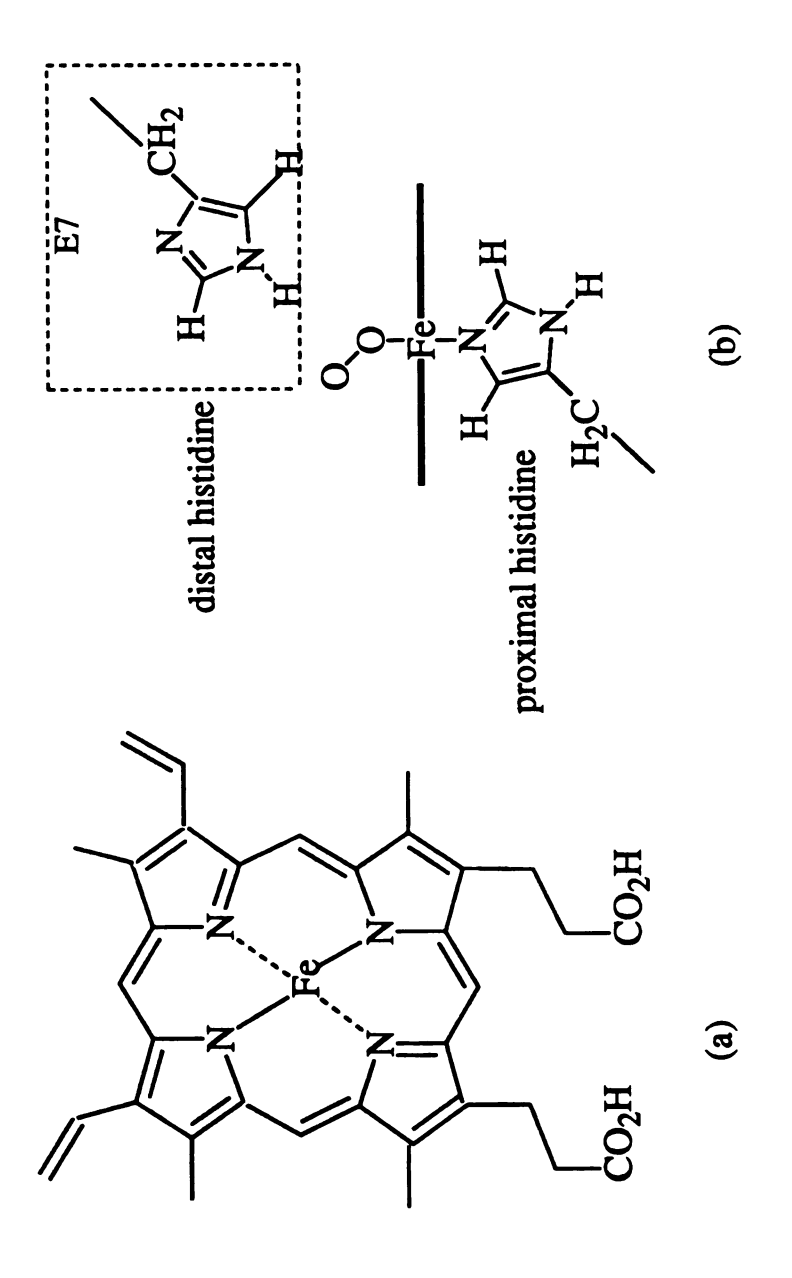


Figure I-2. (a) Structure of Fe(II) protoporphyrin IX. (b) Histidines near the oxygen bound heme active site.

In the native deoxy form, the heme contains a five-coordinated ferrous ion. It recognizes and reversibly binds to dioxygen at its sixth coordination site. Other small substrates, such as CO, can also bind at this site. The amino acid residues dictate the immediate environment around the heme and help to discriminate between CO and O2. The iron atom is approximately 0.5 Å out of the plane of the porphyrin and the Fe-N(imidazole) bond vector is approximately 10° off the heme normal. This iron atom incorporated in the protoporphyrin IX is high-spin (S=2) iron (II). Upon the binding of O₂ to heme, structural and conformational changes occur around the active site. The oxygenated heme has a low-spin six-coordinated iron(II) which is nearly centered in the porphyrin plane. Along with a lateral shift of the protein F helix (Figure I-1), the Fe-N (imidazole) off-axis tilt is reduced. O2 binds in an end-on fashion with a bent geometry.⁶ X-Ray⁷ and neutron diffraction⁸ data have provided strong evidence for H-bonding between the distal histidine and the bound O₂ (Figure I-2B).

Model compounds have been proposed and synthesized to help the understanding of the mechanism of O₂-binding in heme proteins. If we look back at the evolving theories of how the hemoglobin molecule functions, we can see a classic example of the way that protein structures suggest mechanistic theories and models, which in turn suggest new chemical experiments, whose results provide feedback that forces the original theories to be abandoned, modified, qualified, and improved until the truth is finally approached. During the course of the theory development, model compounds have played important roles in understanding the relationships between structure and functions. On the

bases of results from the studies on proteins, models can be designed and synthesized to mimic their active site. Due to its flexibility and simplicity, the synthetic analog approach may lead to a better understanding of the active site than that obtained directly from the protein itself. Without the influence and complexity of the protein, the models provide the essential properties of the active site of the heme protein, and by changing their structure systematically, the functions of the heme protein environment may be revealed.

The sequence of the model studies is as follows: 1) Isolate and purify the proteins; 2) study the structural information and physical properties of the active site; 3) design and synthesize analog molecules; 4) investigate the structural, spectroscopic, and the chemical reactivity properties of the model compounds; 5) compare between the protein and the analogs to reveal new structure-function relationships. A major advantage in the study of synthetic analogs, compared to the heme proteins, is the level of control and flexibility in systematic variation of a single variable (such as axial ligation, binding site polarity, steric restraint, solvent). There are three synthetic challenges in designing synthetic analogs for Hb and Mb⁹: 1) the preservation of coordinative unsaturation at the iron, 2) the prevention of irreversible bimolecular oxidation of the iron, and 3) the control of substrate recognition (specifically O₂ over CO).

The success in synthesis of model compounds capable of binding O₂ reversibly made it possible to study in detail the distal (steric, local polarity, and hydrogen bonding) and proximal binding site effects⁹ (distal and proximal sites are described in Figure I-2). Among them, hydrogen bonding effect as proposed from the distal E7 histidine of hemoglobin is

considered as a major factor affecting O₂ affinity. Therefore, it is important to design and synthesize model compounds to probe this effect.

Besides hemoglobin, another heme protein, cytochrome c oxidase, located at the inner mitochondrial membrane, plays a central role in the cellular respiratory process. This enzyme catalyzes the reduction of O_2 (Equation 1) and functions as a proton pump coupled to electron transfers from cytochome c to O_2 . The free energy developed in this process is used in the synthesis of ATP. It is estimated that 90% of the energy for heart muscle contraction is provided through aerobic metabolism via cytochrome c oxidase.

$$O_2 + 4 \text{ Cyt.}c^{2+} + 4 \text{ H}^+ \xrightarrow{\text{Cyt.}c} 4 \text{ Cyt.}c^{3+} + 2 \text{ H}_2\text{O}$$
 (1)

The enzyme transfers four electrons to bound O_2 one at a time from cytochrome c^{2+} ; four O-H bonds are efficiently formed without release of incompletely reduced O_2 species such as superoxide, H_2O_2 or OH_2 .

It has been well established that the active unit of this enzyme contains four metal centers: two heme groups, associated with heme a and a_3 , and two copper atoms with distinct properties (Figure I-3).¹⁰ Heme a is usually low spin and does not bind ligands while heme a_3 is high spin and capable of binding various ligands, such as O_2 and CO in the ferrous state and cyanide and azide in the ferric state. Heme a serves as a shuttle that mediates the electron transfer from cytochrome c to the heme a_3

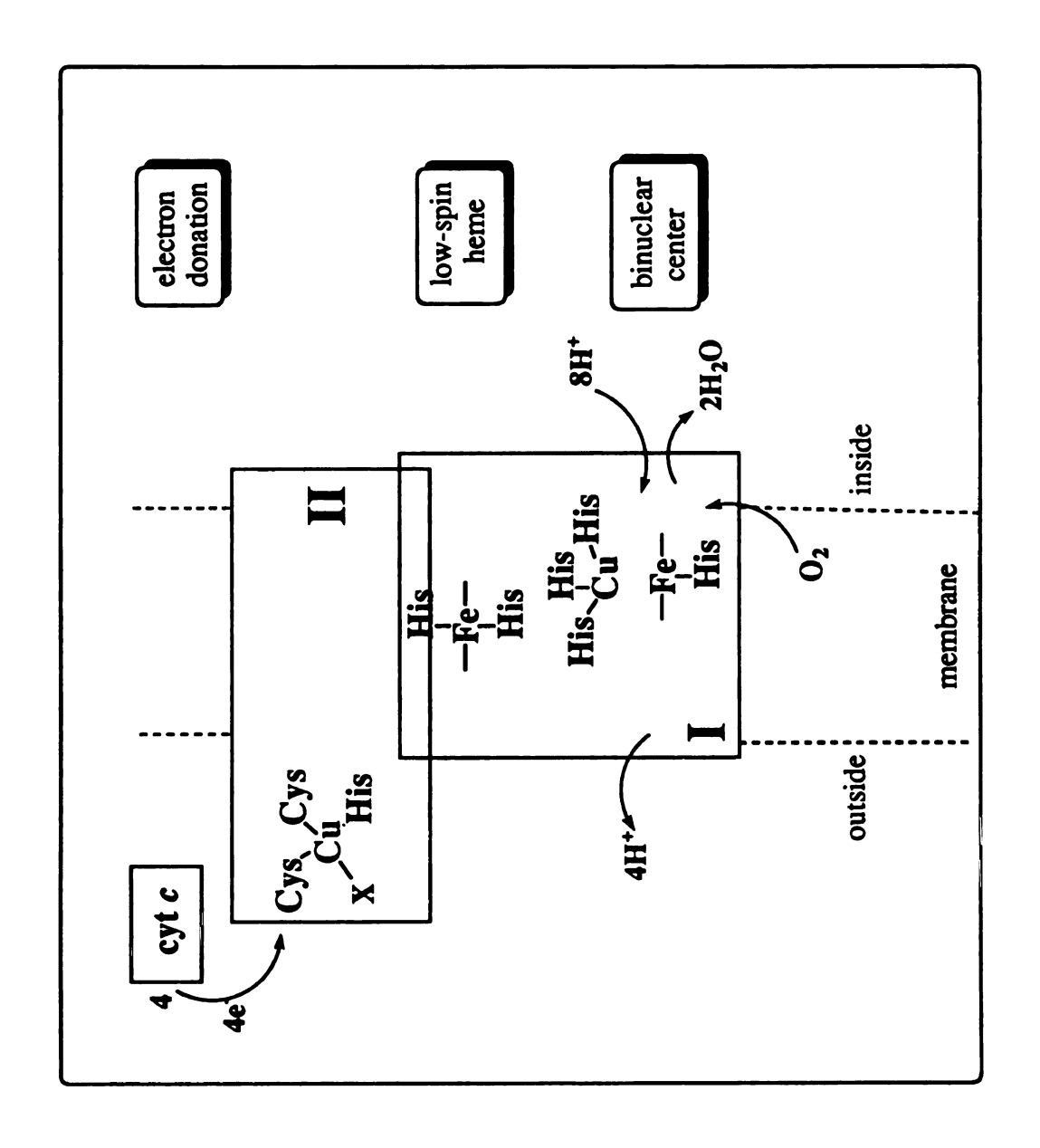


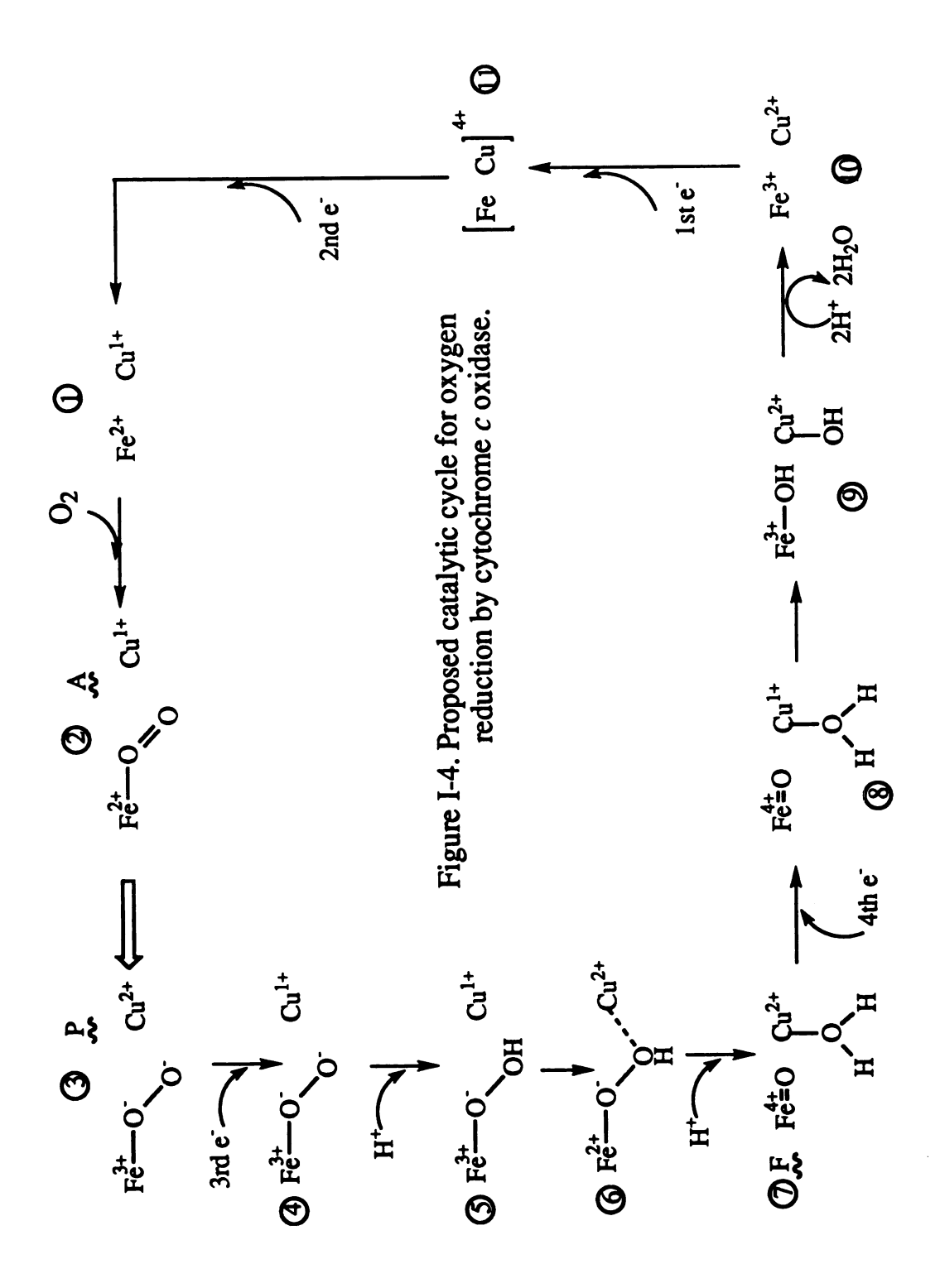
Figure I-3. Cytochrome c oxidase.

Heme a_3 is associated with the binding and subsequent reduction of the O_2 molecule. Electrons are transferred from the heme of cytochrome c, through Cu_A and heme a, to the bimetallic O_2 reduction center which contains heme a_3 and Cu_B .

Although the structural relationship between iron and copper of the enzyme is far from established, it has been suggested that the Fe-Cu distance in the binuclear site is less than 5 Å in the oxidized enzyme, and the Fe-Fe distance between the hemes is 15 to 20 Å.

Many mechanistic studies of the reduction of O₂ to water have been carried out.² The proposed mechanism for dioxygen activation and reduction in cytochrome c oxidase is shown in Figure I-4. The chemistry of equation 1 necessarily involves a number of steps: O₂ binding, electron transfers to oxygen, hydrogen transfers to oxygen, cleavage of O-O bond, and release of products. Some of the intermediates shown in the Figure I-4 have been observed or identified by spectroscopic methods, but not every intermediate is fully established and some of them remain speculative.

In order to understand the mechanism by which cytochrome c oxidase reduces oxygen to water, it is important to clarify the function of CuB. Although μ -peroxo complexes such as Cu-O-O-Fe are expected to be present during the enzymatic cycle, there has been no direct evidence for its existence. Alternatively, as Caughey recently suggested, ¹¹ CuB does not serve as a direct coordination site for O₂ or for its reduction intermediate; its role could be more as an anchor and for electron storage (Figure I-5). The similarity between the function of Cu and H-bonding effect is that they both may serve as polarizing factors to assist in pulling the two oxygen



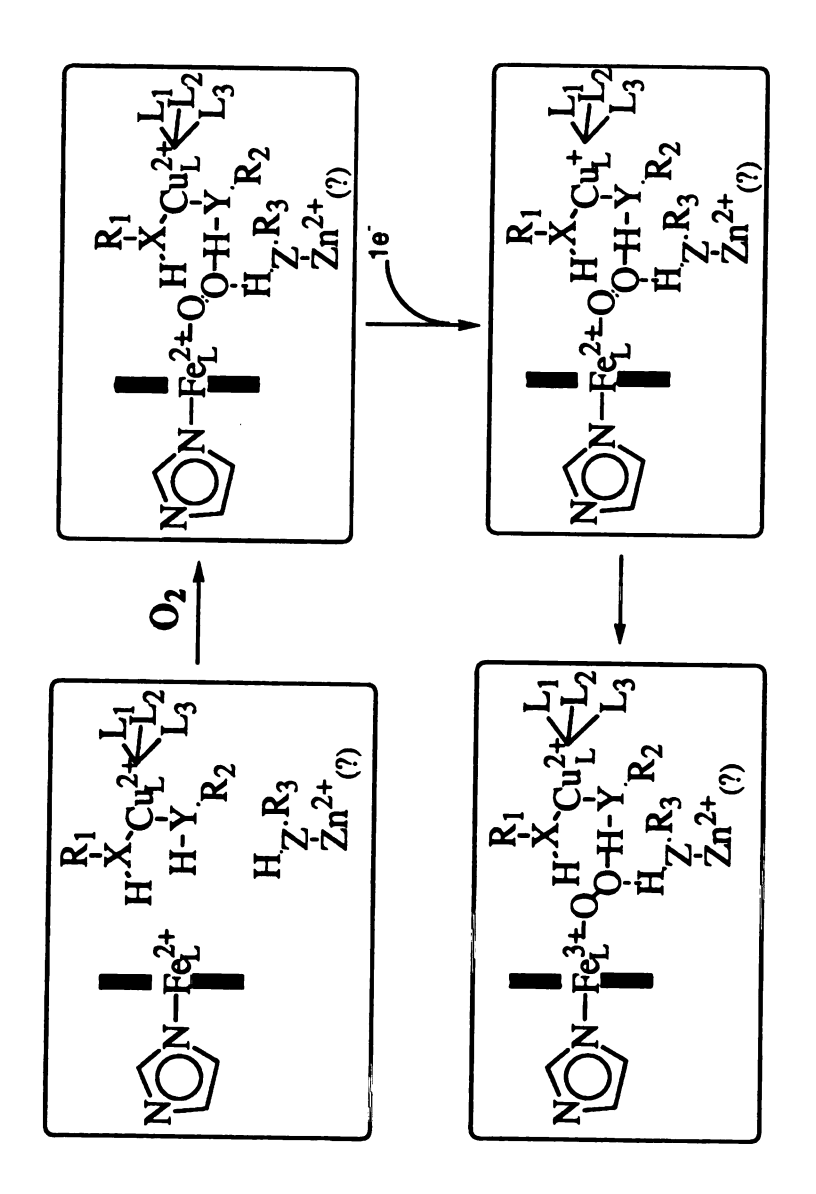
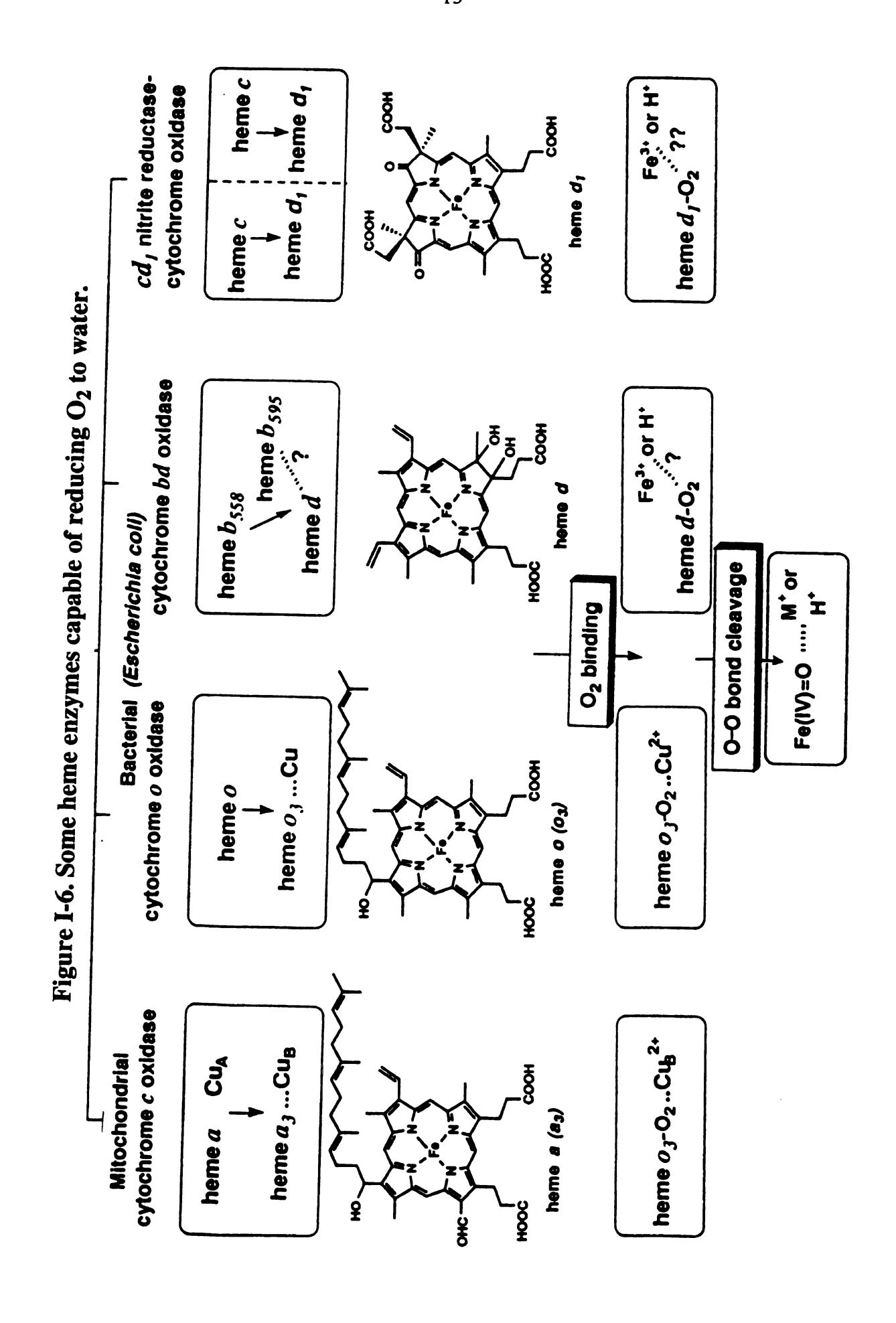


Figure I-5. The reduction pathway of O₂ proposed by Caughey.

atom apart. Therefore, the O₂ adduct can be stabilized as well as reduced easily.

Among the known terminal oxidases in nature (Figure I-6), many bacterial enzymes, such as cytochrome bd oxidase and cd oxidase, do not contain either a copper ion or another heme group at the O₂ coordination site yet the reduction of O₂ to H₂O in these systems occurs unhindered. It is possible that nearby proton donors may provide strong H-bonding to the Fe-O₂ complex thereby facilitating the O-O bond cleavage.

The importance of the hydrogen bonding is also shown in the cytochrome c peroxidase in which hydrogen bonding is thought to promote heterolysis of peroxides by stabilizing a developing negative charge on the leaving group of the substrate. From the crystal structure determination, Poulos¹² showed that peroxidase has a water ligand at the sixth coordination site which in turn is hydrogen-bonded to a distal histidine side chain. Close to the sixth position there are a tryptophan and an arginine side chain. Based on the X-ray crystal structure, Poulos proposed a mechanism (Figure I-7) that utilizes the distal arginine and histidine hydrogen bonds with subsequent proton transfer to effect heterolytic hydroperoxide cleavage.¹³ This transfer has a "push-pull" effect, as discussed by Poulos. 14 In cytochrome c peroxide the proximal histidine hydrogen bonds more strongly to neighboring groups than in the globins. This makes the axial histidine a better electron donor (in other words, a better "push") to the heme than in the globins. This may help to stabilize higher oxidation states of the iron. Meanwhile, the distal histidine serves as a proton donor, while arginine acts to stabilize the developing negative



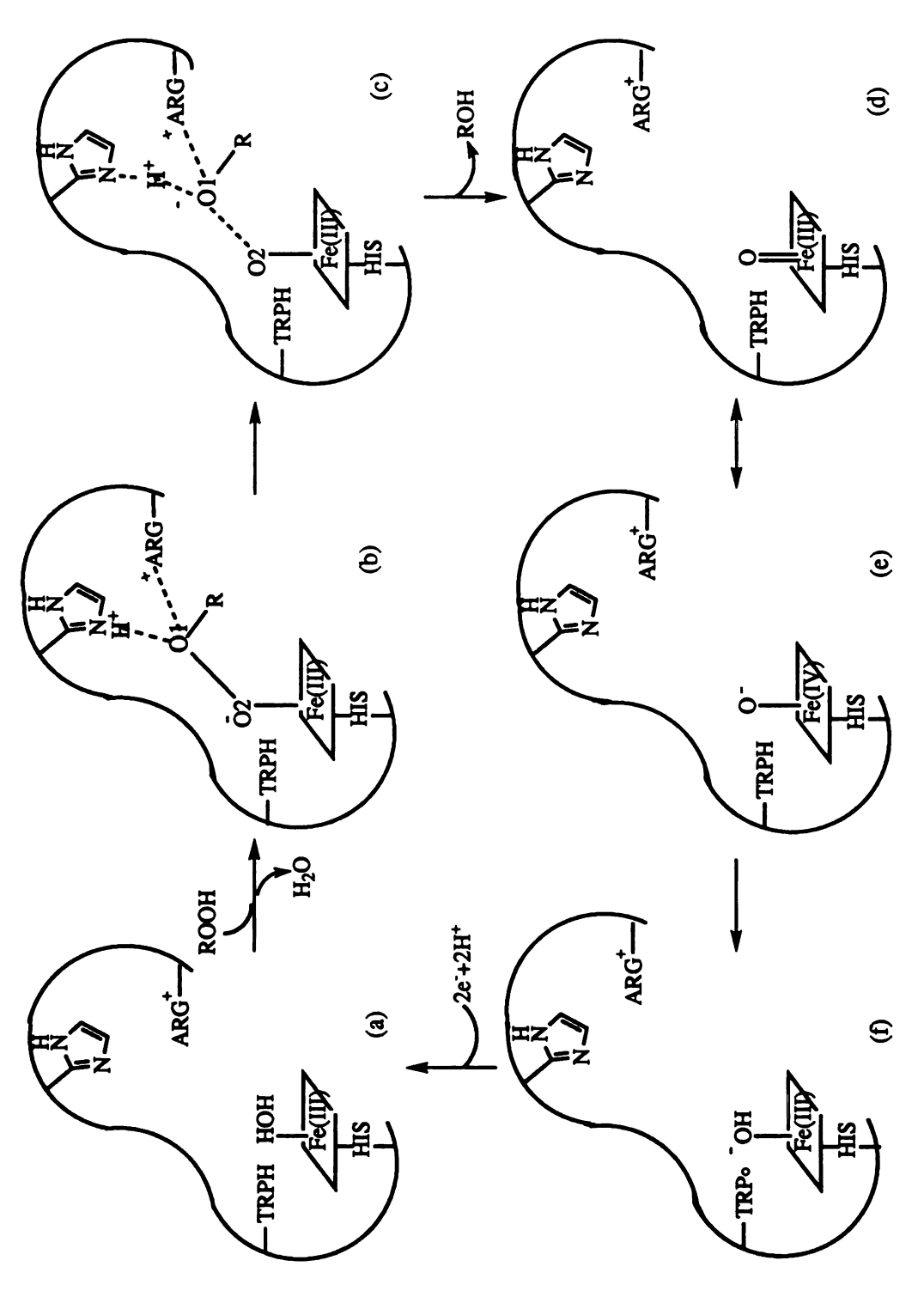


Figure I-7. Schematic representation of the cytochrome c peroxidase heterolytic cleavage of the ROI-02H bond.

charge on the Fe bound oxygen atom. Consequently, the system is more polar than globins and the polar distal side can "pull' apart the O-O bond of the bound peroxide by stabilizing the separating charge.

In cytochrome *P450*, the thiolate ligand aids the cleavage of the O-O bond by "pushing" the electron density from the proximal side on to the metal (Figure I-8). The "pull" element is less evident but may come from hydrogen binding to O₂ by Thr 252, which has been investigated recently by Harris.¹⁵ In the ferrous dioxygen form of the enzyme, a H-bond between T252 and G248 diminishes while the T252 interaction with terminal oxygen of the bound dioxygen simultaneously forms. This T252 not only stabilizes the ferrous dioxygen form of the enzyme, but also helps the formation of compound I.

A variety of metalloporphyrins have been designed and examined for their catalytic effects on O₂ activation and reduction.¹⁶ Chang has shown that dimeric porphyrins substituted with one or two cobalt centers¹⁷ can successfully carry out a four-electron reduction of O₂ electrocatalytically with no hydrogen peroxide intermediate detected (Figure I-9). The most surprising observation is that with only one cobalt ion present in the dimeric porphyrin ligand, it is still capable of catalyzing the four-electron pathway for reduction of O₂. The unexpected high activity might arise from the proximity of the second porphyrin ring which would be protonated in acid. It is conceivable that these protons, juxtaposed to the coordinated O₂, could prevent the premature dissociation of, as well as assist in proton transfer to, the partially reduced O₂ coordinated to the cobalt center in the second porphyrin ring. The function of the second

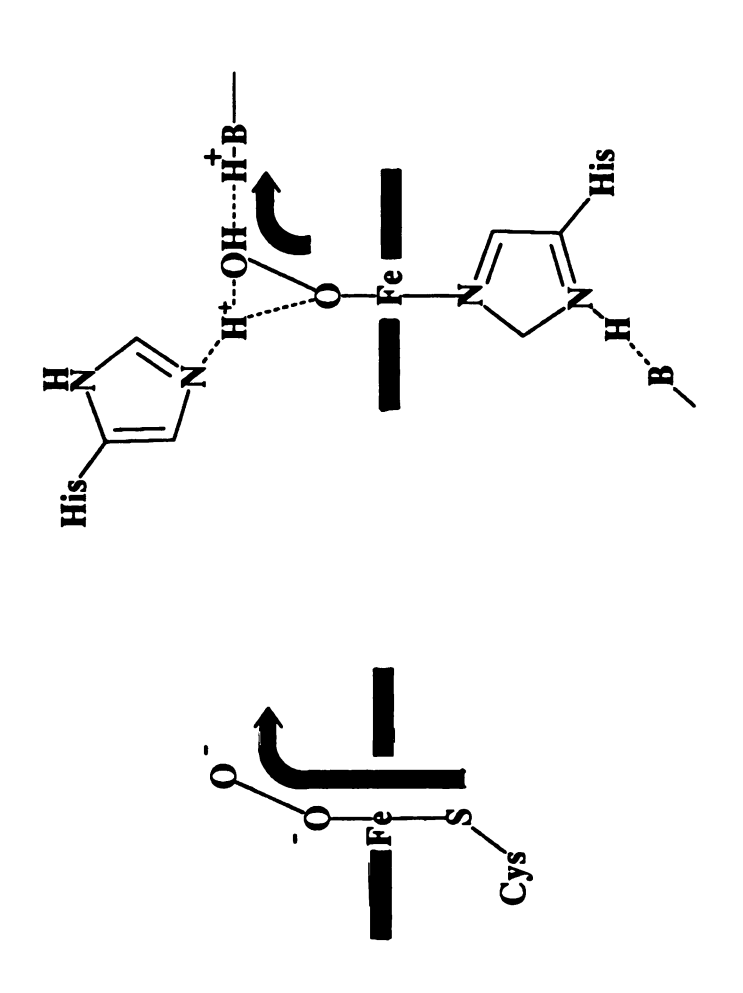


Figure I-8. "Push-pull" for O-O bond cleavage of Fe-bound cytochrome P₄₅₀ (left) and horseradish peroxidase (right).

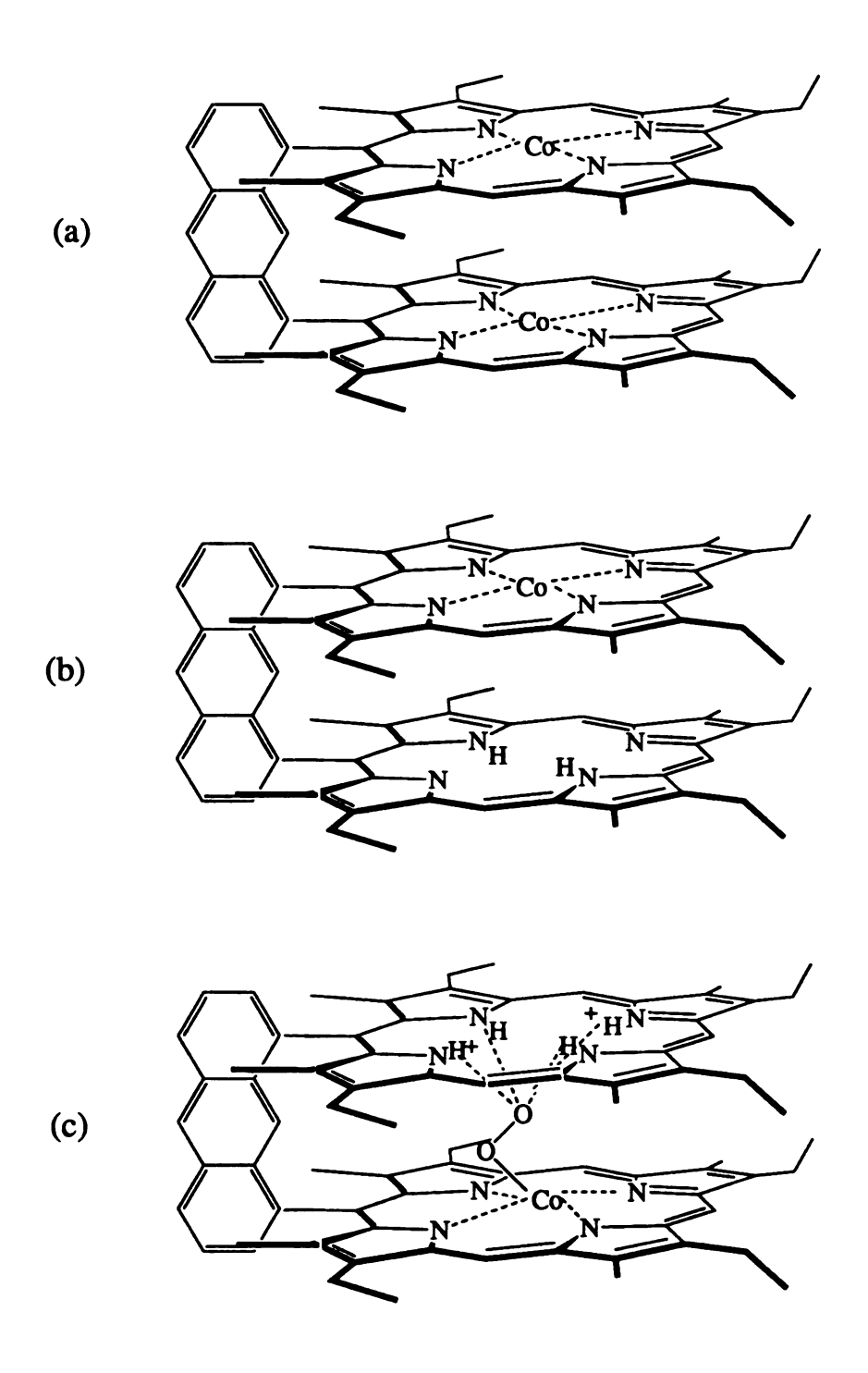


Figure I-9. Anthracene diporphyrins.

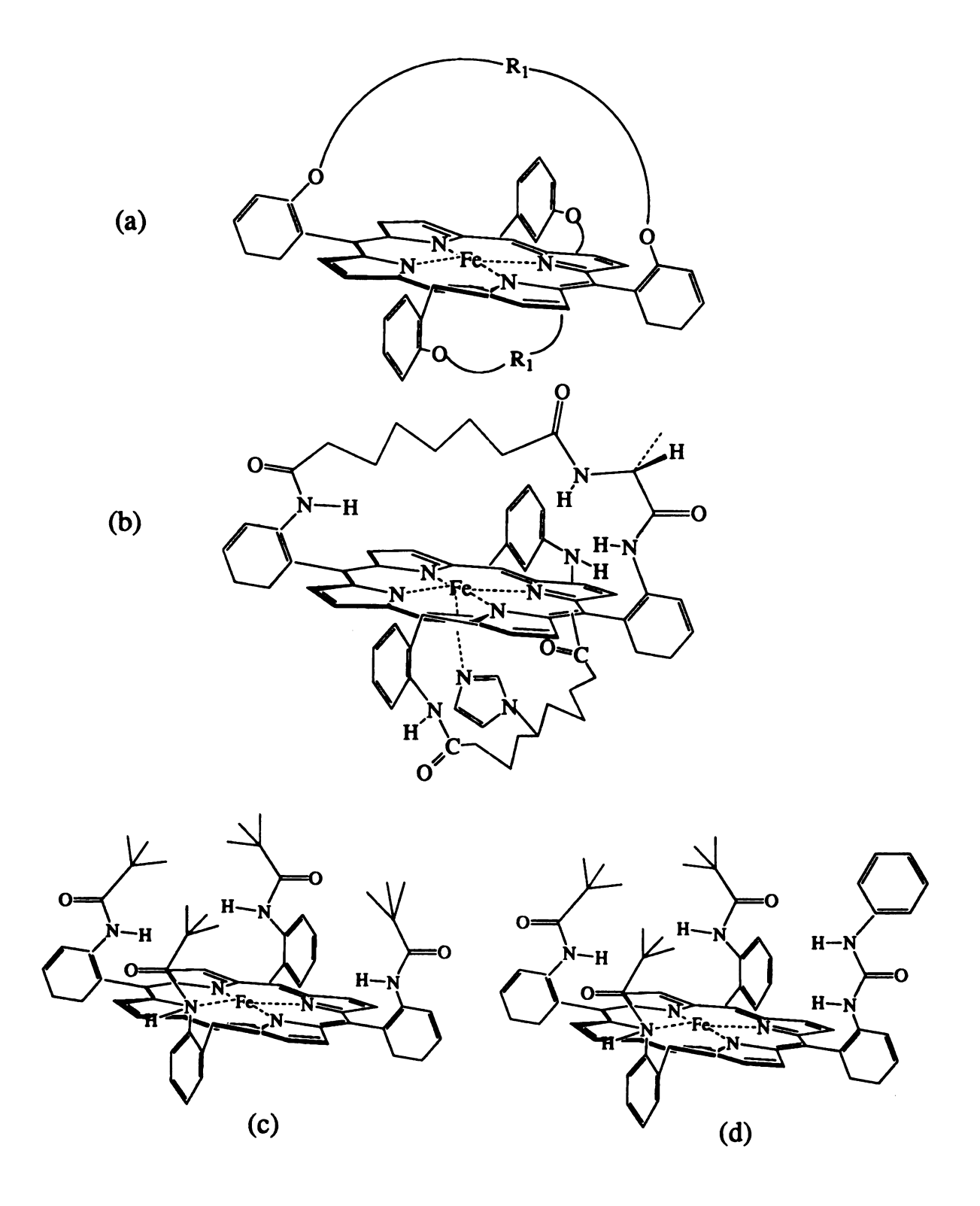
metallic center close to the heme active site is similar to that of a Lewis acid in helping the O-O bond cleavage. Therefore, H-bonding effect has been one focus of various studies of heme proteins and their model systems.

Synthetic models that address the H-bonding interactions first came from solvent effect.²⁰ The affinity of O₂ for cobalt Schiff base complexes increased in the presence of H-bonding solvents. Recently, synthetic models with intramolecular H-bonding ability have also emerged. Some of these models are shown in Figure I-10. In 'picket-fence' porphyrin²¹ the amide proton, located 4Å away from bound dioxygen, does not make direct H-bonding possible. This has been proven by ¹⁷O NMR studies.²² The first successful model is the 'basket-handle' porphyrin.²³ A nearly 10 fold increase in O₂ affinity was observed when an ether linkage was transferred into amide linked basket handle porphyrin. Evidence from ¹H and ¹⁷O NMR verified the interaction of the bound dioxygen with the secondary amide N-H.²² Even greater effects came from an "tailed" porphyrin model equipped with an alcohol or a secondary amide.²⁴ A substituted picket fence porphyrin synthesized by Reed²⁵ showed ca. 10-fold increase when one pivalamide substituent of picket-fence porphyrin is replaced by a phenylurea substituent.

In an effort to create an ideal environment for hydrogen bonding to occur, Chang and Kondylis²⁶ designed a series of U-shaped porphyrin models in which an intramolecular proton donor is juxtaposed to the terminal oxygen atom of the coordinated dioxygen. These models should provide a means of determining quantitatively the influence of H-bonding

FigureI-10. Some structures of porphyrin models for studies of H-bonding effects.

- a) basket handle porphyrin-through ether linkage;
- b) basket handle porphyrin-through amide linkage;
- c) picket-fence porphyein;
- d) substituted picket-fence porphyrin.



on the formation of dioxygen adducts. A series of Co^{II} 1-naphthyl porphyrins substituted with amido, carboxyl, and hydromethoxy at the 8-naphthyl position were prepared (Figure I-11). In the oxygen binding study of these compounds it was observed that the O₂ affinity increased by 1500 fold on going from the Co^{II} naphthalene porphyrin (11a) to the Co^{II} naphthoic acid porphyrin (11d). Kinetic measurements of oxygen binding to metal porphyrin complexes²⁷ have shown that functional groups capable of hydrogen bonding make a significant contribution to the stability of the oxygen-heme complexes by decreasing the dissociation rate of the bound ligand.

While all these models have clearly established the positive effect of enhancing the O₂ affinity, they have not permitted a closer look at how structural and steric perturbations made on the proton donor would influence the heme-substrate reactions. For example, from X-ray and neutron diffraction data it has been noted that the H-bonding between the distal histidine and Fe-O₂ in Mb and Hb is an oblique one. With the H-bond not coplanar with the Fe-O₂ moiety, the oblique interaction raised the possibility of H-bonding correlated with both O₁ and O₂ or only on O₁.

In an attempt to provide better understanding on the influence of H-bonding in O₂ activation, a series of novel model compounds, C-Clamp porphyrins have been designed and synthesized (Figure I-12). This C-clamp porphyrin has a carboxylic acid pointing towards the porphyrin center. This acid functional group combined with the metal ion of the porphyrin furnishes a ditopic binding site for O₂, CO, etc. As shown in Figure I-12, the acid functionality is linked to the porphyrin ring via two

O ₂ Affinity	(11a) R=H, 1 (11b) R=CH ₂ OH 10 (11c) R=CONH ₂ 70 (11d) R=COOH 7500	
R. Co. N.		H-O N-N-N-N-N-N-N-N-N-N-N-N-N-N-N-N-N-N-N

Figure I-11. Naphthalene porphyrin model compounds.

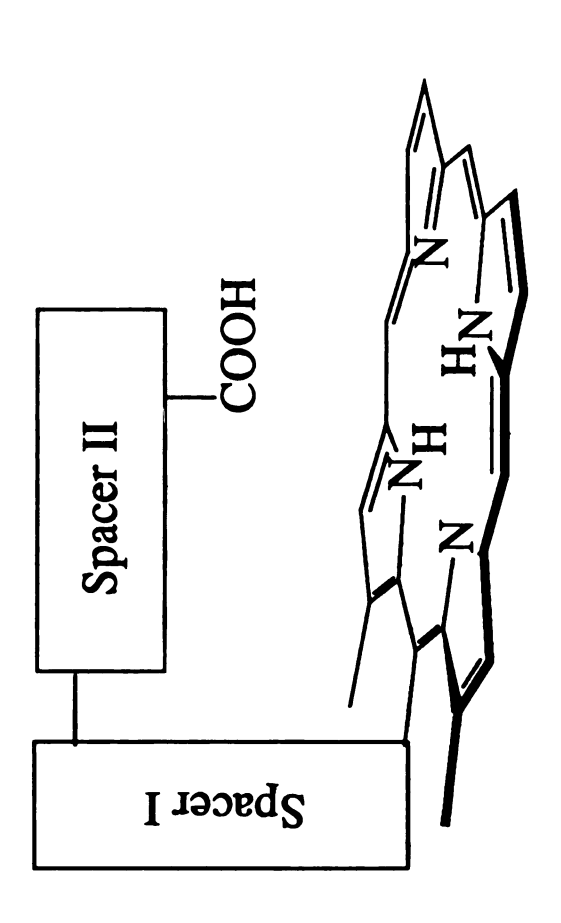


Figure I-12. Essential components of the C-clamp porphyrin.

perpendicular spacers. Spacer I is a rigid aromatic moiety attached to porphyrin meso-position and flanked by two methyl groups to limit its freedom of rotation. Spacer II is conveniently part of the Kemp's triacid whose utility as a convergent building block for molecular receptor has been well demonstrated by Rebek.²⁷ This combination of the Kemp's triacid and a naphthalene or anthracene connector thus provides a C-shaped porphyrin model with a relatively rigid acid hovering over the porphyrin. The structure should minimize the intramolecular attack on the porphyrin ring to avoid self-decomposition, thus allowing further studies on the reaction of H-bonded heme-O₂ species.

Avilés²⁸ has synthesized an anthracene Kemp's acid porphyrin (Figure I-13) and found that the O_2 affinity increase by 90 fold on going from the Co^{II} Kemp's ester porphyrin to the Kemp's acid porphyrin. She also observed that the O_2 affinity increased as the hydrogen-bonding ability of the model compound increased. O_2 affinity for the Co^{II} Kemp's acid model is 14 times better than the O_2 affinity for the alcohol.

The naphthoic acid porphyrin (NAP) still has better O_2 affinity ($P_{1/2}$ = 0.028) than the anthracene Kemp's acid porphyrin (AKAP) ($P_{1/2}$ = 2.4) at -42°C. This may be due to the larger than 4 Å distance between the Kemp's acid and the porphyrin ring in AKAP so that the carboxylic proton may not achieve an optimal interaction with the terminal oxygen of the Co- O_2 complex in order to stabilize it. The O_2 affinity for the naphthalene Kemp's isomer (Figure I-14) is approximately 2.5 times better than the O_2 affinity for the anthracene Kemp's acid. This is surprising since the carboxyl group of the anthracene Kemp's acid is expected to be

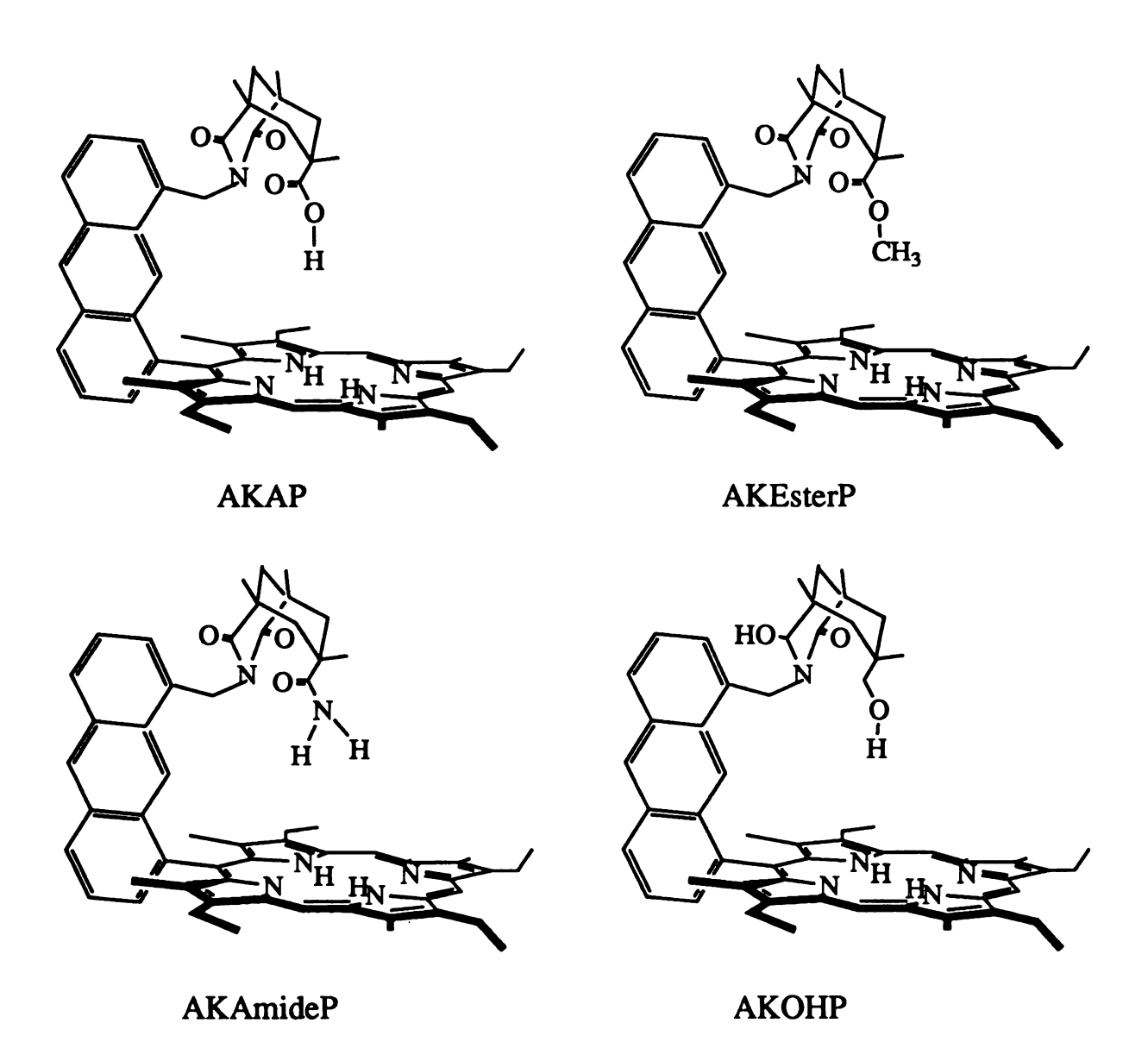


Figure I-13. Structure of series of anthracene Kemp's porphyrins.

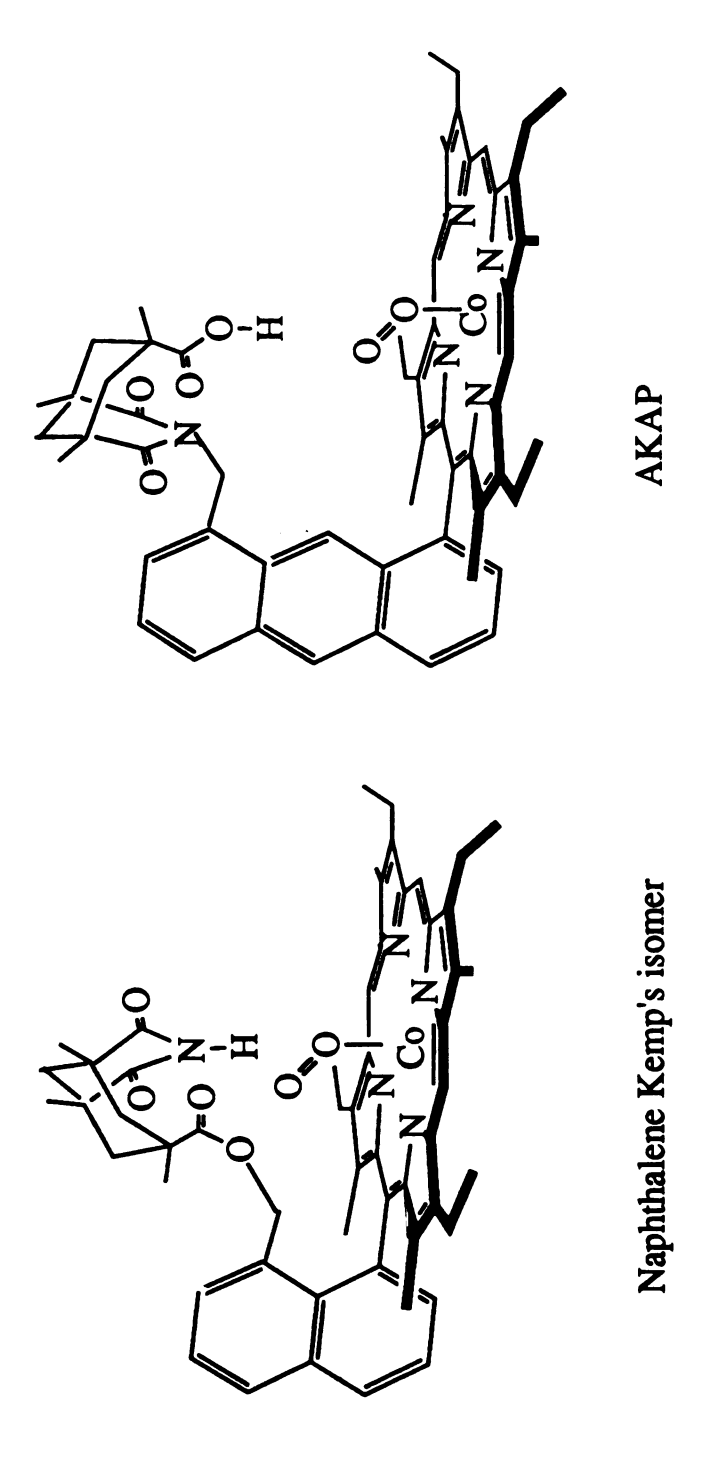


Figure I-14. Co-O₂ complexes of naphthalene Kemp's isomer and anthracene Kemp's acid porphyrin (AKAP).

a better proton donor (pka~4.6) than the imide of the naphthalene Kemp's isomer (pka~9.6). The reason for this may be that the imide proton in this model is positioned closer to the Co-O₂ center, thereby stabilizing it more effectively.

Based on this discussion, the carboxylic acid of the anthracene Kemp's acid porphyrin (AKAP) may be too far away from the bound O₂, and a naphthalene Kemp's acid porphyrin should be a better model. The synthesis of the naphthalene Kemp's acid porphyrin (NKAP) and derivatives are described in Chapter II.

The unique opportunity that the C-clamp porphyrins provided is that these ditopic receptors can accommodate substrates between the NH or metals of the porphyrin and the acid functional group. Guest-host interactions in free base and metallated C-clamp porphyrins is the topic of Chapter III. The recognition of O₂ and O₂ affinity studies will be discussed in Chapter IV. Also in this chapter, comparison between C-clamp porphyrins (NKAP and AKAP) and U-shaped porphyrin will be addressed.

One important intermediate in cytochrome c oxidase and cytochrome P-450 is the ferryl (iron oxo) species. It is still debatable whether H-bonding exists in these natural heme enzymes. Therefore, it is necessary to set up benchmark data on how much the H-bonding affects the vibrational frequency of Fe=O. Stable model compounds, vanadyl (vanadium oxo) porphyrins were used in this study and the result is discussed in Chapter V.

The carbonylated-ruthenium (RuCO) complexes of C-clamp porphyrins are in a 'trans' configuration, in which the CO is on the opposite site of the intramolecular carboxylic acid. In between this acid and the Ru-porphyrin, one solvent molecule, methanol, is trapped and serves as the sixth ligand to the metal. H-bonding from the acid proton affects this methanol trans ligand field and consequently shift the CO vibration. Chapter VI describes the result and X-ray structure of this study.

References

- 1. Perutz, M. F.; Fermi, G.; Luisi, B.; Shaanan, B.; Liddington, R. C. Acc. Chem. Res. 1987, 20, 309-321.
- 2. Babcock, G. T.; Wikström, M. Nature (London), 1992, 356, 301-309.
- Electron Transfer Reactions in Metalloproteins in 'Metal Ions in Biological Systems, Vol. 27, Sigel, H. and Sigel, A; Eds. Dekker, New York, 1991.
- 4. a) Ortiz de Montellano, P. R. Acc. Chem. Res. 1987, 20, 289-294.
 b) "Cytochrome P-450 Structure, Mechanism and Biochemistry".
 Ortiz de Montellano, P. R., Ed., Plenum Press, New York, 1986.
- 5. a) Gunter, M. J.; Turner, P. Coord. Chem. Rev. 1991, 108, 115-161.
 b) Dawson, J. H. Science, 1988, 240, 433-439.
- Jongeward, K. A.; Madge, D.; Taube, D. J.; Marsters, J. C.; Traylor,
 T. G.; Sharma, V. S. J. Am. Chem. Soc. 1988, 110, 380-387.
- 7. a) Shaanan, B. Nature (London) 1982, 296, 683-684.
 b) Condon, P. J.; Royer, W. E. J. Biol. Chem. 1994, 269, 25259-25267.
- Philips, S E. V.; Schoenborn, B. P. Nature (London) 1981, 292, 81-82.
- 9. Suslick, K. S.; Reinert, T. J. J. Chem. Edu. 1985, 62, 974-983.

- Beinert, H.; Griffiths, D. E.; Wharton, D. C.; Sands, R. H. J. Biol. Chem. 1962, 237, 2337-2346.
- a). Yoshikawa, S.; O'Keeffe, D. H.; Caughey, W. S., J. Biol. Chem.,
 1985, 260, 3518-3528.
 - b) Yoshikawa, S.; Caughey, W. S. J. Biol. Chem. 1990, 265, 7945-7958.
- Poulos, T. L.; Freer, S. T.; Alden, R. A.; Edwards, S. L.; Skogland,
 U.; Takio, K.; Eriksson, B.; Xuong, N.; Yonetani, T.; Kraut, J. J. Biol.
 Chem. 1980, 255, 575-580.
- 13. Poulos, T. L.; Kraut, J. J. Biol. Chem. 1980, 255, 8199-8205.
- 14. Poulos, T. L. Adv. Inorg. Biochem. 1987, 7, 1-36.
- 15. Harris, D. L.; Loew, G. H. J. Am. Chem. Soc. 1994, 116, 11671-11674.
- a) Collman, J. P.; Deniserich, P.; Konai, Y.; Marrocco, M.; Koval, C.;
 Anson, F. C. J. Am. Chem. Soc. 1980, 102, 6027-6036.
 - b) Durand, R. R.; Bencosme, C. S.; Collman, J. P.; Anson, F. C. J. Am. Chem. Soc. 1983, 105, 2710-2718.
 - (c) Collman, J. P. J. Electroanal. Chem. 1979, 101, 117-122.
- 17. Liu, H.; Abdalmuhdi, I.; Chang, C. K.; Anson, F. C. J. Phys. Chem. 1985, 89, 665-670.
- 18. Momenteau, M.; Lavalette, D. J. Chem. Soc. Chem. Commun. 1982, 341-343.

- 19. Young, R.; Chang, C. K. J. Am. Chem. Soc., 1985,107, 898-909.
- 20. Drago, R. S.; Cannady, P. J.; Leislie, K. A. J. Am. Chem. Soc. 1980, 102, 6014-6019.
- Jameson, G. B.; Molinaro, F. S.; Ibers, J. A.; Collman, J. P.; Brauman,
 J. I.; Rose, E.; Suslick, K. S. J. Am. Chem. Soc. 1980, 102, 3224-3237.
- 22. Gerothanassis, I. P.; Momenteau, M.; Loock, B. J. Am. Chem. Soc. 1989, 111, 7006-7012.
- 23. Mispelter, J.; Momenteau, M.; Lavalette, D.; Lhoste, J.-M. J. Am. Chem. Soc. 1983, 105, 5165-5166.
- 24. Chang, C. K.; Ward, B.; Young, R.; Kondylis, M. P. J. Macromol. Sci., Chem. 1988, A25, 1307-1326.
- 25. Wuenschell, G. E.; Tetreau, C.; Lavalette, D.; Reed, C. A. J. Am. Chem. Soc. 1992, 114, 3346-3355.
- 26. Chang, C. K.; Kondylis, M. P., J. Chem. Soc. Chem. Commun., 1986, 316-318.
- 27. Rebek, J., Jr. Science, 1987, 235, 1478-1484.
- 28. Aviles, G. M., "Interaction of Intramolecular Carboxylic Acid with Heme-O₂ Complex", Ph.D. Dissertation, Michigan State University, 1991.

CHAPTER II

Synthesis and Characterization of C-Clamp Porphyrin

A. Introduction

As already mentioned in chapter I, distal hydrogen bonding has been considered as one of the important factors affecting reversible dioxygen binding to several O₂ binding heme proteins as well as to cobalt(II) and iron(II) porphyrin models. To design and synthesize model compound that mimic this effect has been a research goal in our group. The naphthoic acid porphyrin (NAP) system, a model capable of intramolecular H-bonding, has displayed high O₂ affinity. However, the curious decomposition of its Co(II) complex³ made the NAP a better model for the studies of heme degradation. Converting this NAP system to the Kemp's triacid porphyrin switches the acid group from the 8-position of the naphthalene ring an overhanging positionand therefore prevent the ring degradation (Figures I-11 and I-12). Additionally, with an acid proton hanging down from a vertical position instead of the

horizontal hydrogen bond donor as in the NAP system, would allow the study of orientation effects about hydrogen bonding.

Our target compound is naphthalene Kemp's acid porphyrin (NKAP) as shown in Figure II-1. Its derivatives, naphthalene Kemp's ester porphyrin (NKEsterP) and naphthalene Kemp's amide porphyrin (NKAmideP), were synthesized as well for comparison purposes.

B. Synthesis

The synthetic strategy is to link the naphthalene (spacer I) with porphyrin followed by linking the Kemp's acid (spacer II) to the naphthalene (Figure I-12). There are two proposed synthetic routes (Figure II-2) to the naphthalene linked porphyrin. One is through a tetrapyrrole pathway, and another is to follow the previous procedure to make a dipyrrole, then by MacDonald 2+2 condensation² to generate NAP. After functional group transformations, a coupling reaction in the last step produces the NKAP.

1. Tetrapyrrole Pathway

This approach is illustrated by the synthesis of a related 2-benzoic acid porphyrin. Starting with a 2-carboxybenzaldehyde and a a,c-biladiene dibromide, the porphyrin benzoate was synthesized in one step (Figure II-3). Since methanol was used as the reaction solvent, the ester was produced as a consequence. The ester was hydrolyzed into acid porphyrin by refluxing with KOH in pyridine for three days.

This implied that if we started with a 1,8-naphthaldehydic acid, the product from coupling with a tetrapyrrole would be a naphthalene ester

C-clamp porphyrin: NKAP

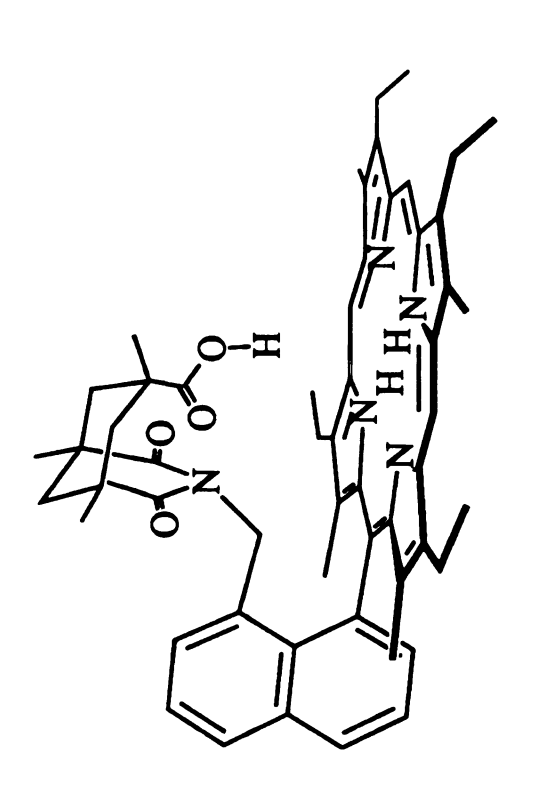


Figure II-1. Target compound NKAP.

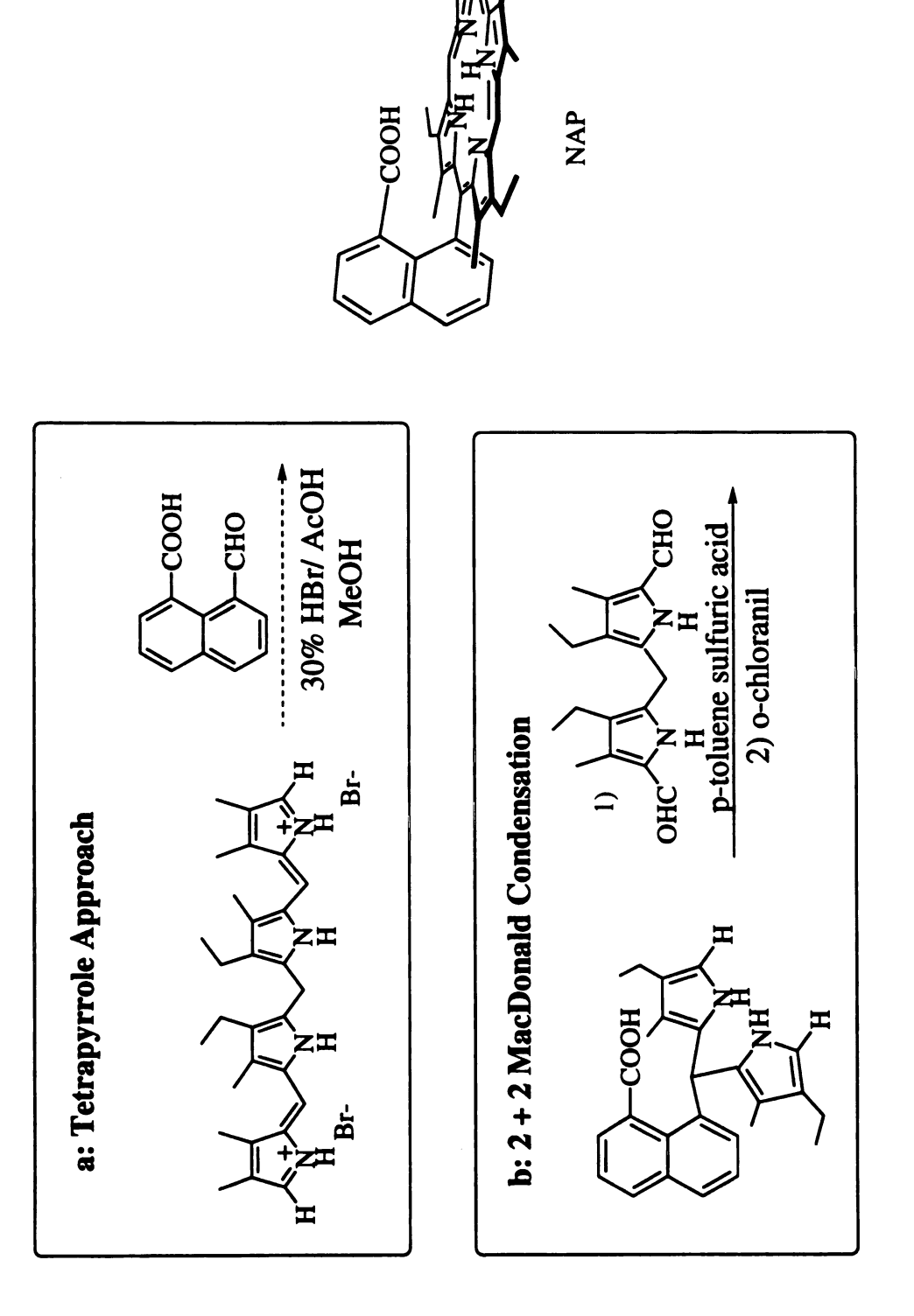
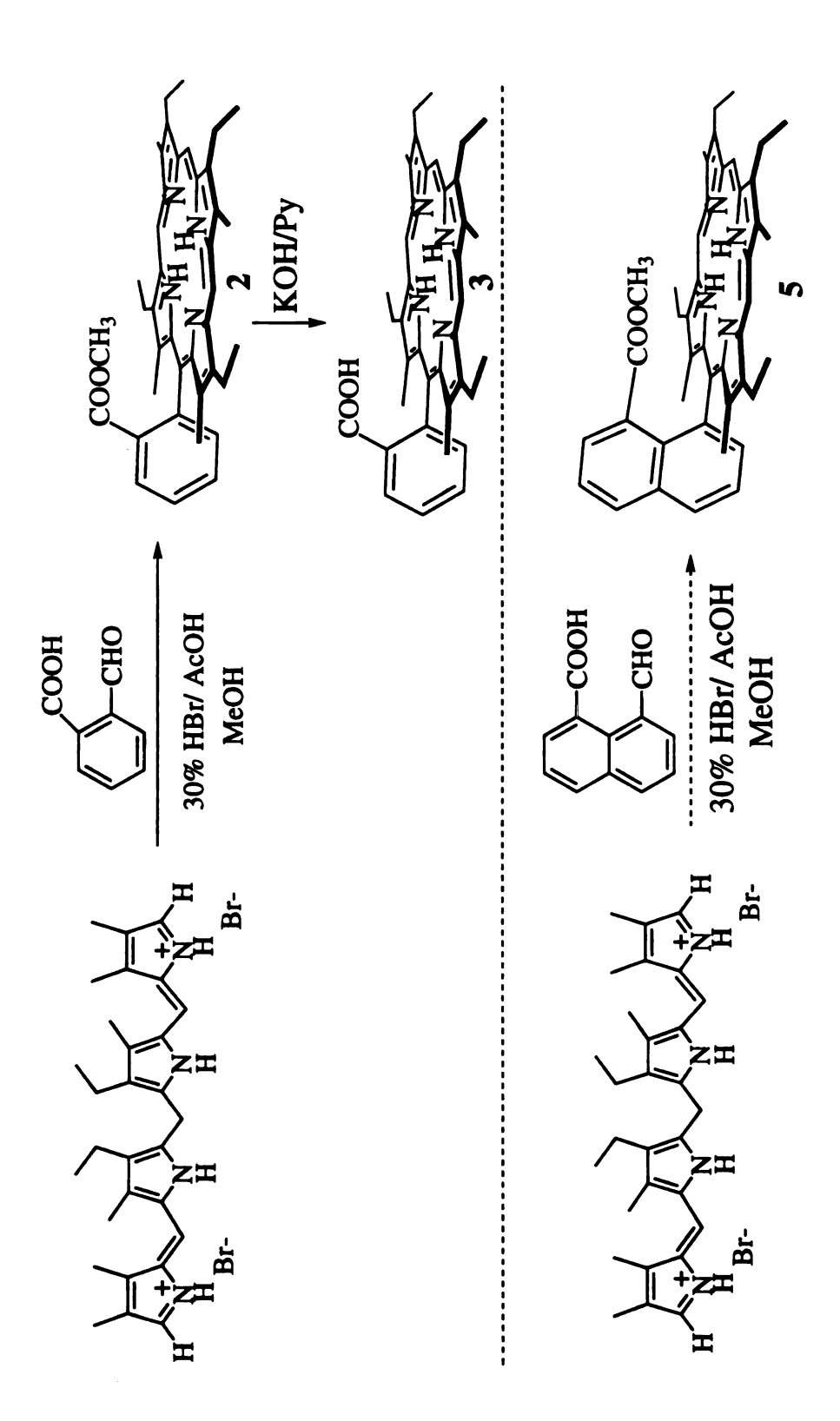


Figure II-2. Two synthetic approaches to naphthalene linked porphyrin.



proposed synthetic pathway to naphthalene ester porphyrin. Figure II-3. Synthetic route to 2-carboxybenzyl porphyrin and

porphyrin (Figure II-3). However, contrary to what we anticipated, the product was not the desired naphthalene ester porphyrin. We obtained a corrole instead (Figure II-4). The evidence came from the strong fluorescence and visible absorptions of the compound at 534, 547 and 592 nm, characteristic absorption of corrole (Figure II-5). Since most of the 8-formyl-1-naphthoic acid might exist in its lactol form as shown in Figure II-6 instead of the free aldehyde form, the acid group was converted into an ester, and the reaction with tetrapyrrole was tried one more time. It still gave corrole as the product indicating that the lactone was not destroyed by converting to ester.

For a typical synthesis of corrole, basic reaction conditions are used.⁴ Our reaction condition was acidic (acetic acid) and seemed to offer reasonably high yield. A control experiment with the a,c-biladiene in 30% HBr/HOAc provided corrin in similar yield.

Even though we were excited about this discovery, we still need to make the target compound NKAP. Therefore, the 2+2 pathway was followed.

2. Dipyrrole Pathway by MacDonald Condensation

The synthesis of the naphthalene Kemp's acid porphyrin (NKAP) is outlined in Figure II-7 and II-9. The starting acid porphyrin NAP (Figure II-2)¹ was converted into naphthalene ester porphyrin by diazomethane. Since direct reduction sometimes gave aluminum porphyrin, the porphyrin ring was protected by transforming to its zinc complex. The ester porphyrin was then reduced with LiAlH₄ in dry THF.

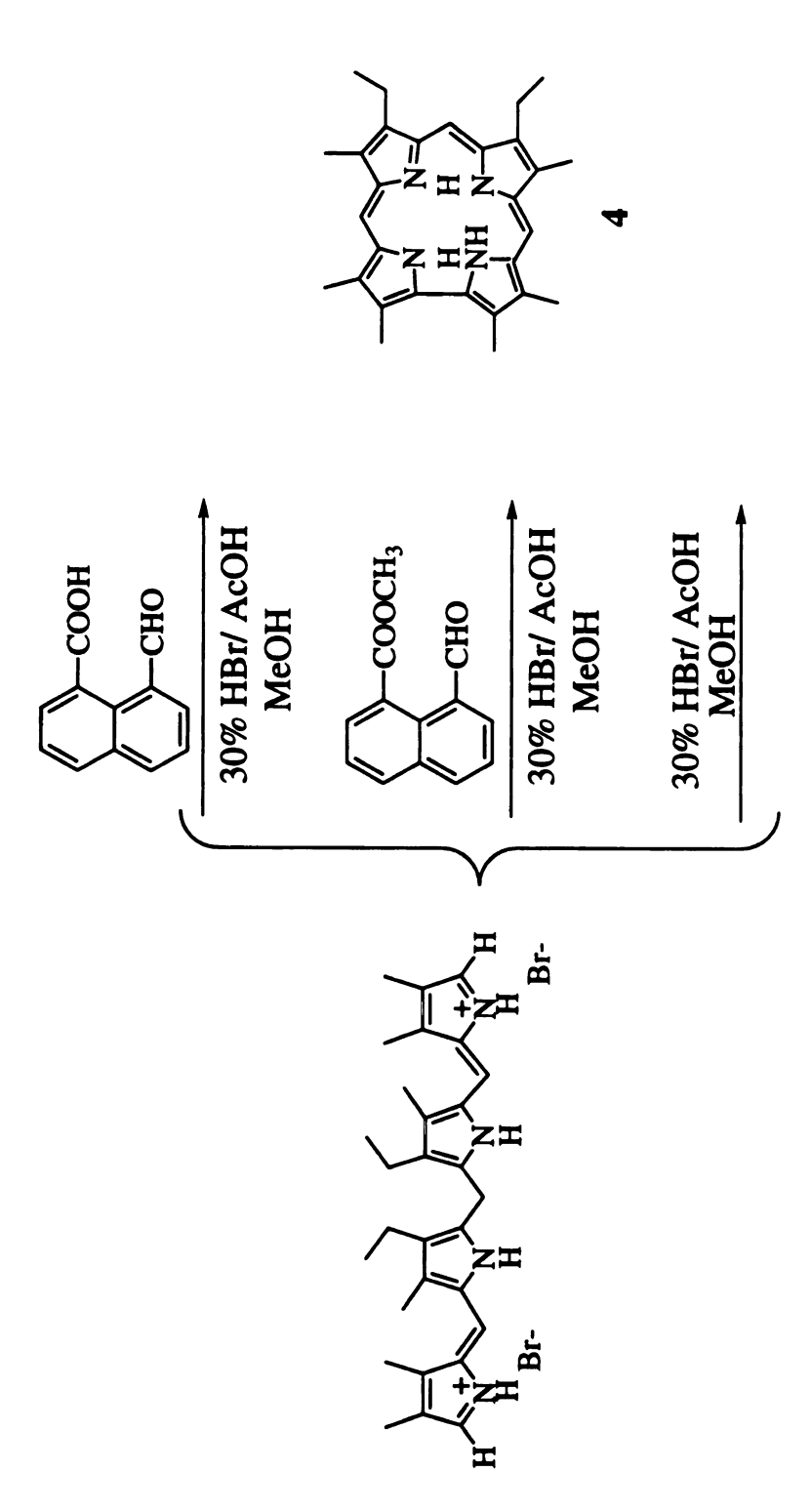
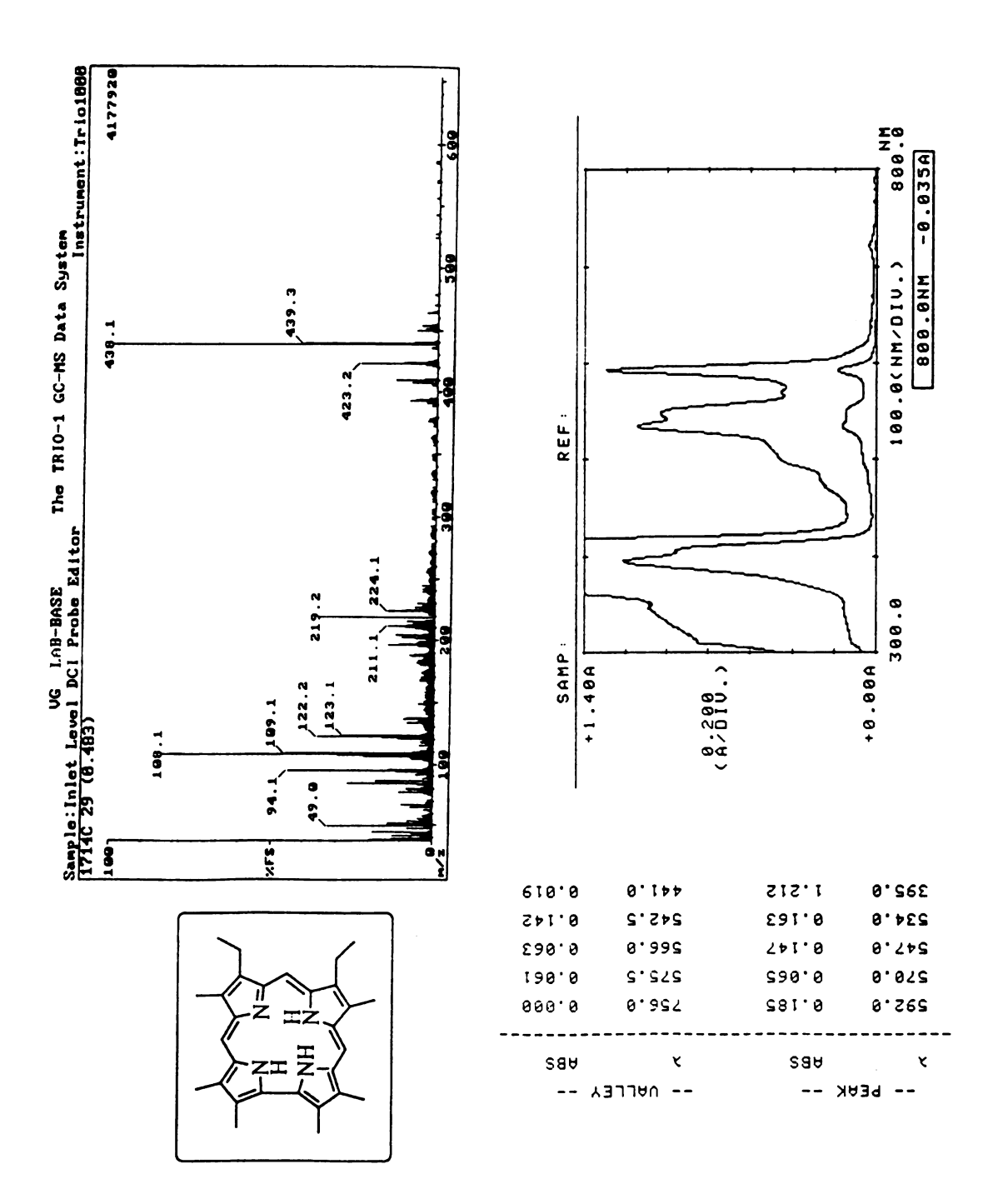


Figure II-4. Synthesis of corrole, failed attempts to make porphyrin.

Figure II-5. MS and UV-vis spectra of corrole.



(a)
$$CCOOH$$
 $CCHO$ CC

Figure II-6. (a) The equilibrium between 8-formal naphthoic acid and its lactone form. (b) The equilibrium between 8-formal naphthoic ester and its lactone form.

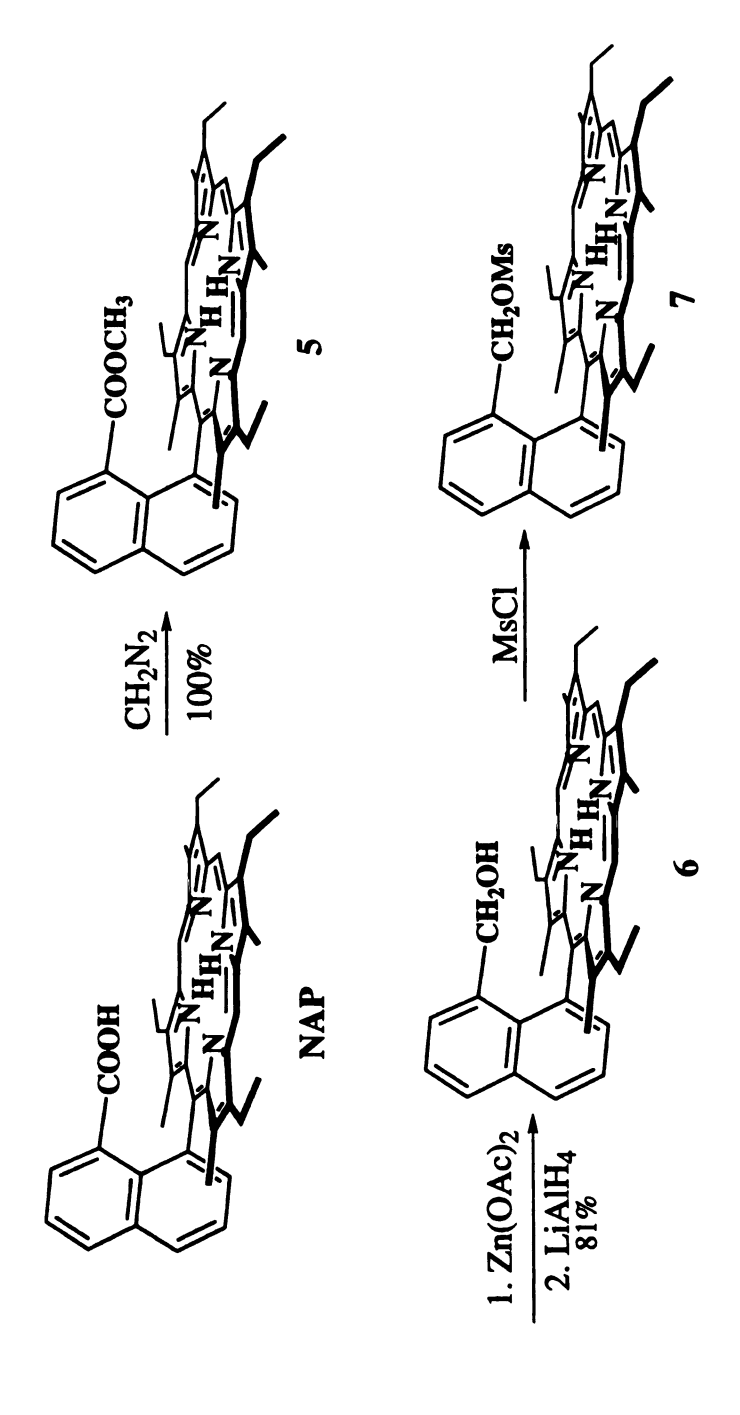


Figure II-7. Synthesis of naphthalene mesylate porphyrin

The resulted alcohol was treated with excess (10 equiv.) methanesulfonyl chloride without heating to minimize decomposition. The excess reagent was removed by vacuum pump.

Direct coupling of the mesylate porphyrin with potassium imide-carboxylate salt has been shown to give Kemp's isomer porphyrin (Figure II-8).⁵ In order to synthesize the target compound, an alternative pathway was employed. Since Rebek's has reported the condensation of various amines with the acid chloride anhydride,⁶ the mesylate was converted into an amine before coupling. The mesylate reacted with excess sodium azide in DMF to give the azido-porphyrin in 99% yield. IR spectrum of this porphyrin showed a strong azide absorption band at 2096 cm⁻¹. After reduction of the zinc azido-porphyrin with LiAlH₄, the amino porphyrin was coupled with the acid chloride-anhydride to generate NKAP (Figure II-9). The overall yield was 60% for NKAP. ¹H NMR of NKAP showed that the capping cyclohexyl protons have substantial upfield shift (Figure II-10). The gem-methyl to the CO₂H was found at -0.26 ppm in NKAP compared to 1.40 ppm in the starting Kemp's acid chloride-anhydride, which is obviously caused by the diamagnetic ring current.

Figure II-11 shows the reactions in synthesizing derivatives of NKAP. The naphthalene Kemp's ester porphyrin (NKEsterP) was obtained in quantitative yield from the reaction of NKAP with diazomethane. In making naphthalene Kemp's amide porphyrin (NKAmideP), NKAP was exposed to oxalyl chloride followed by ammonia. These NKEsterP and NKAmideP were characterized by proton NMR and Mass spectra and used for the purpose of property comparison.

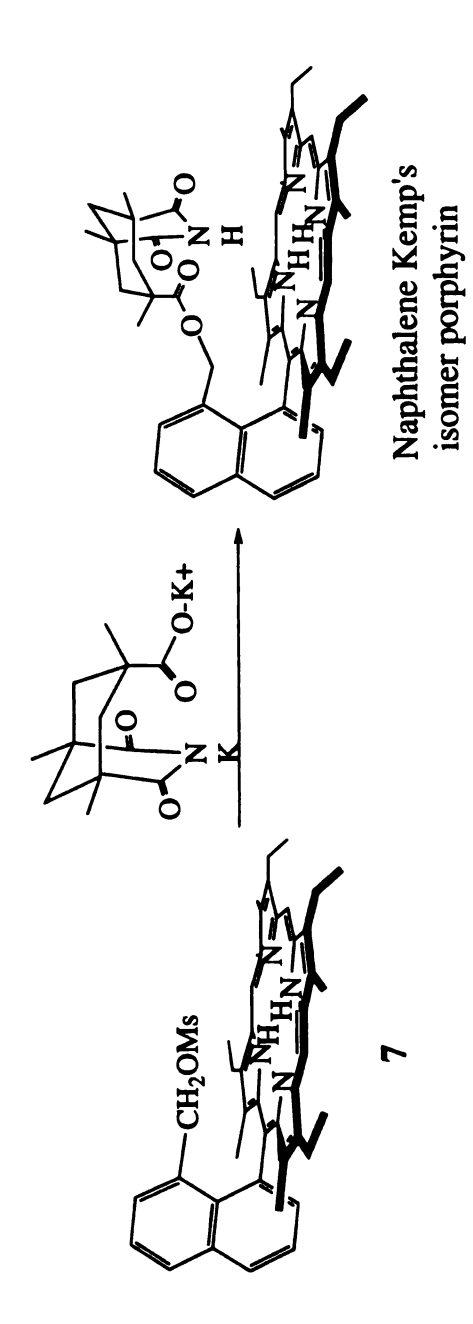


Figure II-8. Naphthalene Kemp's isomer porphyrin.

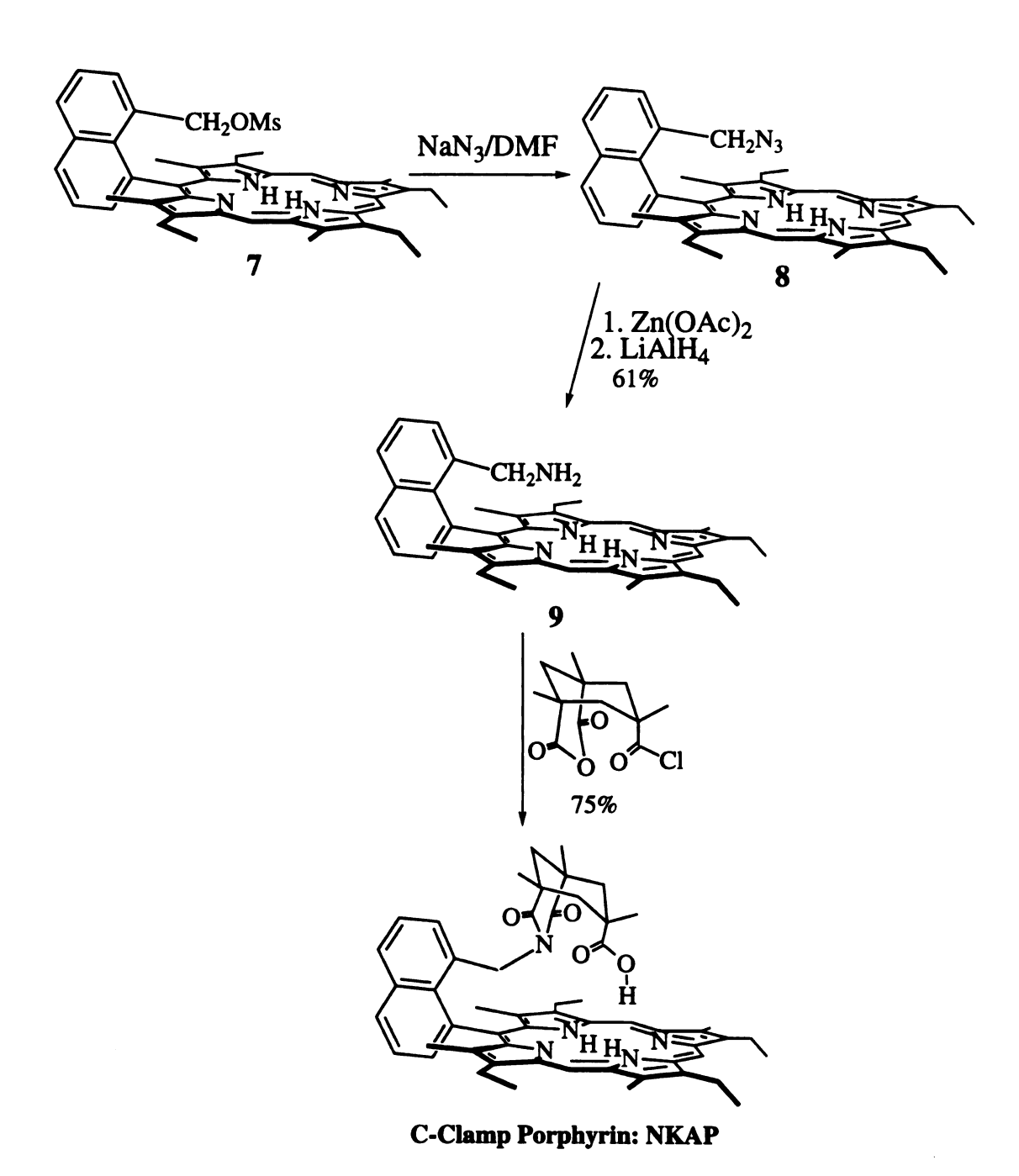
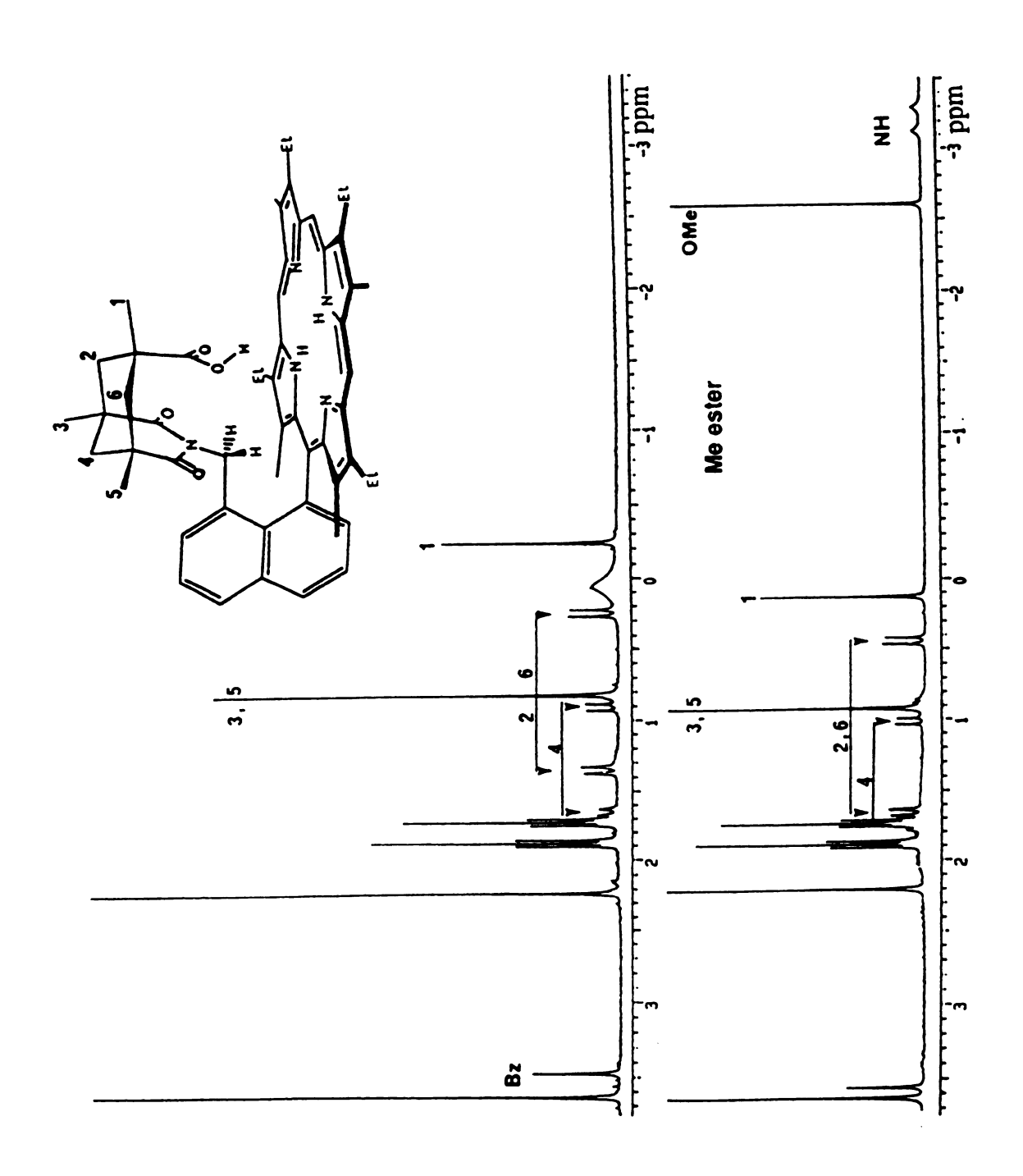


Figure II-9. Synthesis of NKAP.

Figure II-10. ¹H NMR of NKAP and NKEsterP.



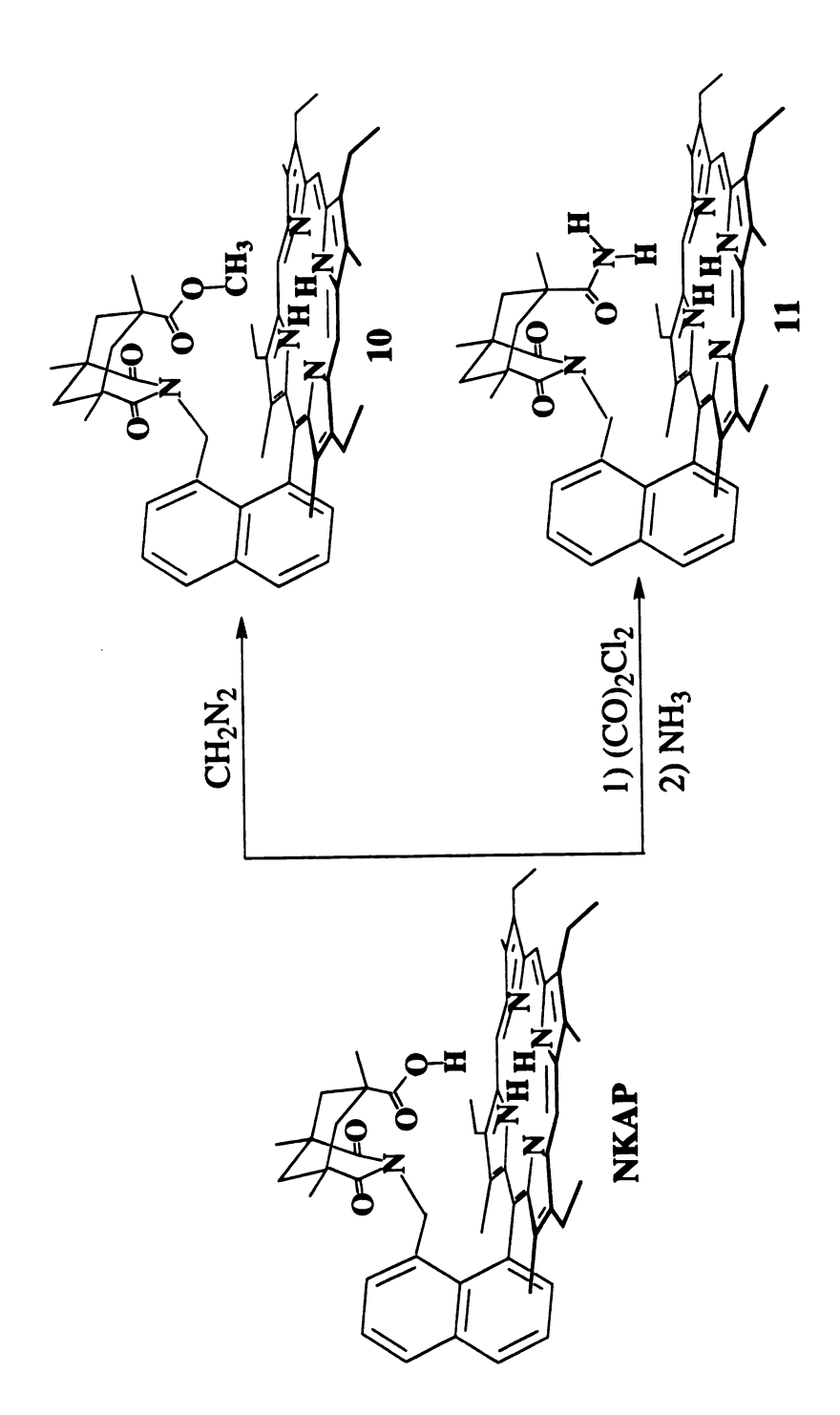
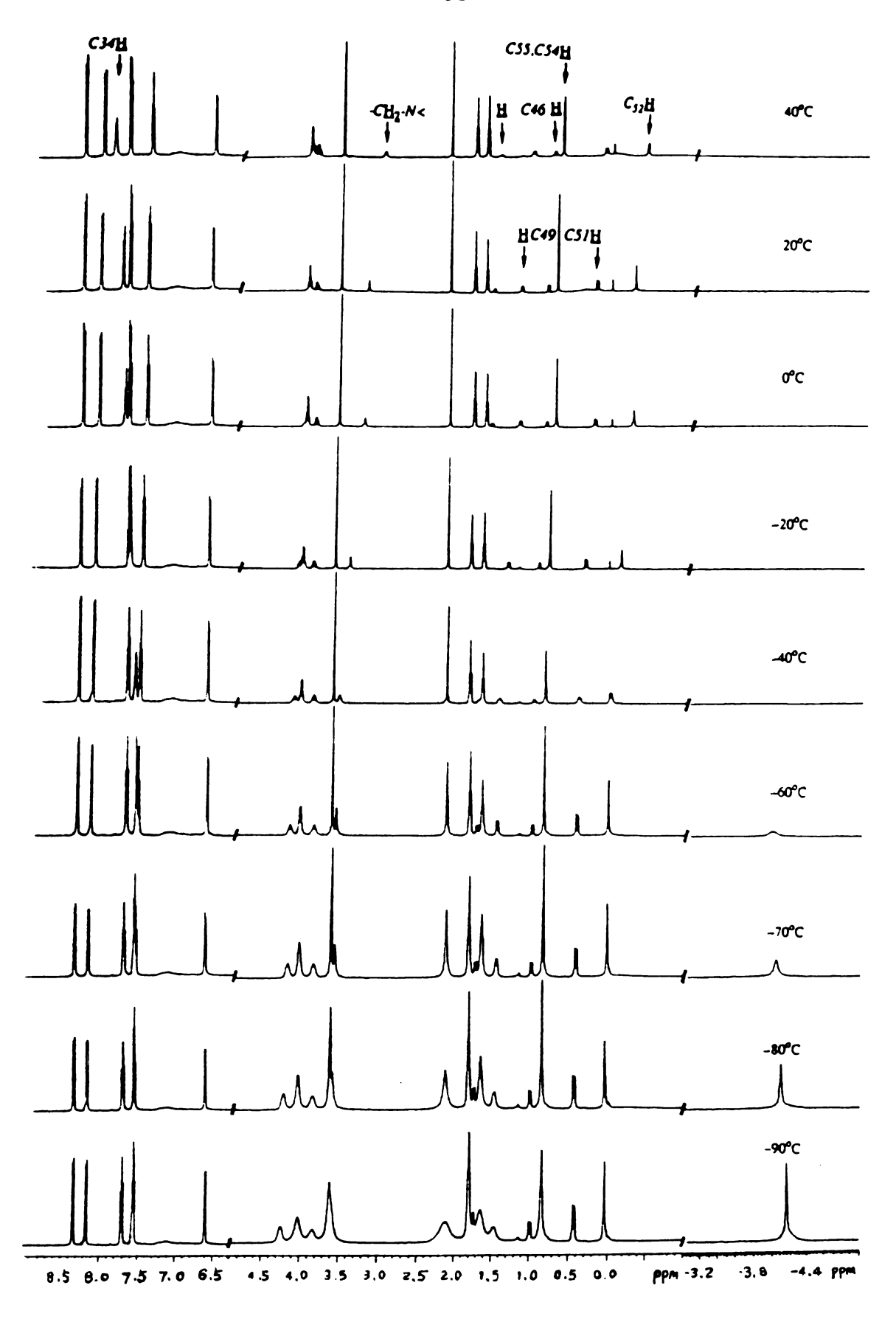


Figure II-11. Synthesis of NKEsterP and NKAmideP.

C. Variant Temperature-NMR

In the ¹H NMR studies of NKAP, the typical NH proton signals in the -3 to -4 ppm region were not detected at room temperature, instead a broad peak around 0 ppm was observed (Figure II-10). This phenomenon suggests proton exchange among the NH protons of the porphyrin and the proton of the carboxylate acid. When the acid group was methylated by CH₂N₂, the NH protons emerged at -3.2 ppm as a doublet. Similar behavior for AKAP was observed. In order to probe the exchange, the variant temperature NMR technique was employed to monitor the dynamics of the proton exchange at 500 MHz in these two systems. The -90 to 40 °C range accessible in CD₂Cl₂ was sufficient to allow the observation of a sharp peak around -4 ppm at -90 °C, which gradually broadened out. When temperature reached 20 °C, a new signal centered at 0 ppm appeared (Figure II-12). Over the entire temperature range (-90 to 40 °C), the signal of the carboxylic acid proton was not obvious, possibly due to overlapping with other signals, and this acid proton was identified later at 3.6 ppm by saturation spin transfer techniques⁸ under conditions of slow exchange. The coalescence temperature detected for NKAP was -10 °C and 15 °C for AKAP. This agrees well with the expectation that in NKAP the acid proton is closer to the porphyrin center and less energy is needed for the coalescence to occur.

Figure II-12. Variant Temperature NMR of NKAP.



D. Experimental

Materials and measurements. Reagents and solvents for synthesis were used as received unless otherwise stated. CH₂Cl₂ and DMF were distilled from CaH₂. THF and toluene were freshly distilled from LiAlH₄. UV-visible spectra were measured on a Cary 219 or a Shimadzu 160 spectrophotometer. ¹H NMR spectra were recorded on Varian Gemini-300 in "100%" CDCl₃ (minimum 99.8 atom % D, Cambridge Isotope Laboratories) with the residual CHCl₃ as the internal standard set at 7.24 ppm. Variant temperature NMR measurements were conducted on Varian 500 MHz spectrometer. Mass spectra were measured from a benchtop VG Trio-1 mass spectrometer or FAB (fast atom bombardment) mass spectra on a JEOL HX-110 HF double focusing spectrometer in the positive ion detection mode. Infrared spectra were obtained from sample film on a NaCl plate and recorded on a Nicolet IR/42 spectrometer.

5-(2-Methoxycarbonylphenyl)-13,17-diethyl-2,3,7,8,12,18-hexamethylporphyrin 2

1,19-Dideoxy-8,12-diethyl-2,3,7,13,17,18-hexamethyl-biladiene-a,c-dihydrobromide (100 mg, 0.166 mmol) and 2-carboxybenzaldehyde (97%, 257 mg, 1.66 mmol) were suspended in 15 ml methanol. To this solution, 4 drops of 30% HBr in acetic acid was added. After being refluxed in the dark for 24 hours under argon, the reaction mixture was cooled and treated with saturated sodium bicarbonate solution. The product was washed with water and extracted by methylene chloride. Chromatography over silica gel using methylene chloride as the eluant gave 34.5 mg of 2 (35.6%). ¹H NMR (300 MHz, CDCl₃) δ ppm -3.19 (d, 2H, NH), 1.84 (6H;

t, Et), 2.38 (6H, s, Me), 2.72 (3H, s, OMe), 3.50 (6H, s, Me), 3.62 (6H, s, Me), 4.05 (4H, q, Et), 9.92 (1H, s, meso), 10.12 (2H, s, meso), phenyl: 7.83 (2H, m), 7.96 (1H, d), 8.37 (1H, d); MS, m/z, 584 (M, 53%); UV-vis λ_{max} nm (rel intens) 404 nm (1.00), 502 (0.08), 536 (0.04), 572 (0.04), 624 (0.01).

5-(2-Carboxyphenyl)-13,17-diethyl-2,3,7,8,12,18-hexamethylporphyrin 3

A KOH solution (4 g in 2 ml H₂O) was added to a pyridine solution of 2 (20 mg, 0.034 mmol). The mixture was heated to reflux under argon for 3 days. The reaction was monitored by TLC which showed a lower R_f upon the product formation. The hot solution was then poured into ice water and washed with brine. The product was extracted with CH₂Cl₂ and purified by TLC plate to provide 19 mg (97%) of 3. ¹H NMR (300 MHz, CDCl₃) δ ppm 0.65 (br, 3H, NH and COOH), 1.69 (6H, t, Et), 2.24 (6H, s. Me), 3.29 (6H, s, Me), 3.45 (6H, s, Me), 3.88 (4H, q, Et), 9.82 (1H, s, meso), 10.02 (2H, s, meso), phenyl: 7.67 (1H, d), 7.75 (2H, m), 8.21 (1H, d); MS, m/z, 570 (M, 81%); UV-vis λ_{max} nm (rel intens) 404 nm (1.00), 503 (0.07), 537 (0.04), 571 (0.04), 622 (0.01).

2,3,7,13,17,18-hexamethyl-8,12-diethylcorrole 4

1,19-Dideoxy-8,12-diethyl-2,3,7,13,17,18-hexamethyl-biladiene-a,c-dihydrobromide (100 mg, 0.166 mmol) and 1,8-naphthaldehydic acid (365 mg, 1.66 mmol) were suspended in 15 ml methanol. To this solution, 4 drops of 30% HBr in acetic acid was added. After being refluxed in the dark for 24 hours under argon, the reaction mixture was cooled and treated with saturated sodium bicarbonate solution. The product was

washed with water and extracted by methylene chloride. Chromatography on a silica gel column using methylene chloride as the eluant gave 30 mg of corrole 4 (41%). Under the same reaction condition, using methyl 8-formyl-1-naphthoate as starting material gave the same product.

1,19-Dideoxy-8,12-diethyl-2,3,7,13,17,18-hexamethyl-biladiene-a,c-dihydrobromide (100 mg, 0.166 mmol) was dissolved in 15 ml methanol. To this solution, 4 drops of 30% HBr in acetic acid was added. After being refluxed in the dark for 24 hours under argon, the reaction mixture was cooled and treated with saturated sodium bicarbonate solution. The product was washed with water and extracted by methylene chloride. Chromatography over silica gel using methylene chloride as the eluant gave 30 mg corrole 4 (41%). ¹H NMR (300 MHz, CDCl₃) δ ppm 1.74 (t, 6H, Et), 3.31 (s, 6H, Me), 3.40 (s, 6H, Me), 3.48 (s, 6H, Me), 3.87 (q, 4H, Et), 9.18 (s, 1H, meso), 9.27 (s, 2H, meso); MS, m/z, 438 (M, 100%); UV-vis λ_{max} nm (rel intens) 395 nm (1.00), 534 (0.13), 547 (0.12), 592 (0.15).

5-(8-Methoxycarbonyl-1-naphthyl)-2,8,13,17-tetraethyl-3,7,12,18-tetramethylporphyrin 5

5-(8-Hydroxycarbonyl-1-naphthyl)-2,8,13,17-tetraethyl-3,7,12,18-tetramethyl porphyrin (NAP) (1.09 g, 1.65 mmol) was dissolved in 200 ml THF. To this solution, 10 equivalents of freshly prepared diazomethane ether solution was added and stirred at room temperature for 30 minutes. 5% HOAc (40 ml) was added slowly to quench the excess diazomethane. The THF was removed and the residue was redissolved in methylene chloride, washed with saturated NaHCO₃ solution and water, dried over anhydrous Na₂SO₄. Purification by column chromatography over silica

gel with methylene chloride as eluant gave purple crystals in quantitative yield of 5: 1 H NMR (300 MHz, CDCl₃) δ ppm -3.10 (2H, d, NH), 0.07 (3H, OMe), 1.71 (6H; t, Et), 1.88 (6H, t Et), 2.13 (6H, s, Me), 3.65 (6H, s, Me), 3.94 (4H, q, Et), 4.08 (4H, q, Et), 9.97 (1H, s, meso), 10.17 (2H, s, meso), naphthyl: 7.61 (1H, s), 7.63 (1H, t), 7.78 (1H, t), 8.00 (1H, d), 8.16 (1H, t); 8.34 (1H, d); MS, m/z 662 (M, 100%); UV-vis λ_{max} nm (rel intens) 407nm (1.00), 505 (0.08), 538 (0.05), 573 (0.04), 627 (0.02).

5-[8-(Hydroxymethyl)-1-naphthyl]-2,8,13,17-tetraethyl-3,7,12,18-tetramethylporphyrin 6.

To 5-(8-methoxycarbonyl-1-naphthyl)-2,8,13,17-tetraethyl-3,7,12,18-tetramethylporphyrin 5 (2.1 g, 3.17 mmol) dissolved in methylene chloride (400 ml) was added a saturated methanol solution of zinc acetate containing sodium acetate. The mixture was heated to reflux for 10 minutes before being washed with water (50 ml), dried over Na₂SO₄ and evaporated to dryness to give the zinc porphyrin. To this material dissolved in freshly distilled THF (300 ml), a suspension of LiAlH₄ (0.5 g) in THF was added slowly. The reaction solution was stirred at room temperature for another hour. Completion of the reaction was monitored on TLC by the disappearance of the fast moving starting material. After the reduction was complete, the mixture was quenched by addition of ice water and the product was isolated by extraction with CH₂Cl₂ from water. The crude product was purified by column chromatography over silica gel using 2% MeOH/CH₂Cl₂. The purified zinc porphyrin was redissolved in methylene chloride (200 ml), and demetalated by washing with 10% HCl (200 ml). The organic solution was then washed with saturated NaHCO₃, water and dried over anhydrous

Na₂SO₄. Evaporation afforded 1.63 g (81%) purple crystal of 6. ¹H NMR (300 MHz, CDCl₃) δ ppm -3.09 (2H, d, NH), 0.20 (1H, t, OH), 1.71 (6H; t, Et), 1.88 (6H, t Et), 2.13 (6H, s, Me), 3.08 (2H, d, CH₂O₋), 3.65 (6H, s, Me), 3.96 (4H, m, Et), 4.08 (4H, q, Et), 9.97 (1H, s, meso), 10.17 (2H, s, meso), naphthyl: 7.61 (1H, s), 7.63 (1H, d), 7.78 (1H, t), 8.01 (1H, d); 8.17 (1H, t), 8.35 (1H, d); MS, m/e (relative intensity) 634 (M⁺, 86.89); UV-vis λ_{max} nm (ϵ_{M}) 625 (2100), 572 (6400), 538 (6500), 503 (15000), 405 (190000).

5-[8-(Methanesulfonylmethyl)-1-naphthyl]-2,8,13,17-tetraethyl-3,7,12,18-tetramethylporphyrin 7.

The above alcohol 6 (100 mg, 0.16 mmol) was dissolved in 5 ml dry methylene chloride with 3 drops of trimethylamine. To this mixture stirred under argon in an ice bath, methanesulfonyl chloride (2 ml) was slowly added. The system was continuously stirred for 14 hours at room temperature. The solvent and excess methanesulfonyl chloride was pumped away with a vacuum pump (room temperature until almost dry, then at 60°C for 2 hours). This product was used for the next step without further purification.

5-[8-(Azidomethyl)-1-naphthyl]-2,8,13,17-tetraethyl-3,7,12,18-tetramethylporphyrin 8.

The porphyrin mesylate 7 was dissolved in dry DMF (10 ml) and sodium azide (300 mg) was added. The mixture was heated to 90°C for 5 hours under argon. After the reaction was done, water was added to the solution and the porphyrin was extracted to the organic layer by methylene chloride. The crude product was purified by column chromatography over

silica gel using methylene chloride as solvent and crystallized from CH₂Cl₂/CH₃OH (3:2) to give 103 mg (99%) of 8. ¹H NMR (300 M Hz, CDCl₃) δ ppm -3.08 (2H, d, NH), 1.73 (6H; t, Et), 1.89 (6H, t Et), 2.12 (6H, s, Me), 2.95 (2H, d, CH₂N₃), 3.66 (6H, s, Me), 3.98 (4H, q, Et), 4.10 (4H, q, Et), 9.99 (1H, s, meso), 10.19 (2H, s, meso), naphthyl: 7.49 (1H, d), 7.64 (1H, t), 7.80 (1H, t), 8.03 (1H, dd); 8.22 (1H, d), 8.36 (1H, dd); FAB-MS, m/e (relative intensity) 660 (M+1, 3.17); UV-vis λ_{max} nm (ϵ_{M}) 625 (2100), 572 (6400), 538 (6500), 503 (15000), 405 (190000); IR: 2096 cm⁻¹ (strong).

5-[8-(Aminomethyl)-1-naphthyl]-2,8,13,17-tetraethyl-3,7,12,18-tetramethylporphyrin 9.

Zinc was inserted into 50 mg of porphyrin 8 using the procedure described previously for porphyrin 5. To the dried zinc porphyrin dissolved in freshly distilled THF (15 ml), cooled in ice bath and stirred under argon, a suspension of LiAlH4 (20 mg) in THF was added slowly. The mixture was stirred for another 10 minutes. The reduction was monitored by TLC as the product has a relative smaller R_f value compared to that of the starting material. After the reaction was done, ice water was added cautiously to the reaction flask. The THF was evaporated, and the porphyrin was extracted into methylene chloride and evaporated to dryness. Column chromatography (silica, CH₂Cl₂) provided the pure zinc amino-porphyrin. The zinc complex was then partitioned between CH₂Cl₂ and 10% HCl, and the CH₂Cl₂ layer of porphyrin was washed with saturated NaHCO₃, water, and evaporated to give 29 mg (61%) of 9. ¹H NMR (300 MHz, CDCl₃) δ ppm -3.09(2H, br, NH), 0.89 (2H, t, NH₂), 1.70 (6H; t, Et), 1.88 (6H, t Et), 2.12 (6H, s, Me), 2.39 (2H, s, CH₂N), 3.65

(6H, s, Me), 3.88 (2H, q, Et), 3.97 (2H, q Et), 4.08 (4H, q, Et), 9.97 (1H, s, meso), 10.16 (2H, s, meso), naphthyl: 7.52 (1H, d), 7.61 (1H, t), 7.77 (1H, t), 8.00 (1H, dd); 8.13 (1H, dd), 8.32 (1H, dd); MS, m/e (relative intensity) 633 (M⁺, 2.56); UV-vis λ_{max} nm (ε_{M}) 625 (2100), 572 (6400), 538 (6500), 503 (15000), 405 (190000).

5-{8-[endo-7-(Hydroxycarbonyl)-1,5,7-trimethyl-2,4-dioxo-3-azabicyclo[3,3,1]non-3-yl]-methyl-1-naphthyl}-2,8,13,17-tetraethyl-3,7,12,18-tetramethylporphyrin (NKAP).

The Kemp's imide-acid chloride was prepared as reported previously⁶. 9 (57 mg, 0.09 mmol) was dissolved in freshly distilled toluene (5 ml) and stirred under argon. To this solution, a catalytic amount of dimethylaminopyridine (DMAP) and 2,6-di-t-butylpyridine (46 mg) and Kemp's imide-acid chloride (28 mg, 1.0 mmol) were added. The mixture was refluxed under argon for 19 hours. The solvent was evaporated and methylene chloride was added. Purification from preparative TLC plate (silica gel, 1% CH₃OH/CH₂Cl₂) and recrystallization from CH₂Cl₂/CH₃OH (3:2) gave 77 mg (75%) of NKAP. mp: 298°C dec; ¹H NMR (300 MHz, CDCl₃) δ ppm 1.73 (6H; t, Et), 1.88 (6H, t, Et), 2.21 (6H, s, Me), 3.28 (2H, s, CH₂N), 3.62 (6H, s, Me), 3.82-4.08 (8H, m, Et), 9.93 (1H, s, meso), 10.19 (2H, s, meso), naphthyl: 6.67 (1H, d), 7.45 (1H, t), 7.69 (1H, t), 7.78 (1H, dd); 8.04 (1H, d), 8.27 (1H, dd), Kemp's: -0.26 (3H, s, Me), 0.23 (2H, d, CH₂), 0.80 (6H, s, Me), 0.88 (1H, d, CH₂), 1.30 (2H, t, CH₂), 1.63 (1H, d, CH₂); MS, m/e (relative intensity) 855 (M⁺, 7.86); UV-vis λ_{max} nm (ϵ_{M}) 622 (2000), 570 (6300), 540 (6000), 507 (12000), 406 (140000).

5-{8-[endo-7-(Methoxycarbonyl)-1,5,7-trimethyl-2,4-dioxo-3-azabicyclo[3,3,1]non-3-yl]-methyl-1-naphthyl}-2,8,13,17-tetraethyl-3,7,12,18-tetramethylporphyrin 10

NKAP (10 mg, 0.012 mmol) was dissolved in 10 ml freshly distilled THF. 10 equivalents of fresh prepared diazomethane ether solution was added and the mixture was stirred at room temperature for 30 minutes. 5% Acetic acid (1 ml) was then added to quench the excess diazomethane. After THF was evaporated, the product was extracted with methylene chloride and washed with saturated solution of NaHCO3 and water. The removal of the solvent and recrystallized from CH3OH/CH2Cl2 (2:3) afforded quantitative yield of 10: ¹H NMR (300 MHz, CDCl3) δ ppm -3.22 (2H, d, NH), 1.74 (6H; t, Et), 1.86 (6H, t, Et), 2.20 (6H, s, Me), 3.56 (2H, s, CH2N<), 3.63 (6H, s, Me), 3.92-4.11 (8H, m, Et), 9.89 (1H, s, meso), 10.16 (2H, s, meso), naphthyl: 6.58 (1H, d), 7.46 (1H, t), 7.70 (1H, t), 7.82 (1H, dd); 8.08 (1H, d), 8.28 (1H, dd), Kemp's: -2.61 (3H, s, -OCH3), 0.13 (3H, s, Me), 0.44 (2H, d, CH2), 0.92 (6H, s, Me), 1.02 (1H, d, CH2), 1.66 (2H, t, CH2), 1.76 (1H, d, CH2); MS, m/z 869 (M, 58%); UV-vis λ max nm (rel intens) 406 nm (1.00), 504 (0.09), 538 (0.04), 573 (0.04), 627 (0.01).

 $5-\{8-[endo-7-(Aminocarbonyl)-1,5,7-trimethyl-2,4-dioxo-3-azabicyclo[3,3,1]non-3-yl]-methyl-1-naphthyl\}-2,8,13,17-tetraethyl-3,7,12,18-tetramethylporphyrin 11$

To a solution of NKAP (15 mg, 0.018 mmol) in 2 ml dry methylene chloride, oxalyl chloride (3 ml) was added. The mixture was stirred under argon for 6 hours at room temperature. The excess oxalyl chloride was pumped away by vacuum pump. Dry methylene chloride (20 ml) was

introduced to dissolve the compound and ammonia gas was bubbled in for 20 minutes. The solvent was evaporated and the residue was purified on a preparative TLC plate (silica gel, 1% CH₃OH/CH₂Cl₂) to give 14 mg (95 %) of 11: 1 H NMR (300 MHz, CDCl₃) δ ppm -3.16 (2H, br, NH), -1.19 (2H, br, -CONH₂), 1.75 (6H; t, Et), 1.89 (6H, t, Et), 2.22 (6H, s, Me), 3.60 (2H, s, CH₂N<), 3.64 (6H, s, Me), 3.94-4.11 (8H, m, Et), 9.93 (1H, s, meso), 10.17 (2H, s, meso), naphthyl: 6.73 (1H, d), 7.49 (1H, t), 7.69 (1H, t), 7.76 (1H, dd); 8.08 (1H, d), 8.30 (1H, dd), Kemp's: -1.19 (2H, s, CONH₂), -0.19 (3H, s, Me), 0.32 (2H, d, CH₂), 0.83 (6H, s, Me), 0.90 (1H, d, CH₂), 1.24 (2H, t, CH₂), 1.65 (1H, d, CH₂); MS, m/z 854 (M, 100%); UV-vis λ_{max} nm (rel intens) 407 nm (1.00), 506 (0.08), 540 (0.04), 570(0.04), 623 (0.01).

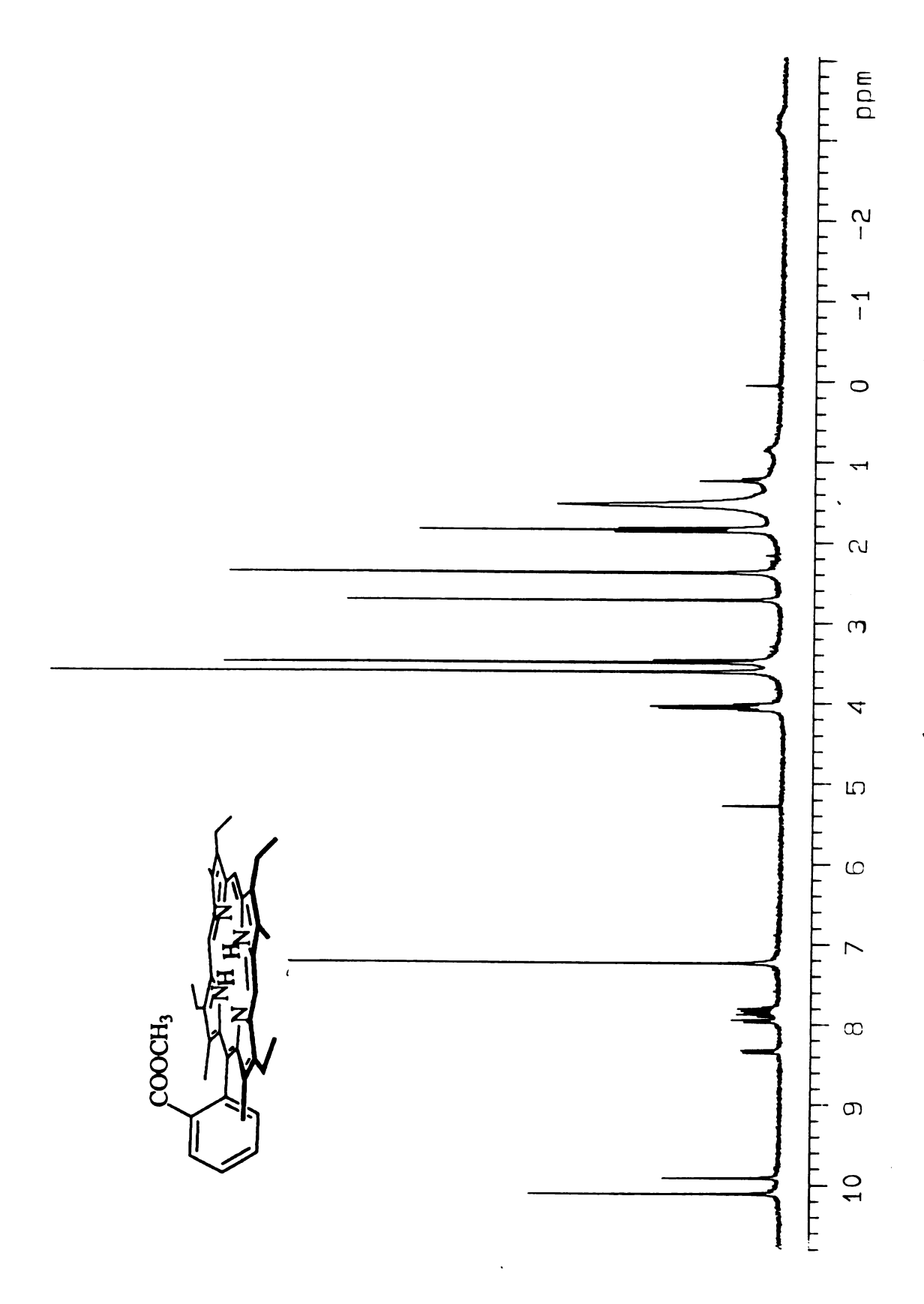


Figure II-13. ¹H NMR spectrum of 2.

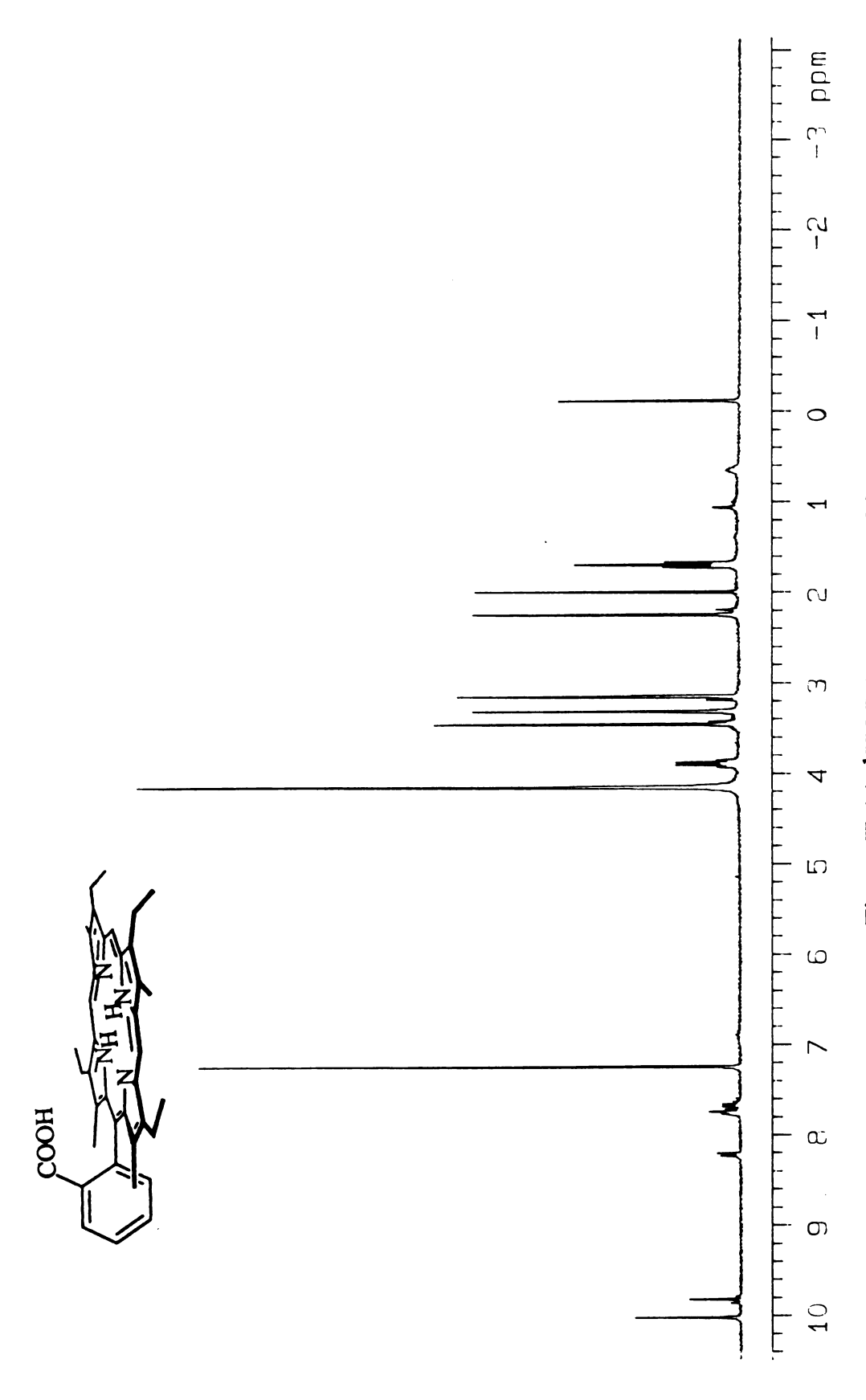


Figure II-14. ¹H NMR spectrum of 3.

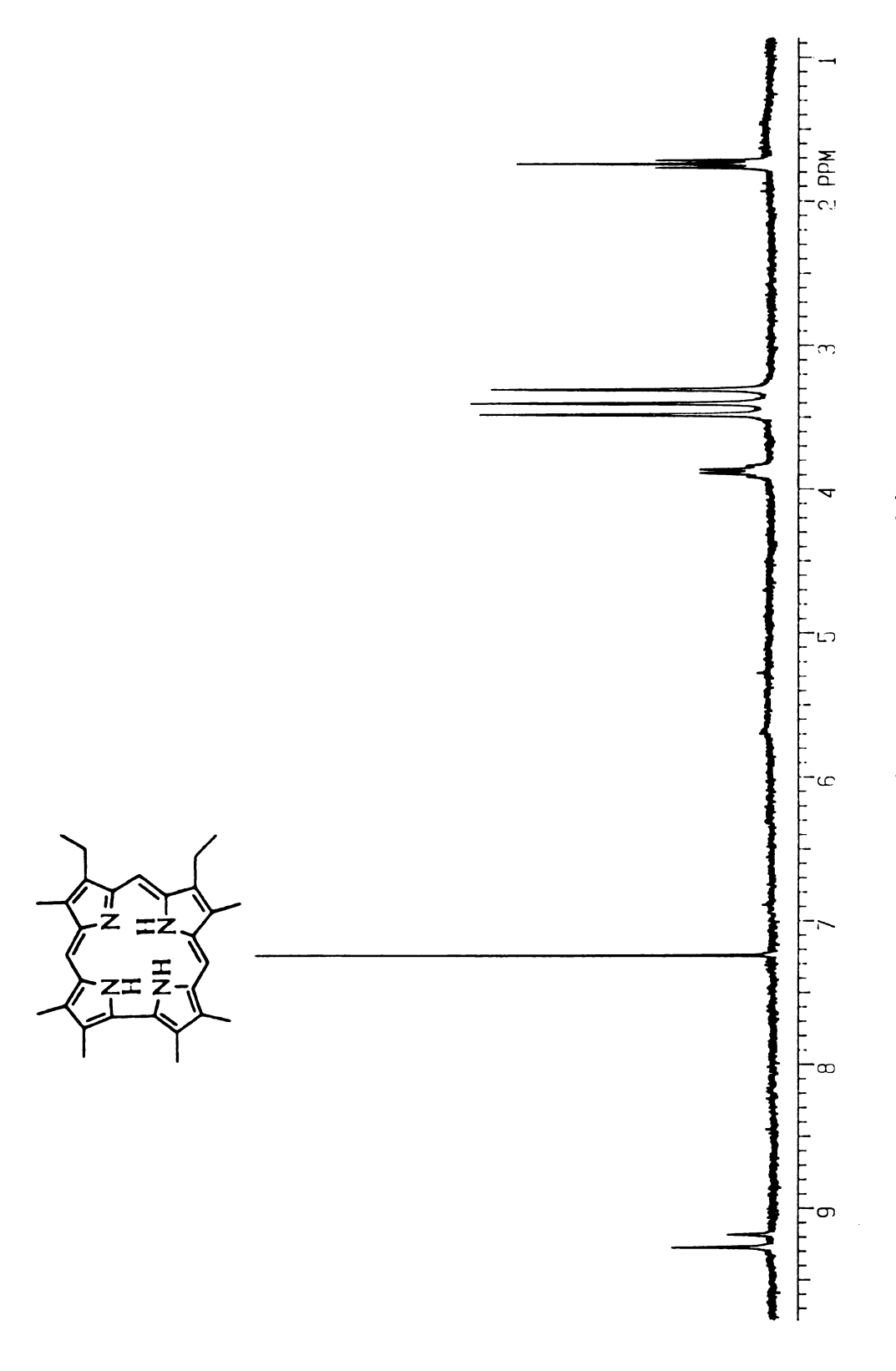


Figure II-15. ¹H NMR spectrum of 4.

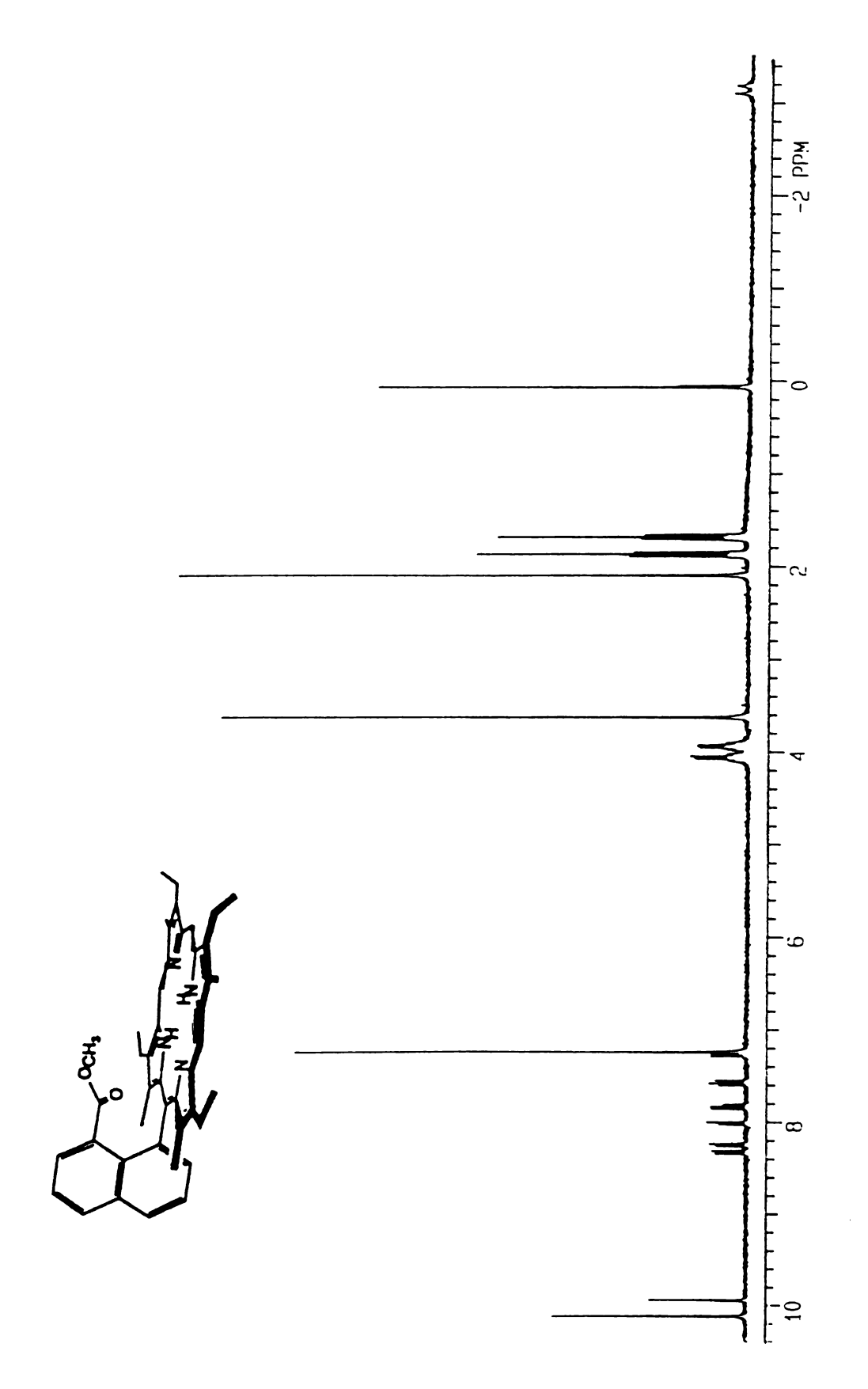


Figure II-16. ¹H NMR spectrum of 5.

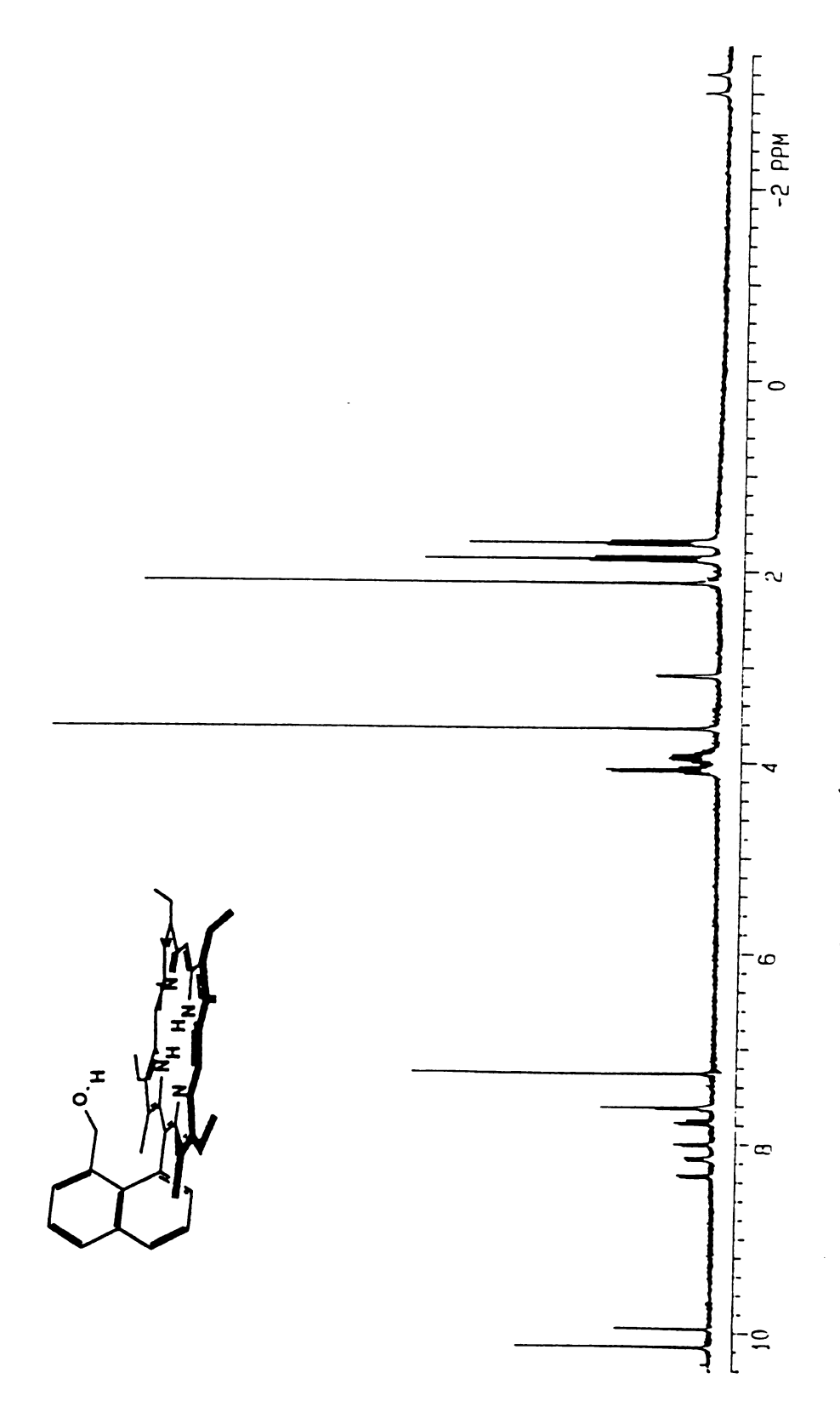


Figure II-17. ¹H NMR spectrum of 6.

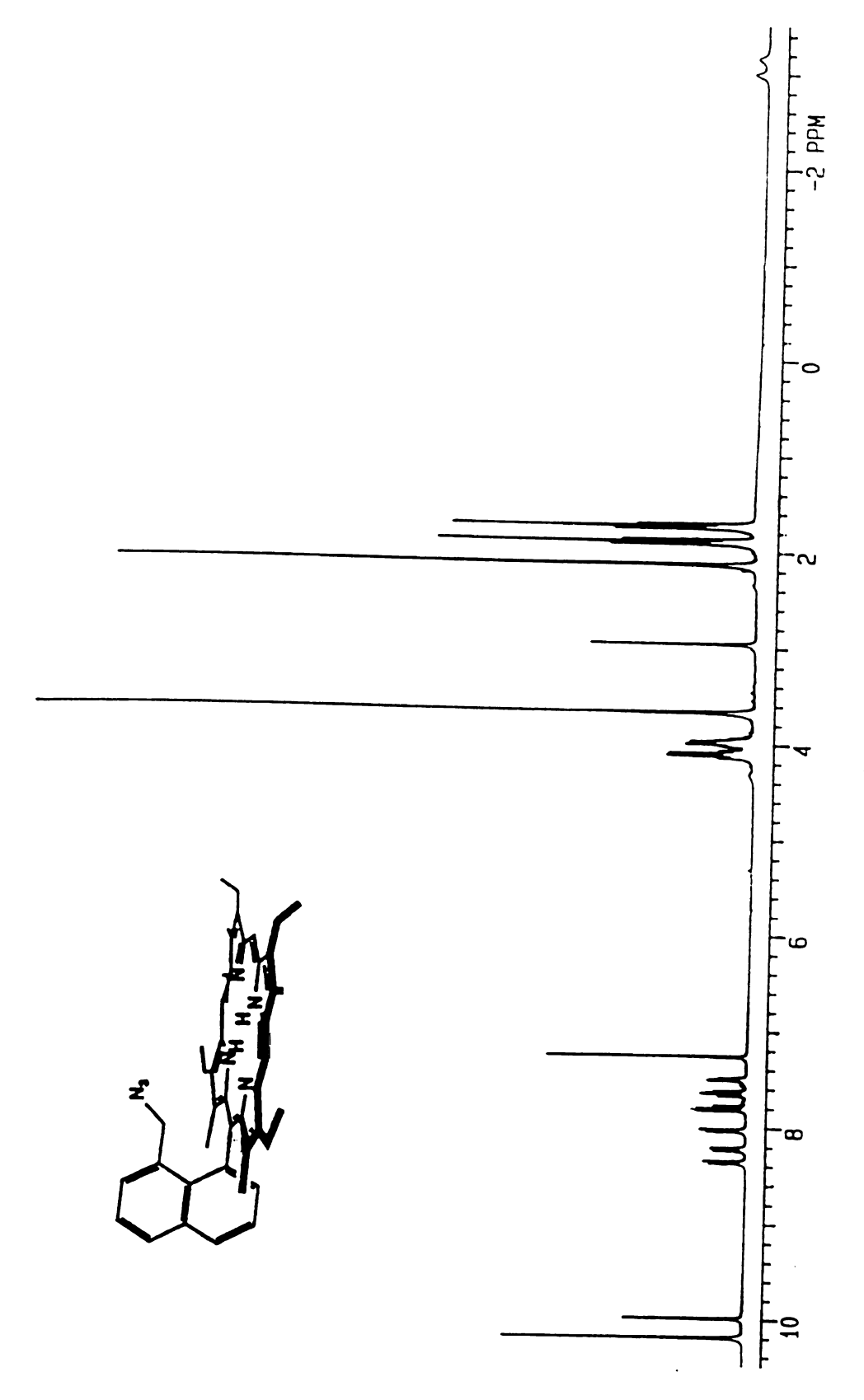


Figure II-18. ¹H NMR spectrum of 8.

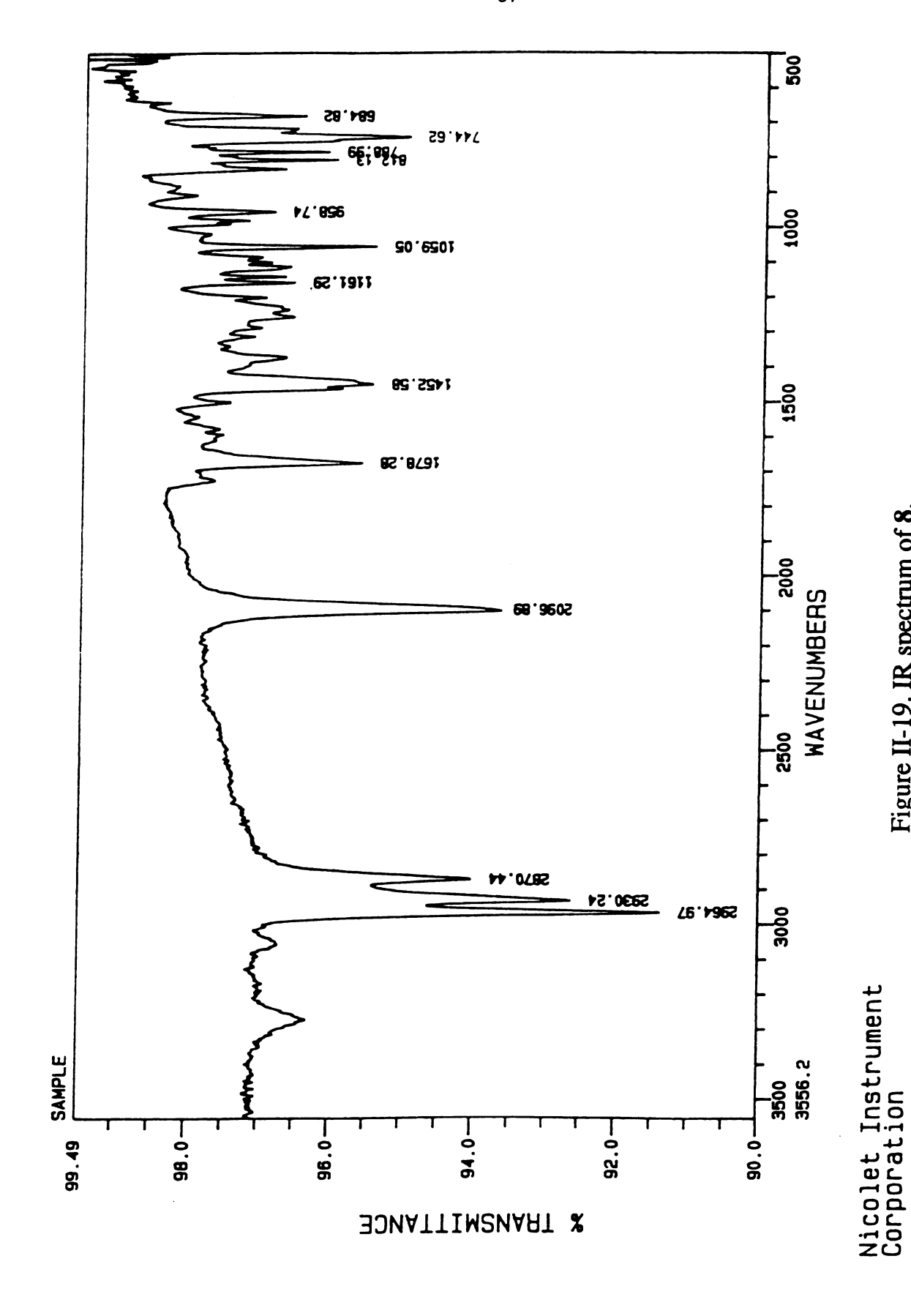
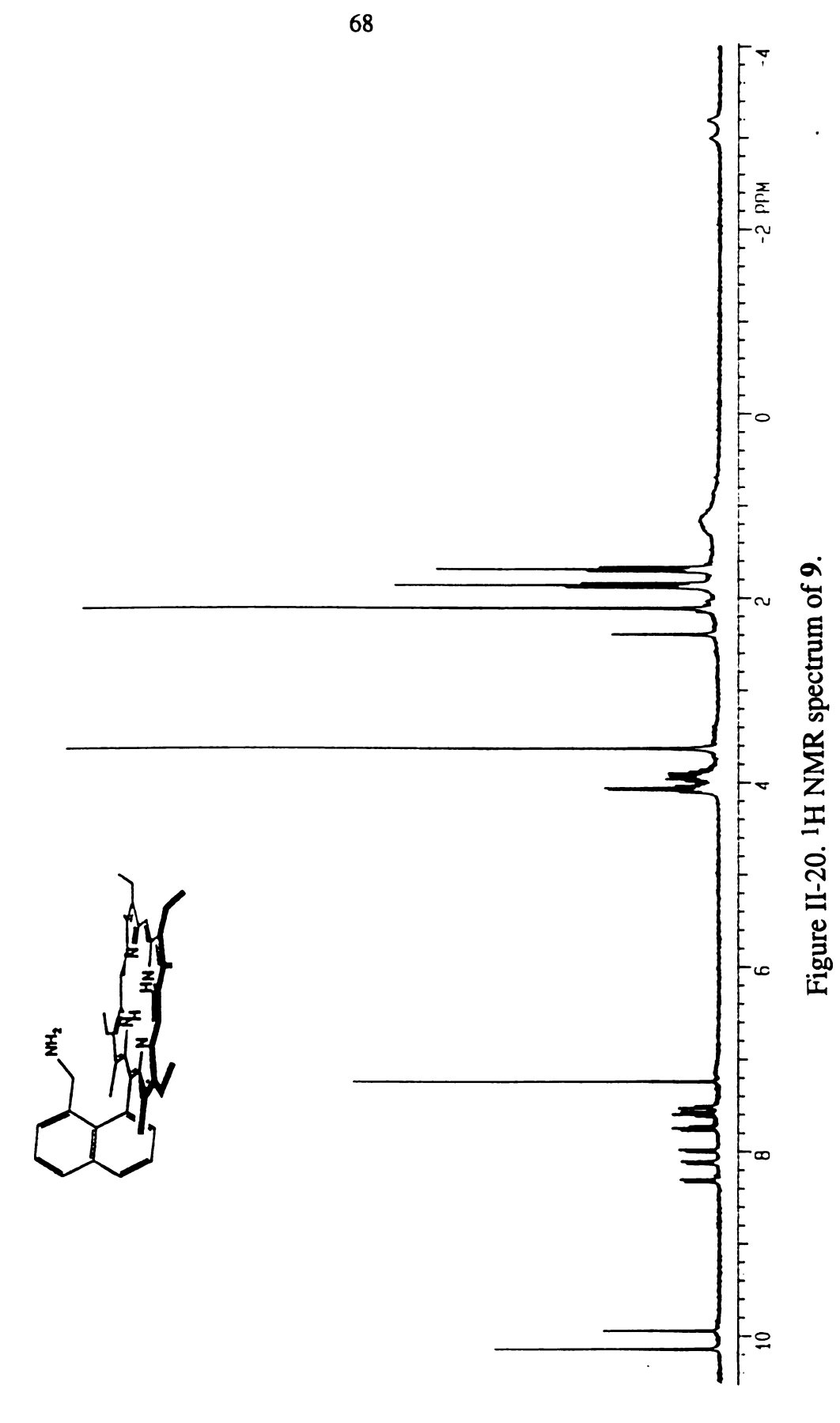


Figure II-19. IR spectrum of 8.



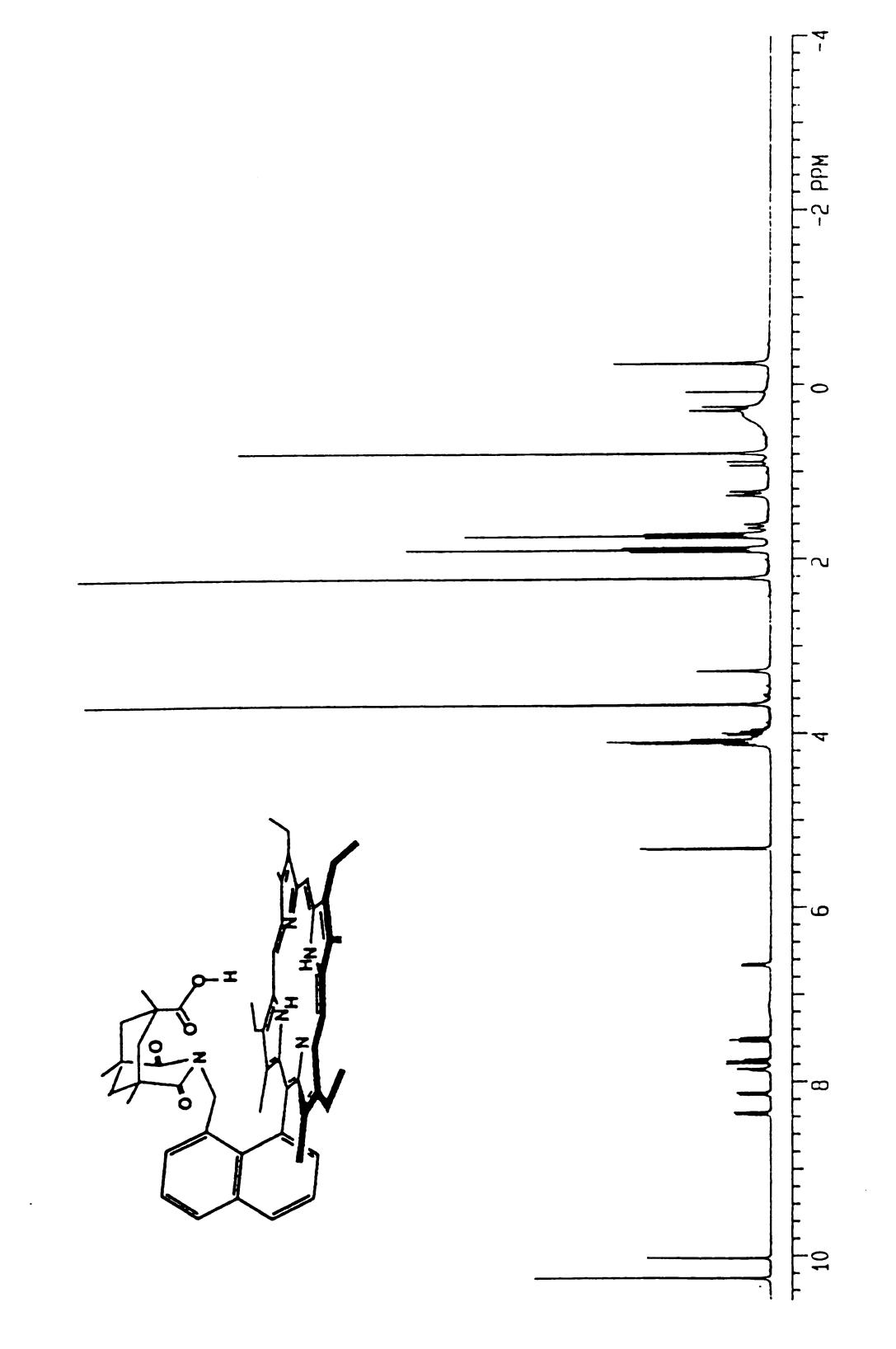


Figure II-21. ¹H NMR spectrum of NKAP.

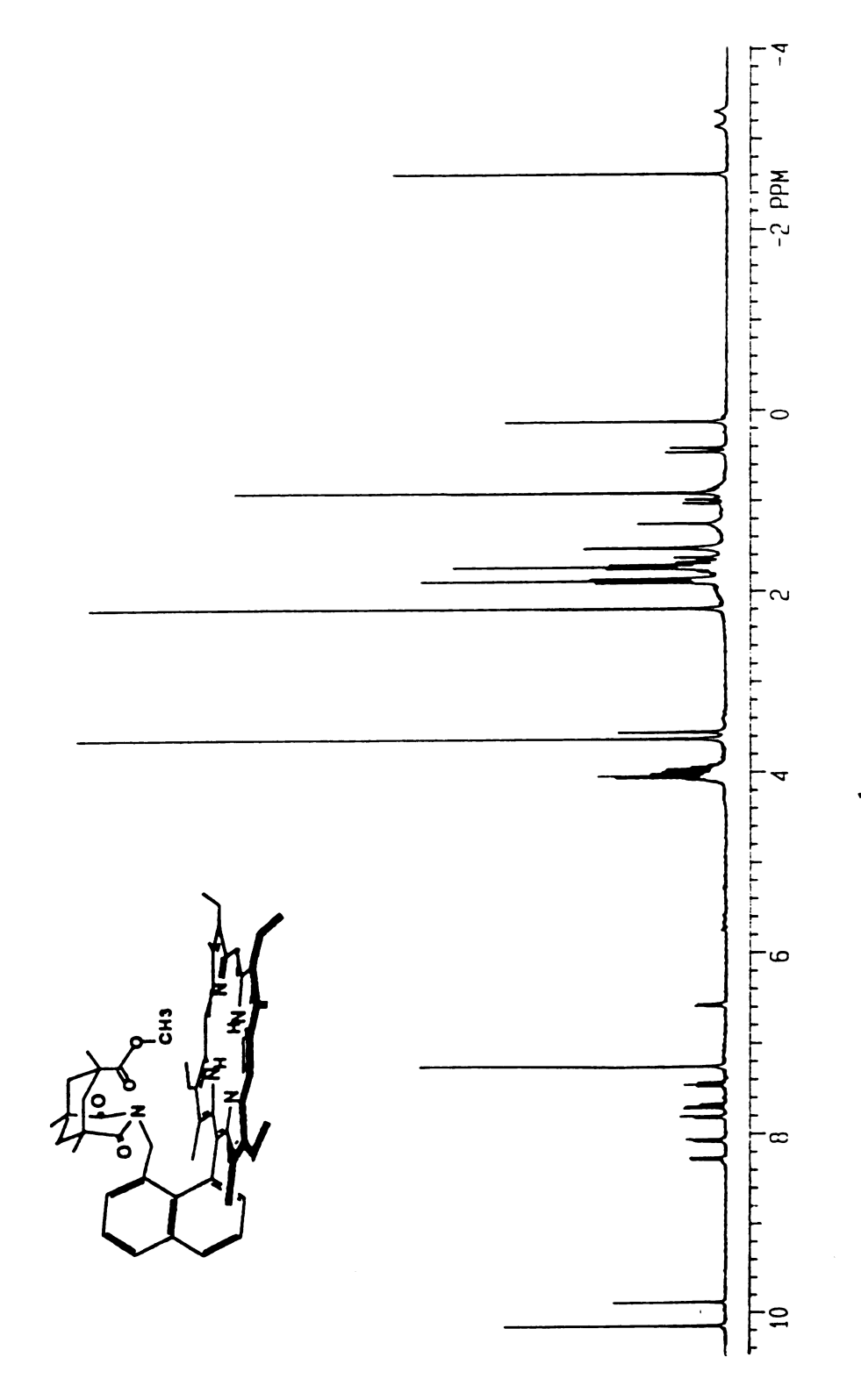


Figure II-22. ¹H NMR spectrum of 10.

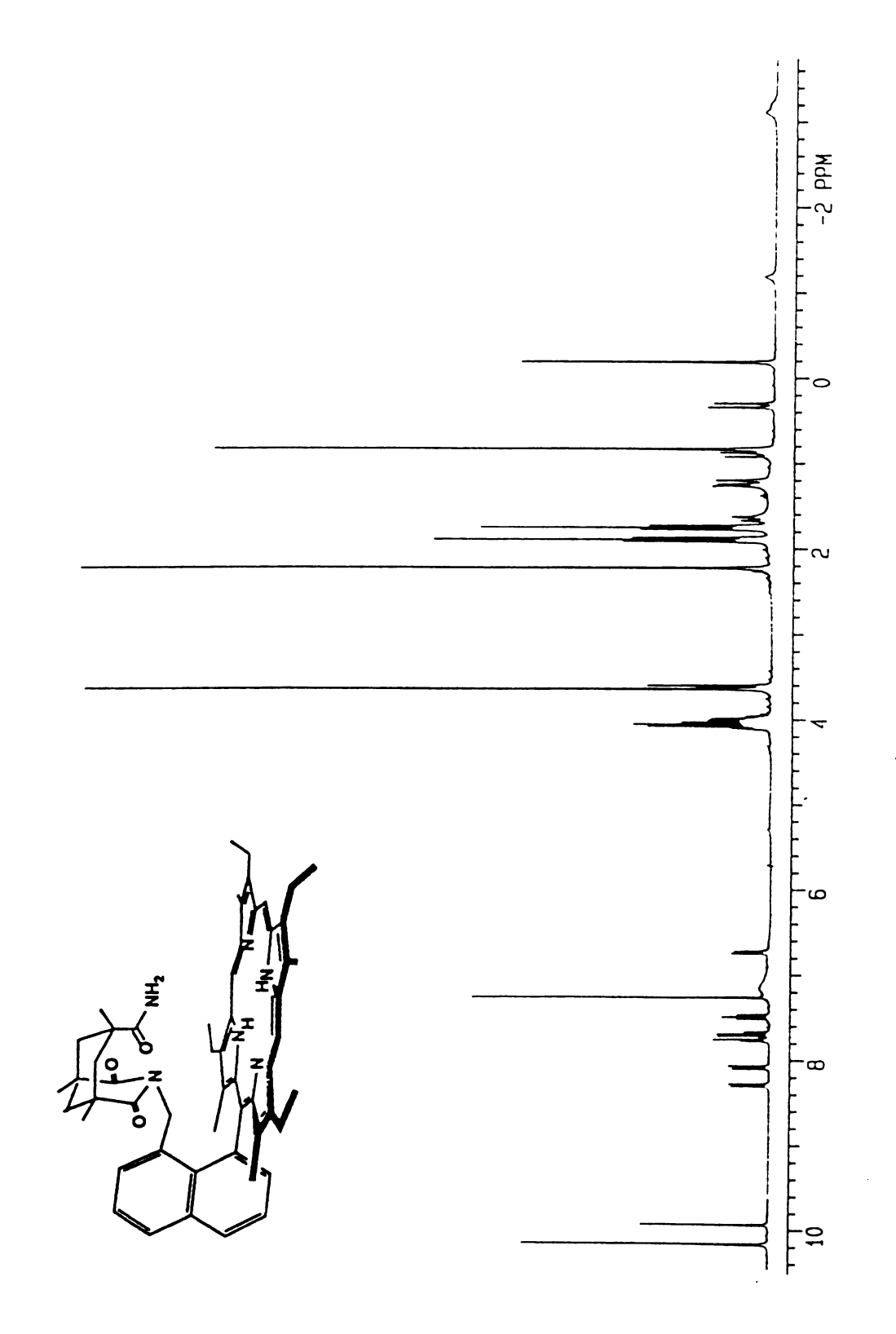


Figure II-23. ¹H NMR spectrum of 11.

E. References

- 1. Chang, C. K.; Kondylis, M. P. J. Chem. Soc. Chem. Commun. 1986, 316-318.
- 2. Paine, J. B., III, in "The Porphyrins", Dolphin, D. Ed.; Academic Press, 1978. Vol. I, p177
- 3. Chang, C. K.; Avilés, G.; Bag, N. J. Am. Chem. Soc. 1994, 116, 12127-12128.
- 4. a) Harris, R. L. N.; Johnson, A. W.; Kay, I. T. J. Chem. Soc. (C) 1966, 22-29.
 - b) Dolphin, D.; Harris, R. L. N.; Huppatz, J. L.; Johnson, A. W.; Kay, I. T. J. Chem. Soc. (C) 1966, 30-40.
 - c) Engel, J.; Gossauer, A.; Johnson, A. W. J. Chem. Soc. Perkin I 1978, 871-875.
 - d) Pandey, R. K.; Zhou, H.; Gerzevske, K.; Smith, K. M. J. Chem. Soc. Chem. Commun. 1992, 183-185.
- 5. Avilés, G. M., "Interaction of Intramolecular Carboxylic Acid with Heme-O₂ Complex", Ph.D. Dissertation, Michigan State University, 1991.
- Rebek, J., Jr.; Marshall, L.; Wolak, R.; Parris, K.; Kolloran, M.;
 Askew, B.; Nemeth, D.; Islam, N. J. Am. Chem. Soc. 1985, 107, 7476-7481.
- 7. a) Sandström, J. "Dynamic NMR Spectroscopy". Academic Press: New York, 1982, p97.

- b) Õki, M. "Applications of Dynamic NMR Spectroscopy to Organic Chemistry". VCH Publishers: Deerfield, 1985, p 1-12.
- 8. Dahlquist, F. W.; Longmuir, K. J.; Du Vernet, R. B. J. Magn. Reson. 1975, 17, 406-410.

CHAPTER III

Hydrogen Bonding in Molecular Recognition: Inclusion

Complex and Substrate Recognition by C-Clamp Porphyrins

A. Introduction

Molecular recognition plays an important role in biological systems. Highly specific interactions between proteins and ligands provide the basis for protein function. There have been extensive studies focusing on the design and synthesis of biomimetic host-guest systems that may provide insights to biological processes. In efforts to mimic heme proteins, numerous model porphyrins have been synthesized for studies of mainly metal-centered interactions such as dioxygen binding. The porphyrin macrocycle, despite the crucial biological functions of its metal derivatives, usually does not have enough functionalized binding sites to interact with substrates. However, the porphyrin ring can be easily linked to other functional groups at the peripheral meso and β -pyrrole positions. Recent advances in the synthesis of functionalized porphyrins have made it possible

to develop porphyrin-based receptors with a variety of sizes, shapes and functional surfaces. The relatively rigid and disk-shaped porphyrins are suitable to serve as frameworks in building molecular clefts that function independently of the porphyrin. The presence of N-H protons or metal ion at the porphyrin center can provide additional binding sites to aid the complexation of guest molecules. The flexibility in design and synthesis makes modified porphyrins useful not only in mimicking their biochemical functions, but also in developing new types of receptors for artificial molecular recognition. The mechanism which allows the binding of specific ligand can be ascribed to hydrogen bonding, π - π stacking and metal-ligand coordination. Various porphyrin receptors have been designed for recognizing amino acids, nucleobase pairs, barbiturates and polyols.³

In Chapter II, we already discussed the synthesis of a novel C-clamp shaped molecular receptor in which a porphyrin ring is supplemented by a carboxylic acid group pointing towards the porphyrin center. This acid functional group combined with the pyrrole NH or metal ion of the porphyrin furnishes a ditopic binding site capable of specific substrate recognition. The combination of the Kemp's triacid and a naphthalene or a anthracene connector thus gives a C-shaped receptor with a relatively rigid acid hovering over the porphyrin. The C-clamp porphyrins have been used to enhance O₂ binding to the Co(II) porphyrin,⁴ which will be discussed later in Chapter IV. In this chapter, the emphasis will be on the formation of inclusion complexes with small neutral guest molecules.⁵

B. Experimental

1. Crystal Structure Analysis.

Data collection was performed on a Nonius CAD4 diffractometer at room temperature using graphite-monochromated Cu K_{α} or Mo K_{α} radiation. The crystals used for analysis were of approximate dimensions 0.30 x 0.35 x 0.40 mm for NKAP and 0.40 x 0.40 x0.70 mm for ZnNKAP. The unit cell parameters were determined by a least square fit of 25 machine-centered reflections having 20 values in the ranges of 39.6-44.4° for NKAP and 20.10-27.12° for ZnNKAP. The intensity data were reduced and corrected for Lorentz and polarization factors using the applied programs. Semiempirical absorption corrections were applied. The crystal structures were solved by direct methods using the NRCVAX program package. All non-hydrogen atoms were refined anisotropically. The hydrogen atoms of the carboxylic group and methanol were located from the difference map and refined positionally. All other hydrogen atoms were calculated with fixed isotropic thermal parameters. highest difference Fourier peak was 0.31 and 0.35 e Å-3 for NKAP and ZnNKAP, respectively. For NKAP, the final R is 0.047 and Rw is 0.044; and for ZnNKAP, R and Rw are 0.040 and 0.042, respectively.

2. Determination of Binding Constants.

a) NMR Method. The receptor molecules NKAP, AKAP, ZnNKAP and ZnAKAP (2-5 x 10⁻³ M in 0.8 ml CDCl₃) were titrated with a solution of the substrate (2-5 M) dissolved in CDCl₃ or methanol-d₄. The downfield shifts of the naphthyl and anthryl methylene protons linked to the imide were monitored as a function of substrate concentration. Addition was

continued until up to 10-15 equivalents of the substrate have been added. The resultant titration curve was analyzed by nonlinear regression methods.⁶

- b) UV-Vis Method. A similar protocol to a) was followed. The increase in absorbance of the Soret peak of the molecular complex and the decrease of the receptor Soret peak were monitored upon the addition of substrate molecules.
- c) DSC Method. DSC measurements were carried out for the NKAP-H₂O crystal under N₂ with heating rate at 5 °C/min.

C. Results and Discussion

1. Structure of Receptors and Their Znic Complexes

The crystal structures of NKAP and ZnNKAP are shown by the ORTEP drawings in Figures III-1 and III-2, respectively. Crystal data and refinement parameters are given in Table III-1. Table III-2 lists the atomic coordinates of non-hydrogen atoms. The data for selected bond distances and angles for both compounds are given in Table III-3. For both compounds, the porphyrin structural features essentially remain unchanged.

X-ray structure analysis of NKAP receptor showed a C-shaped structure with the acid pointing towards the porphyrin (Figure II-1).⁴ The cavity between the porphyrin and the acid is occupied by a water molecule of crystallization. As shown in Figure II-2, there are multiple H-bonds that brought about the water inclusion. To accommodate this H₂O molecule, the porphyrin ring undergoes several noticeable deformations at the

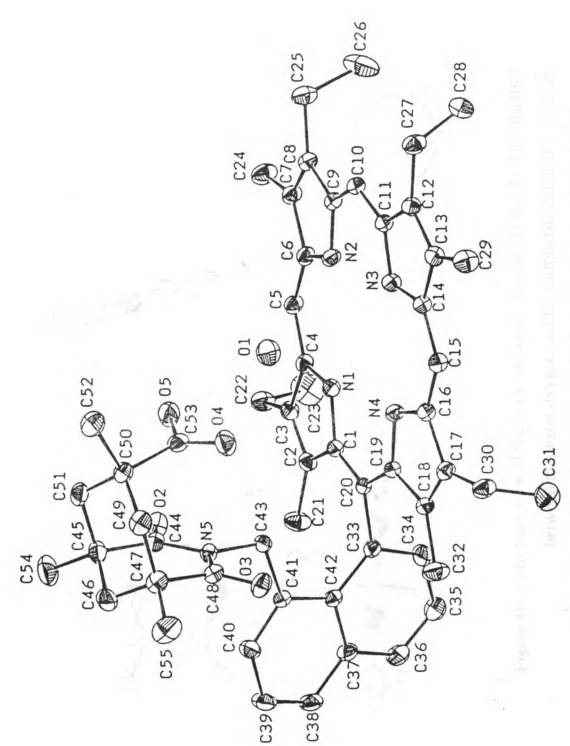


Figure III-1. (a) ORTEP plot and labeling scheme for NKAP-H₂O.

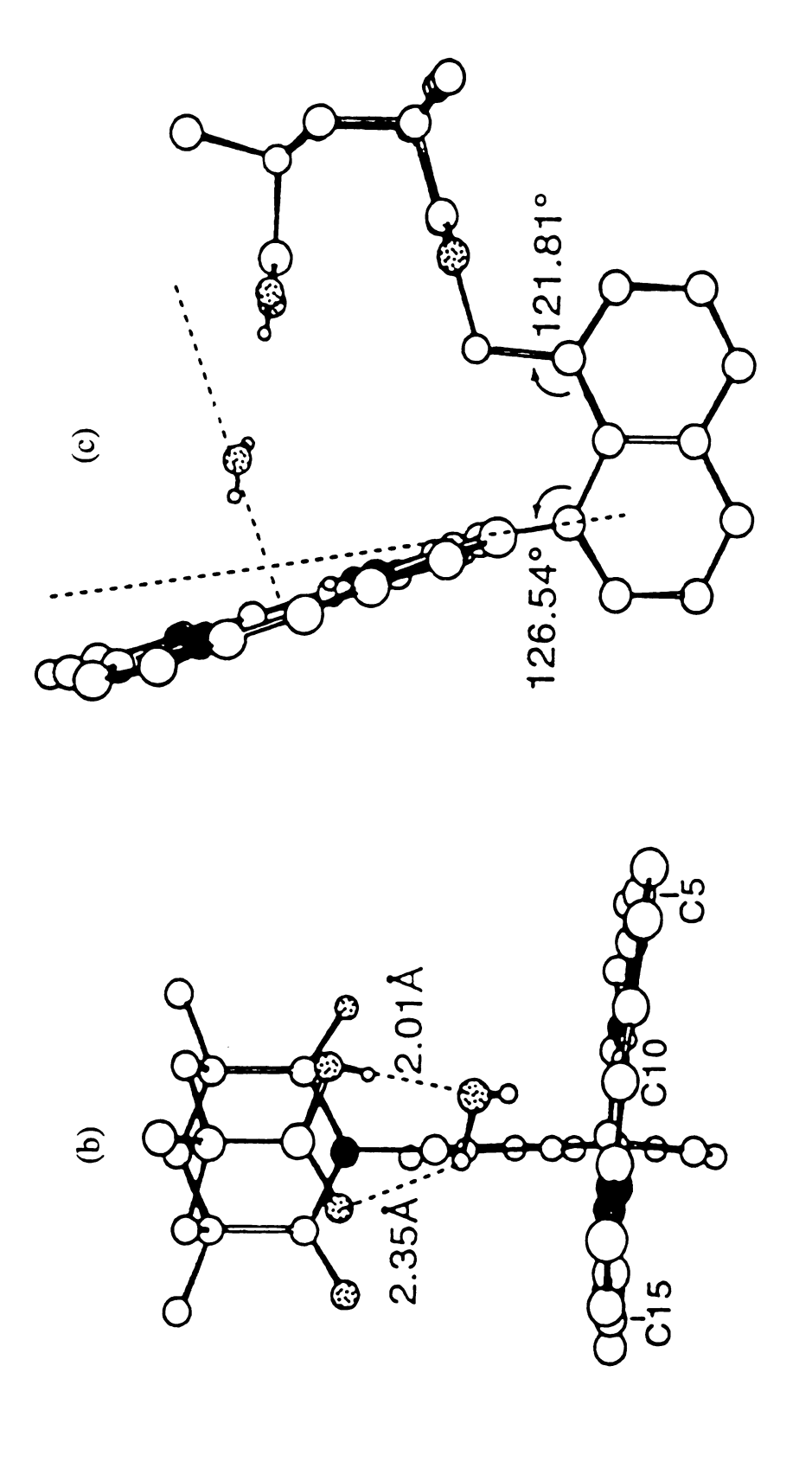


Figure III-1. (b) Side view of the X-ray structure showing H-bonds. The distance between the water oxygen and the porphyrin center is 2.31(4) Å.

(c) Another view showing distortions around the C20-C33 connetor.

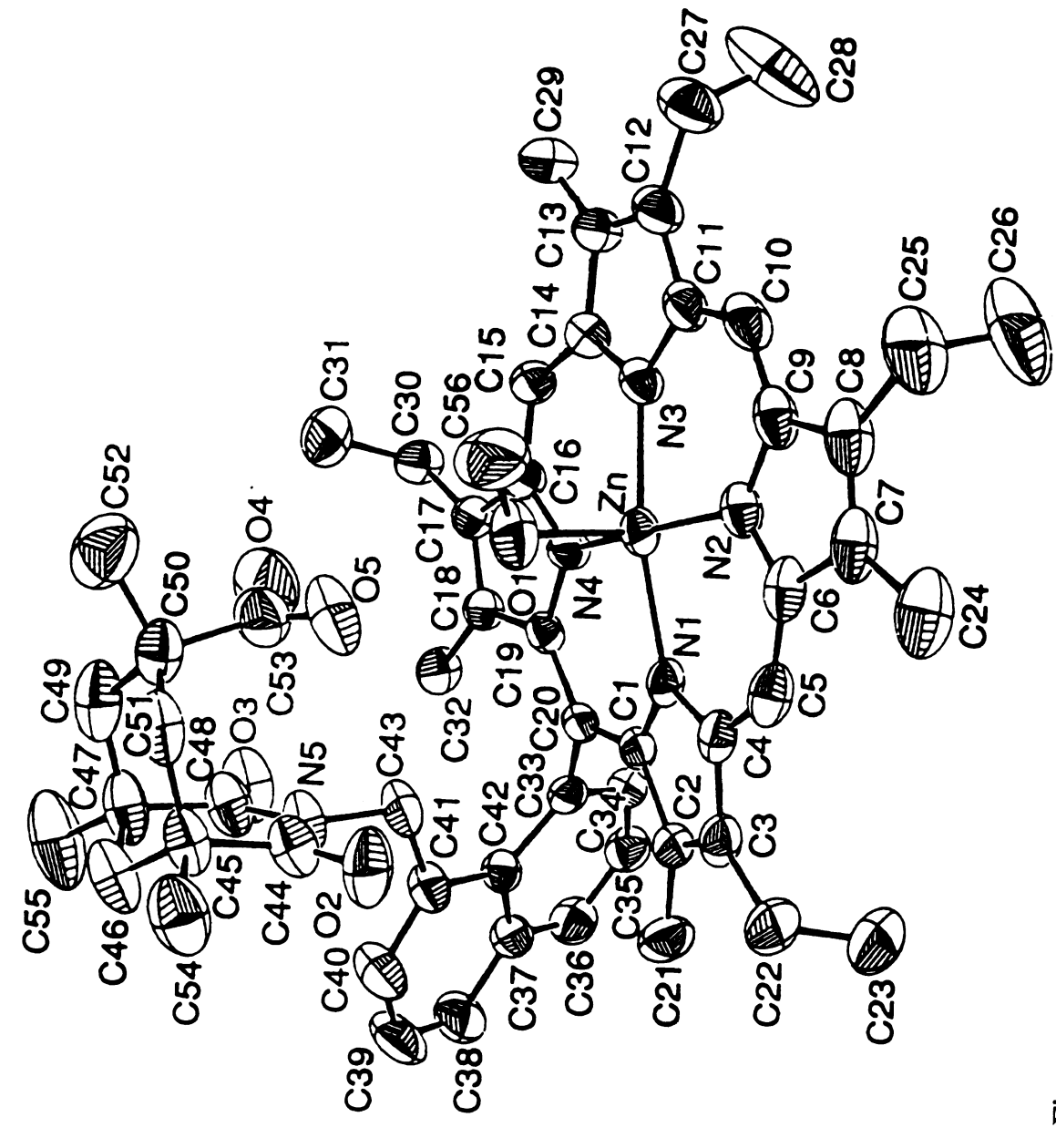


Figure III-2. (a) ORTEP plot and labeling scheme for ZnNKAP-MeOH.

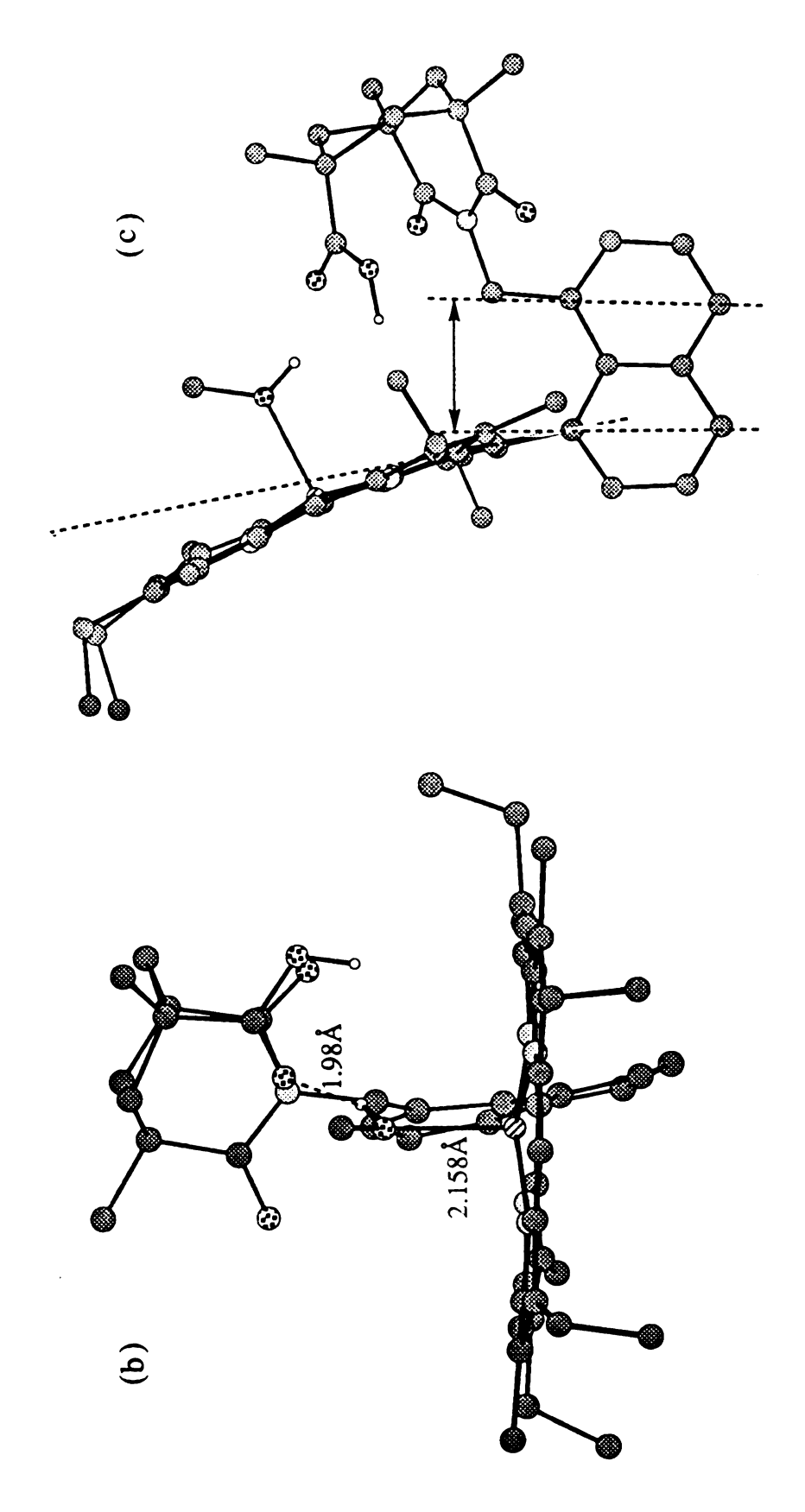


Figure III-2. (b) Side view of the X-ray structure of ZnNKAP-methanol.

(c) Side view from another angle showing the porphyrin outward bending.

Table III-1. Crystallographic Data of NKAP and ZnNKAP

	NKAP	ZnNKAP
Formula	C55N5O5H63	ZnC56N5O5H63
fw	876.14	951.51
cryst syst	monoclinic	Triclinic
space group	C 2/c	PĪ
a, Å	19.557(4)	9.1228(2)
b, Å	11.9541(17)	11.789(9)
c, Å	42.602(8)	23.583(5)
α, deg	90	76.58(4)
β, deg	105.201(17)	86.83(2)
γ, deg	90	88.28(4)
v, å3	9611(3)	2462.9(20)
Z	8	2
Q(calc), gcm ⁻³	1.211	1.283
μ, cm ⁻¹	0.58	0.56
transm coeff	0.974-0.9994	0.9629-0.9965
scan speed, deg min-1	1.37-8.24	2.35-8.24
scan width, deg	$2(0.85 + 0.35\tan\theta)$	$2(0.65 + 0.35 \tan \theta)$
no. of measd reflns	6008	8662
no. of obsd reflns	4758 (I>2σ(I))	5855(I>2σ(I))
no. of refined params	608	609
R, Rw	0.0047, 0.044	0.040, 0.042
Gof	1.39	1.80

Table III-2. Atomic Parameters x, y, z and B_{iso} for NKAP and ZnNKAP with E.S.D.'s. refer to the last digit printed

NKAP

	x	у	z	Biso
NI	0.81974(13)	0.27970(20)	0.13701(5)	3.40(12)
N2	0.85113(13)	0.25643(20)	0.07115(6)	3.62(12)
N3	0.76212(13)	0.44434(21)	0.04749(5)	3.53(12)
N4	0.73450(12)	0.47166(20)	0.11398(6)	3.31(11)
N5	0.55610(12)	0.21342(19)	0.15560(5)	3.10(10)
C1	0.80080(15)	0.30197(25)	0.16530(7)	3.19(13)
C2	0.83606(16)	0.2196 (3)	0.18915(7)	3.53(14)
C3	0.87552(16)	0.1533 (3)	0.17488(7)	3.58(14)
C4	0.86535(15)	0.19145(25)	0.14188(7)	3.40(14)
C5	0.89815(16)	0.1445 (3)	0.11993(7)	3.72(15)
C6	0.89269(16)	0.17341(25)	0.08793(7)	3.58(14)
C 7	0.92817(17)	0.1185 (3)	0.06643(8)	3.95(15)
C 8	0.90534(17)	0.1681 (3)	0.03695(7)	3.98(15)
C9	0.85686(16)	0.25603(25)	0.03987(7)	3.51(14)
C10	0.82159(16)	0.3284 (3)	0.01580(7)	3.53(14)
C11	0.77853(16)	0.4167 (3)	0.01917(7)	3.39(13)
C12	0.74591(17)	0.4964 (3)	-0.00529(7)	3.67(15)
C13	0.71053(16)	0.5708 (3)	0.00866(7)	3.85(15)

Table III-2 (cont'd)

C14	0.72091(15)	0.53772(25)	0.04230(7)	3.29(13)
C15	0.69491(16)	0.5901 (3)	0.06537(7)	3.70(14)
C16	O.70031(15)	0.56221(25)	0.09775(7)	3.35(13)
C17	0.67009(16)	0.6251 (3)	0.11962(7)	3.76(14)
C18	0.68640(16)	0.5709 (3)	0.14874(7)	3.69(14)
C19	0.72788(15)	0.47243(24)	0.14537(7)	3.13(13)
C20	0.75743(14)	0.39216(24)	0.16893(7)	2.96(12)
C21	0.83102(20)	0.2024 (3)	0.22384 (8)	5.41(19)
C22	0.92520(19)	0.0616 (3)	0.19019 (8)	4.88(17)
C23	0.99932(23)	0.1014 (4)	0.20408 (12)	8.4(3)
C24	0.97957(21)	0.0236 (3)	0.07582(9)	5.67(20)
C25	0.92755(20)	0.1440 (3)	0.00633(8)	5.35(19)
C26	0.98527(24)	0.2210 (5)	0.00283(11)	9.5(3)
C27	0.75334(20)	0.4964 (3)	-0.03951 (8)	5.09(19)
C28	0.8213 (3)	0.5462(4)	-0.04242 (11)	8.8(3)
C29	0.66651(20)	0.6672(3)	-0.00752 (8)	5.41(18)
C30	0.63022(19)	0.7335 (3)	0.11179(8)	4.75(17)
C31	0.67496(23)	0.8333 (3)	0.12511(11)	7.14(25)
C32	0.66376(23)	0.6098 (3)	0.17786(9)	6.23(22)
C33	0.75342(15)	0.41373(25)	0.20349 (7)	3.28(13)
C34	0.80892(18)	0.4764 (3)	0.22124(8)	4.93(17)
C35	0.81811(20)	0.4982 (q)	0.25425(8)	6.05(20)
C36	0.77259(19)	0.4542 (3)	0.26962 (8)	5.21(18)
C37	0.71325(17)	0.3926 (3)	0.25261 (7)	3.92(16)

Table III-2 (cont'd)

C38 0.66601(19) 0.3512 (3) 0.26961(7) 4.89(18) C39 0.60741(19) 0.2951 (3) 0.25414(8) 5.26(19) C40 0.59394(17) 0.2746(3) 0.22066 (7) 4.39(16) C41 0.63891(15) 0.30858(24) 0.20266 (7) 3.17(13) C42 0.70138(15) 0.37104(24) 0.21839(7) 3.16(13) C43 0.62095(15) 0.2808 (3) 0.15661 (7) 3.39(13) C44 0.56349(16) 0.0969 (3) 0.15819(7) 3.65(15) C45 0.49721(18) 0.0256 (3) 0.14707(8) 4.36(16) C46 0.43416(18) 0.0907 (3) 0.15122(9) 5.39(19) C47 0.42544(16) 0.1997 (3) 0.13208(8) 4.60(16) C48 0.49196(16) 0.2702 (3) 0.14426(7) 3.76(14) C49 0.41458(17) 0.2702 (3) 0.09585(8) 4.95(17) C50 0.47024(17) 0.0969 (3) 0.08750 (7) 4.19(15) C51 0.48519(18) -0.0029 (3) 0.11068(8) 4.72(17) C52 0.44276(22)					
C40 0.59394(17) 0.2746(3) 0.22066 (7) 4.39(16) C41 0.63891(15) 0.30858(24) 0.20266 (7) 3.17(13) C42 0.70138(15) 0.37104(24) 0.21839(7) 3.16(13) C43 0.62095(15) 0.2808 (3) 0.15661 (7) 3.39(13) C44 0.56349(16) 0.0969 (3) 0.15819(7) 3.65(15) C45 0.49721(18) 0.0256 (3) 0.14707(8) 4.36(16) C46 0.43416(18) 0.0907 (3) 0.15122(9) 5.39(19) C47 0.42544(16) 0.1997 (3) 0.13208(8) 4.60(16) C48 0.49196(16) 0.2702 (3) 0.14426(7) 3.76(14) C49 0.41458(17) 0.2702 (3) 0.09585(8) 4.95(17) C50 0.47024(17) 0.0969 (3) 0.08750 (7) 4.19(15) C51 0.48519(18) -0.0029 (3) 0.11068(8) 4.72(17) C52 0.44276(22) 0.0540 (4) 0.05245(9) 6.48(21) C53 0.53636(18) 0.1634 (3) 0.08684(7) 4.43(17) C54 0.50753(25)	C38	0.66601(19)	0.3512 (3)	0.26961(7)	4.89(18)
C41 0.63891(15) 0.30858(24) 0.20266 (7) 3.17(13) C42 0.70138(15) 0.37104(24) 0.21839(7) 3.16(13) C43 0.62095(15) 0.2808 (3) 0.15661 (7) 3.39(13) C44 0.56349(16) 0.0969 (3) 0.15819(7) 3.65(15) C45 0.49721(18) 0.0256 (3) 0.14707(8) 4.36(16) C46 0.43416(18) 0.0907 (3) 0.15122(9) 5.39(19) C47 0.42544(16) 0.1997 (3) 0.13208(8) 4.60(16) C48 0.49196(16) 0.2702 (3) 0.14426(7) 3.76(14) C49 0.41458(17) 0.2702 (3) 0.09585(8) 4.95(17) C50 0.47024(17) 0.0969 (3) 0.08750 (7) 4.19(15) C51 0.48519(18) -0.0029 (3) 0.11068(8) 4.72(17) C52 0.44276(22) 0.0540 (4) 0.05245(9) 6.48(21) C53 0.53636(18) 0.1634 (3) 0.08684(7) 4.43(17) C54 0.50753(25) -0.0825 (3) 0.16708(11) 7.23(25) C55 0.36205(20) <td>C39</td> <td>0.60741(19)</td> <td>0.2951 (3)</td> <td>0.25414(8)</td> <td>5.26(19)</td>	C39	0.60741(19)	0.2951 (3)	0.25414(8)	5.26(19)
C42 0.70138(15) 0.37104(24) 0.21839(7) 3.16(13) C43 0.62095(15) 0.2808 (3) 0.15661 (7) 3.39(13) C44 0.56349(16) 0.0969 (3) 0.15819(7) 3.65(15) C45 0.49721(18) 0.0256 (3) 0.14707(8) 4.36(16) C46 0.43416(18) 0.0907 (3) 0.15122(9) 5.39(19) C47 0.42544(16) 0.1997 (3) 0.13208(8) 4.60(16) C48 0.49196(16) 0.2702 (3) 0.14426(7) 3.76(14) C49 0.41458(17) 0.2702 (3) 0.09585(8) 4.95(17) C50 0.47024(17) 0.0969 (3) 0.08750 (7) 4.19(15) C51 0.48519(18) -0.0029 (3) 0.11068(8) 4.72(17) C52 0.44276(22) 0.0540 (4) 0.05245(9) 6.48(21) C53 0.53636(18) 0.1634 (3) 0.08684(7) 4.43(17) C54 0.50753(25) -0.0825 (3) 0.16708(11) 7.23(25) C55 0.36205(20) 0.2661 (4) 0.13668(12) 7.9(3) 01 0.68795(16)	C40	0.59394(17)	0.2746(3)	0.22066 (7)	4.39(16)
C43 0.62095(15) 0.2808 (3) 0.15661 (7) 3.39(13) C44 0.56349(16) 0.0969 (3) 0.15819(7) 3.65(15) C45 0.49721(18) 0.0256 (3) 0.14707(8) 4.36(16) C46 0.43416(18) 0.0907 (3) 0.15122(9) 5.39(19) C47 0.42544(16) 0.1997 (3) 0.13208(8) 4.60(16) C48 0.49196(16) 0.2702 (3) 0.14426(7) 3.76(14) C49 0.41458(17) 0.2702 (3) 0.09585(8) 4.95(17) C50 0.47024(17) 0.0969 (3) 0.08750 (7) 4.19(15) C51 0.48519(18) -0.0029 (3) 0.11068(8) 4.72(17) C52 0.44276(22) 0.0540 (4) 0.05245(9) 6.48(21) C53 0.53636(18) 0.1634 (3) 0.08684(7) 4.43(17) C54 0.50753(25) -0.0825 (3) 0.16708(11) 7.23(25) C55 0.36205(20) 0.2661 (4) 0.13668(12) 7.9(3) 01 0.68795(16) 0.2419 (3) 0.07700(8) 8.79(19) 02 0.62148(12)	C41	0.63891(15)	0.30858(24)	0.20266 (7)	3.17(13)
C44 0.56349(16) 0.0969 (3) 0.15819(7) 3.65(15) C45 0.49721(18) 0.0256 (3) 0.14707(8) 4.36(16) C46 0.43416(18) 0.0907 (3) 0.15122(9) 5.39(19) C47 0.42544(16) 0.1997 (3) 0.13208(8) 4.60(16) C48 0.49196(16) 0.2702 (3) 0.14426(7) 3.76(14) C49 0.41458(17) 0.2702 (3) 0.09585(8) 4.95(17) C50 0.47024(17) 0.0969 (3) 0.08750 (7) 4.19(15) C51 0.48519(18) -0.0029 (3) 0.11068(8) 4.72(17) C52 0.44276(22) 0.0540 (4) 0.05245(9) 6.48(21) C53 0.53636(18) 0.1634 (3) 0.08684(7) 4.43(17) C54 0.50753(25) -0.0825 (3) 0.16708(11) 7.23(25) C55 0.36205(20) 0.2661 (4) 0.13668(12) 7.9(3) 01 0.68795(16) 0.2419 (3) 0.07700(8) 8.79(19) 02 0.62148(12) 0.05716(19) 0.16892(6) 5.22(11) 03 0.49101(12)	C42	0.70138(15)	0.37104(24)	0.21839(7)	3.16(13)
C45 0.49721(18) 0.0256 (3) 0.14707(8) 4.36(16) C46 0.43416(18) 0.0907 (3) 0.15122(9) 5.39(19) C47 0.42544(16) 0.1997 (3) 0.13208(8) 4.60(16) C48 0.49196(16) 0.2702 (3) 0.14426(7) 3.76(14) C49 0.41458(17) 0.2702 (3) 0.09585(8) 4.95(17) C50 0.47024(17) 0.0969 (3) 0.08750 (7) 4.19(15) C51 0.48519(18) -0.0029 (3) 0.11068(8) 4.72(17) C52 0.44276(22) 0.0540 (4) 0.05245(9) 6.48(21) C53 0.53636(18) 0.1634 (3) 0.08684(7) 4.43(17) C54 0.50753(25) -0.0825 (3) 0.16708(11) 7.23(25) C55 0.36205(20) 0.2661 (4) 0.13668(12) 7.9(3) 01 0.68795(16) 0.2419 (3) 0.07700(8) 8.79(19) 02 0.62148(12) 0.05716(19) 0.16892(6) 5.22(11) 03 0.49101(12) 0.37086(18) 0.14487(6) 5.05(12) 04 0.53502(19)	C43	0.62095(15)	0.2808 (3)	0.15661 (7)	3.39(13)
C46 0.43416(18) 0.0907 (3) 0.15122(9) 5.39(19) C47 0.42544(16) 0.1997 (3) 0.13208(8) 4.60(16) C48 0.49196(16) 0.2702 (3) 0.14426(7) 3.76(14) C49 0.41458(17) 0.2702 (3) 0.09585(8) 4.95(17) C50 0.47024(17) 0.0969 (3) 0.08750 (7) 4.19(15) C51 0.48519(18) -0.0029 (3) 0.11068(8) 4.72(17) C52 0.44276(22) 0.0540 (4) 0.05245(9) 6.48(21) C53 0.53636(18) 0.1634 (3) 0.08684(7) 4.43(17) C54 0.50753(25) -0.0825 (3) 0.16708(11) 7.23(25) C55 0.36205(20) 0.2661 (4) 0.13668(12) 7.9(3) 01 0.68795(16) 0.2419 (3) 0.07700(8) 8.79(19) 02 0.62148(12) 0.05716(19) 0.16892(6) 5.22(11) 03 0.49101(12) 0.37086(18) 0.14487(6) 5.05(12) 04 0.53502(19) 0.26306(21) 0.08102(6) 6.01(14)	C44	0.56349(16)	0.0969 (3)	0.15819(7)	3.65(15)
C47 0.42544(16) 0.1997 (3) 0.13208(8) 4.60(16) C48 0.49196(16) 0.2702 (3) 0.14426(7) 3.76(14) C49 0.41458(17) 0.2702 (3) 0.09585(8) 4.95(17) C50 0.47024(17) 0.0969 (3) 0.08750 (7) 4.19(15) C51 0.48519(18) -0.0029 (3) 0.11068(8) 4.72(17) C52 0.44276(22) 0.0540 (4) 0.05245(9) 6.48(21) C53 0.53636(18) 0.1634 (3) 0.08684(7) 4.43(17) C54 0.50753(25) -0.0825 (3) 0.16708(11) 7.23(25) C55 0.36205(20) 0.2661 (4) 0.13668(12) 7.9(3) 01 0.68795(16) 0.2419 (3) 0.07700(8) 8.79(19) 02 0.62148(12) 0.05716(19) 0.16892(6) 5.22(11) 03 0.49101(12) 0.37086(18) 0.14487(6) 5.05(12) 04 0.53502(19) 0.26306(21) 0.08102(6) 6.01(14)	C45	0.49721(18)	0.0256 (3)	0.14707(8)	4.36(16)
C48 0.49196(16) 0.2702 (3) 0.14426(7) 3.76(14) C49 0.41458(17) 0.2702 (3) 0.09585(8) 4.95(17) C50 0.47024(17) 0.0969 (3) 0.08750 (7) 4.19(15) C51 0.48519(18) -0.0029 (3) 0.11068(8) 4.72(17) C52 0.44276(22) 0.0540 (4) 0.05245(9) 6.48(21) C53 0.53636(18) 0.1634 (3) 0.08684(7) 4.43(17) C54 0.50753(25) -0.0825 (3) 0.16708(11) 7.23(25) C55 0.36205(20) 0.2661 (4) 0.13668(12) 7.9(3) 01 0.68795(16) 0.2419 (3) 0.07700(8) 8.79(19) 02 0.62148(12) 0.05716(19) 0.16892(6) 5.22(11) 03 0.49101(12) 0.37086(18) 0.14487(6) 5.05(12) 04 0.53502(19) 0.26306(21) 0.08102(6) 6.01(14)	C46	0.43416(18)	0.0907 (3)	0.15122(9)	5.39(19)
C49 0.41458(17) 0.2702 (3) 0.09585(8) 4.95(17) C50 0.47024(17) 0.0969 (3) 0.08750 (7) 4.19(15) C51 0.48519(18) -0.0029 (3) 0.11068(8) 4.72(17) C52 0.44276(22) 0.0540 (4) 0.05245(9) 6.48(21) C53 0.53636(18) 0.1634 (3) 0.08684(7) 4.43(17) C54 0.50753(25) -0.0825 (3) 0.16708(11) 7.23(25) C55 0.36205(20) 0.2661 (4) 0.13668(12) 7.9(3) 01 0.68795(16) 0.2419 (3) 0.07700(8) 8.79(19) 02 0.62148(12) 0.05716(19) 0.16892(6) 5.22(11) 03 0.49101(12) 0.37086(18) 0.14487(6) 5.05(12) 04 0.53502(19) 0.26306(21) 0.08102(6) 6.01(14)	C47	0.42544(16)	0.1997 (3)	0.13208(8)	4.60(16)
C50 0.47024(17) 0.0969 (3) 0.08750 (7) 4.19(15) C51 0.48519(18) -0.0029 (3) 0.11068(8) 4.72(17) C52 0.44276(22) 0.0540 (4) 0.05245(9) 6.48(21) C53 0.53636(18) 0.1634 (3) 0.08684(7) 4.43(17) C54 0.50753(25) -0.0825 (3) 0.16708(11) 7.23(25) C55 0.36205(20) 0.2661 (4) 0.13668(12) 7.9(3) 01 0.68795(16) 0.2419 (3) 0.07700(8) 8.79(19) 02 0.62148(12) 0.05716(19) 0.16892(6) 5.22(11) 03 0.49101(12) 0.37086(18) 0.14487(6) 5.05(12) 04 0.53502(19) 0.26306(21) 0.08102(6) 6.01(14)	C48	0.49196(16)	0.2702 (3)	0.14426(7)	3.76(14)
C51 0.48519(18) -0.0029(3) 0.11068(8) 4.72(17) C52 0.44276(22) 0.0540(4) 0.05245(9) 6.48(21) C53 0.53636(18) 0.1634(3) 0.08684(7) 4.43(17) C54 0.50753(25) -0.0825(3) 0.16708(11) 7.23(25) C55 0.36205(20) 0.2661(4) 0.13668(12) 7.9(3) 01 0.68795(16) 0.2419(3) 0.07700(8) 8.79(19) 02 0.62148(12) 0.05716(19) 0.16892(6) 5.22(11) 03 0.49101(12) 0.37086(18) 0.14487(6) 5.05(12) 04 0.53502(19) 0.26306(21) 0.08102(6) 6.01(14)	C49	0.41458(17)	0.2702 (3)	0.09585(8)	4.95(17)
C52 0.44276(22) 0.0540 (4) 0.05245(9) 6.48(21) C53 0.53636(18) 0.1634 (3) 0.08684(7) 4.43(17) C54 0.50753(25) -0.0825 (3) 0.16708(11) 7.23(25) C55 0.36205(20) 0.2661 (4) 0.13668(12) 7.9(3) 01 0.68795(16) 0.2419 (3) 0.07700(8) 8.79(19) 02 0.62148(12) 0.05716(19) 0.16892(6) 5.22(11) 03 0.49101(12) 0.37086(18) 0.14487(6) 5.05(12) 04 0.53502(19) 0.26306(21) 0.08102(6) 6.01(14)	C50	0.47024(17)	0.0969 (3)	0.08750 (7)	4.19(15)
C53 0.53636(18) 0.1634 (3) 0.08684(7) 4.43(17) C54 0.50753(25) -0.0825 (3) 0.16708(11) 7.23(25) C55 0.36205(20) 0.2661 (4) 0.13668(12) 7.9(3) 01 0.68795(16) 0.2419 (3) 0.07700(8) 8.79(19) 02 0.62148(12) 0.05716(19) 0.16892(6) 5.22(11) 03 0.49101(12) 0.37086(18) 0.14487(6) 5.05(12) 04 0.53502(19) 0.26306(21) 0.08102(6) 6.01(14)	C51	0.48519(18)	-0.0029 (3)	0.11068(8)	4.72(17)
C54 0.50753(25) -0.0825 (3) 0.16708(11) 7.23(25) C55 0.36205(20) 0.2661 (4) 0.13668(12) 7.9(3) 01 0.68795(16) 0.2419 (3) 0.07700(8) 8.79(19) 02 0.62148(12) 0.05716(19) 0.16892(6) 5.22(11) 03 0.49101(12) 0.37086(18) 0.14487(6) 5.05(12) 04 0.53502(19) 0.26306(21) 0.08102(6) 6.01(14)	C52	0.44276(22)	0.0540 (4)	0.05245(9)	6.48(21)
C55 0.36205(20) 0.2661 (4) 0.13668(12) 7.9(3) 01 0.68795(16) 0.2419 (3) 0.07700(8) 8.79(19) 02 0.62148(12) 0.05716(19) 0.16892(6) 5.22(11) 03 0.49101(12) 0.37086(18) 0.14487(6) 5.05(12) 04 0.53502(19) 0.26306(21) 0.08102(6) 6.01(14)	C53	0.53636(18)	0.1634 (3)	0.08684(7)	4.43(17)
01 0.68795(16) 0.2419 (3) 0.07700(8) 8.79(19) 02 0.62148(12) 0.05716(19) 0.16892(6) 5.22(11) 03 0.49101(12) 0.37086(18) 0.14487(6) 5.05(12) 04 0.53502(19) 0.26306(21) 0.08102(6) 6.01(14)	C54	0.50753(25)	-0.0825 (3)	0.16708(11)	7.23(25)
02 0.62148(12) 0.05716(19) 0.16892(6) 5.22(11) 03 0.49101(12) 0.37086(18) 0.14487(6) 5.05(12) 04 0.53502(19) 0.26306(21) 0.08102(6) 6.01(14)	C55	0.36205(20)	0.2661 (4)	0.13668(12)	7.9(3)
03 0.49101(12) 0.37086(18) 0.14487(6) 5.05(12) 04 0.53502(19) 0.26306(21) 0.08102(6) 6.01(14)	01	0.68795(16)	0.2419 (3)	0.07700(8)	8.79(19)
04 0.53502(19) 0.26306(21) 0.08102(6) 6.01(14)	02	0.62148(12)	0.05716(19)	0.16892(6)	5.22(11)
	03	0.49101(12)	0.37086(18)	0.14487(6)	5.05(12)
05 0.59258(13) 0.10340(21) 0.09106(7) 6.30(15)	04	0.53502(19)	0.26306(21)	0.08102(6)	6.01(14)
	05	0.59258(13)	0.10340(21)	0.09106(7)	6.30(15)

Table III-2 (cont'd)	ZnNKAP

	····			
	х	у	Z	Biso
Zn	0.21688(4)	0.99502(3)	0.201917(16)	3.083(15)
N1	0.11388(24)	0.95417(19)	0.28328(10)	2.88(11)
N2	0.0500(3)	1.11057(20)	0.17041(11)	3.45(11)
N3	0.3400(3)	1.06924(19)	0.12723(10)	3.32(11)
N4	0.40098(25)	0.91124(19)	0.23933(10)	2.90(10)
N5	0.1902(3)	0.48962(20)	0.33522(12)	4.06(13)
C 1	0.1654(3)	0.89152(23)	0.33569(12)	2.83(13)
C2	0.0498(3)	0.88513(25)	0.38157(13)	3.40(14)
C3	-0.0699(3)	0.9397(3)	0.35530(14)	3.60(16)
C4	-0.0291(3)	0.98464(24)	0.29473(13)	3.25(14)
C5	-0.1199(3)	1.0558(3)	0.25494(15)	3.86(16)
C 6	-0.0847(3)	1.1161(3)	0.19870(14)	3.75(15)
C 7	-0.1797(4)	1.1981(3)	0.16130(15)	4.52(17)
C8	-0.1016(4)	1.2410(3)	0.11127(15)	4.76(18)
C 9	0.0432(4)	1.1849(3)	0.11672(14)	3.98(15)
C10	0.1560(4)	1.2010(3)	0.07456(14)	4.29(16)
C 11	0.2947(4)	1.14885(25)	0.07881(13)	3.75(15)
C12	0.4119(4)	1.1659(3)	0.03356(14)	4.31(17)
C13	0.5266(4)	1.0963(3)	0.05507(13)	3.93(16)
C14	0.4799(3)	1.03586(25)	0.11373(13)	3.52(14)
C15	0.5648(3)	0.9549(3)	0.15144(13)	3.55(14)

Table III-2 (cont'd)

		 		
C16	0.5295(3)	0.89722(24)	0.20870(12)	3.12(13)
C17	0.6269(3)	0.81650(24)	0.24498(13)	3.18(13)
C18	0.5576(3)	0.78370(24)	0.29839(12)	3.04(13)
C19	0.4146(3)	0.84476(22)	0.29541(12)	2.73(13)
C20	0.3075(3)	0.83959(22)	0.34129(12)	2.67(12)
C21	0.0503(4)	0.8331(3)	0.44636(15)	5.18(18)
C22	-0.2181(4)	0.9552(3)	0.38370(16)	4.84(19)
C23	-0.2310(5)	1.0607(4)	0.40887(20)	6.98(24)
C24	-0.3346(4)	1.2298(3)	0.17810(19)	6.24(22)
C25	-0.1479(4)	1.3353(3)	0.06045(18)	6.53(22)
C26	-0.1186(7)	1.4562(4)	0.06808(24)	10.4(3)
C27	0.4033(5)	1.2453(3)	-0.02657(15)	5.95(21)
C28	0.4659(6)	1.3622(4)	-0.03040(23)	10.6(3)
C29	0.6736(4)	1.0808(3)	0.02562(15)	5.29(20)
C30	0.7755(3)	0.7798(3)	0.22534(14)	3.82(15)
C31	0.7703(4)	0.6845(4)	0.19210(17)	5.59(20)
C32	0.6201(3)	0.6948(3)	0.34833(14)	3.96(16)
C33	0.3538(3)	0.78687(24)	0.40214(12)	2.87(13)
C34	0.4298(3)	0.86005(24)	0.42665(13)	3.33(14)
C35	0.4734(4)	0.8287(3)	0.48423(14)	4.09(16)
C36	0.4324(4)	0.7246(3)	0.51831(13)	4.16(16)
C37	0.3508(3)	0.6471(3)	0.49632(13)	3.61(14)
C38	0.2993(4)	0.5436(3)	0.53457(15)	5.14(19)

Table III-2 (cont'd)

C39	0.2183(5)	0.4688(3)	0.51496(16)	5.99(21)
C40	0.1941(4)	0.4887(3)	0.45534(16)	5.40(19)
C41	0.2428(4)	0.58623(25)	0.41585(13)	3.71(15)
C42	0.3166(3)	0.67258(24)	0.43659(12)	3.04(13)
C43	0.2259(4)	0.59858(25)	0.35129(14)	4.11(16)
C44	0.0492(4)	0.4801(3)	0.31609(15)	4.27(17)
C45	0.0224(4)	0.3774(3)	0.29002(15)	4.33(17)
C46	0.1110(4)	0.2726(3)	0.32199(17)	5.36(20)
C47	0.2729(4)	0.2989(3)	0.31522(17)	5.15(19)
C48	0.3036(4)	0.4064(3)	0.33738(15)	4.70(17)
C49	0.3226(4)	0.3252(3)	0.25072(19)	5.89(22)
C50	0.2364(4)	0.4235(3)	0.21058(16)	4.87(19)
C51	0.0725(4)	0.4051(3)	0.22488(16)	4.86(19)
C52	0.2734(5)	0.4187(4)	0.14656(19)	7.6(3) .
C53	0.2788(4)	0.5458(3)	0.21248(16)	5.38(20)
C54	-0.1416(4)	0.3536(3)	0.29604(19)	6.27(23)
C55	0.3629(5)	0.1949(3)	0.34799(23)	8.6(3)
C56	0.0918(6)	0.8678(4)	0.11137(18)	8.3(3)
O 1	0.1305(3)	0.85711(18)	0.16790(10)	5.19(12)
O2	-0.0425(3)	0.55350(20)	0.31960(12)	5.95(14)
О3	0.4216(3)	0.42435(20)	0.35399(11)	5.83(14)
O4	0.4203(3)	0.55604(24)	0.22004(14)	7.85(18)
O5	0.1949(3)	0.62726(20)	0.20503(13)	7.24(16)
HO1	0.159(4)	0.798(3)	0.1842(15)	8.4(10) .

Table III-3. Selected Bond Distances (Å) and Angles (deg) and Their Estimated Standard Deviations for NKAP and ZnNKAP.

	NKAP		ZnNKAP
	Distances		
		Zn-N1	2.0482(24)
		Zn-N2	2.063(3)
O(1)-HO(5)	2.01(3)	Zn-N3	2.063(3)
		Zn-N4	2.0578(24)
		Zn-O	2.1587(24)
	**************************************	O(4)-HO(5)	1.657(3)
	Angles		
		N1-Zn-N2	91.36(10)
		N1-Zn-N4	87.45(9)
O(5)-HO(5)-O(1)	173(4)	N2-Zn-N3	87.44(10)
		N3-Zn-N4	90.63(9)
		O(4)-HO(5)-O(5)	159(4)

naphthalene connector. Not only is the C20-C33-C42 angle at $126.54(25)^{\circ}$ larger than $123.5(6)^{\circ}$ found in the parent naphthoic acid, but the porphyrin plane also bends outwardly by as much as 9° from the C20-C33 axis (Figure III-1c), resulting in a bigger "bite" than otherwise possible. Laterally, the C20-C33 bond deviates from the naphthalene plane by tilting about 6° in the C5 direction and is supplemented by further distortions at C20 (the C19-C20-C33 angle of $117.57(25)^{\circ}$ is larger than the C1-C20-C33 angle of $115.06(25)^{\circ}$), to displace the porphyrin core to the right (Figure III-1b), presumably to achieve the best alignment with the water proton. Despite this, it is significant that the imide-to-naphthalene linkage retains its near perfect alignment and C_2 symmetry (with only a slight rotation along the C43-N5 bond). Undoubtedly, much of this rigidity arises from the nonbonding interaction between the C43 methylene and the porphyrin whereby the substituent at C43 obtains a predictable conformation.

The zinc complex of NKAP crystallized from methylene chloride solution layered with methanol has a methanol molecule as axial ligand with the O-Zn distance of 2.1587(24) Å (Figure III-2a). The methanolic proton is H-bonded to the carbonyl group of the Kemp's acid with a distance of 1.98(3) Å. In order to accommodate this H-bond, the superstructure is twisted off center (Figure 2b). The naphthalene spacer and the porphyrin ring also distort severely from the ideal C20-C33 axis (Figure 2c). The "jaw-opening" observed in ZnNKAP is even greater than that in the free base NKAP.

In both structures, the porphyrin skeleton remains essentially unchanged. The X-ray structures clearly indicate that the NKAP system is

ideal for binding small, preferably monoatomic substrates. By inference supported by molecular modeling, the AKAP compounds with a greater porphyrin to acid distance should serve as good receptors for larger substrates.

2. Substrate Binding Studies

The magnitude of molecular inclusion is followed by ¹H NMR studies, UV-vis spectroscopy and differential scanning calorimetry.

a) Substrate Binding of Metal-free Systems

The magnitude of molecular inclusion was followed by ¹H NMR titration carried out in CDCl₃. Upon stepwise addition of guest molecules into the porphyrin solution, all the protons of the Kemp's acid superstructure exhibited downfield shift due to less diamagnetic ring current. This downfield shift suggested that upon binding of the guest molecule, a "jaw-opening" motion occurred at the porphyrin-spacer I conjunction. On the other hand, along this motion, the naphthyl proton on C34 experienced an upfield shift due to the tilting of naphthalene, bringing this proton closer to the porphyrin. A similar shift was also observed for the corresponding proton on anthracene in AKAP. The binding constants were derived from the chemical shift of naphthyl or anthryl methylene protons as well as by distinctive shifts of other protons during the titration process.

For studying the H₂O binding to NKAP, it is crucial that all reagents and the NMR tube are as anhydrous as possible. The binding of water to NKAP is strong enough that the saturation point can be reached before the

solubility of water in CDCl₃ becomes a problem.⁷ Figure III-3 displays ¹H NMR spectra showing the chemical shift of the naphthyl methylene proton at varying concentrations of water.

The DSC (differential scanning calorimetry) analysis was also applied to the solid crystals of NKAP- H_2O . The DSC (Figure III-4) showed two endothermic peaks, with the first one attributable to dehydration and the second peak coinciding with the melting of the compound. Continuous heating led to decomposition. The heat flow associated with the first peak is 18.76 J g^{-1} , indicating that the water binding energy is about $-15 \pm 1 \text{ kJ mol}^{-1}$.

For the AKAP binding of imidazole or purine, the interaction presumably relies on multipoint recognition as depicted by the computer model (Figures III-6, 7). The titration (Figure III-5) data give a 1:1 complex with binding constants of 2550 and 2600 M⁻¹ for imidazole and purine, respectively. As purine is a weaker base than imidazole (Table III-4), the comparable binding strength of the two bases suggests that the intrinsic basicity is not the determining binding force. In our systems, π - π interactions between the guest and host molecules need not to be considered. Therefore, the attractive forces solely come from the H-bonding network.

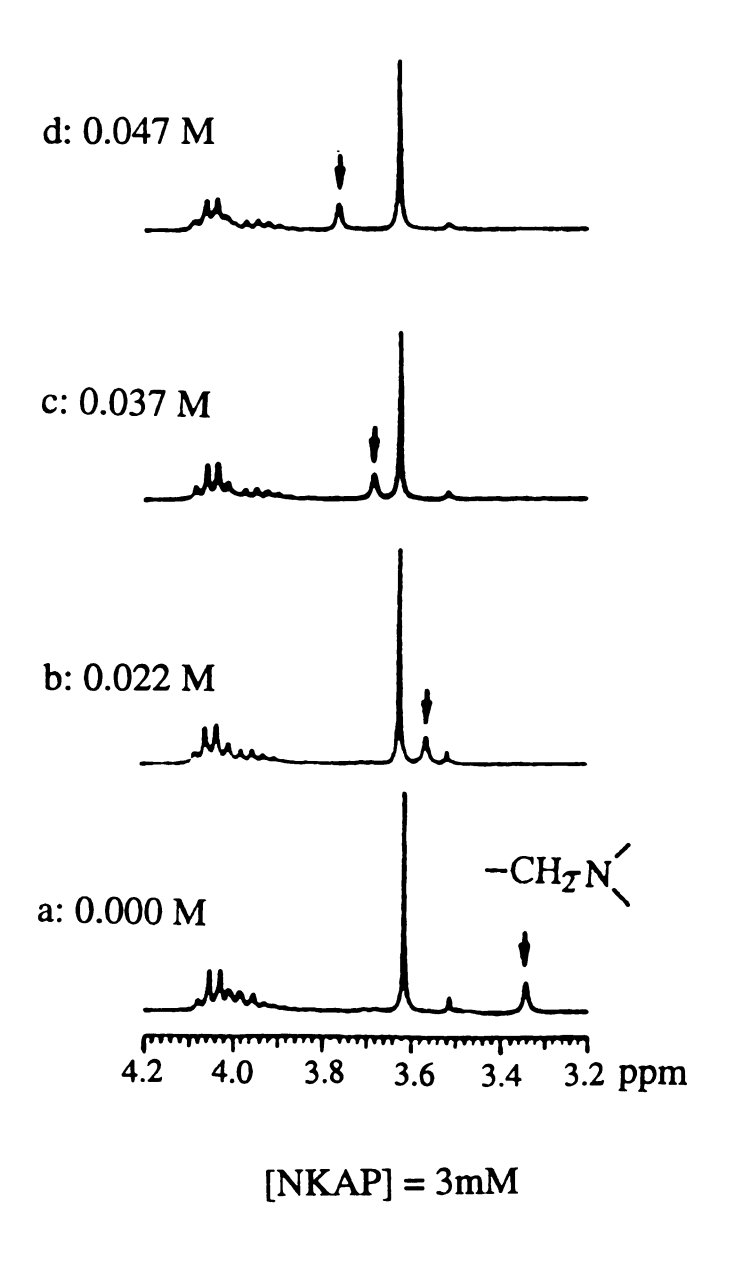


Figure III-3. ¹H NMR titration of H_2O into NKAP. [NKAP] = 3 mM, [H_2O] in a: 0.000; b: 0.022; c: 0.037; d: 0.047 M.

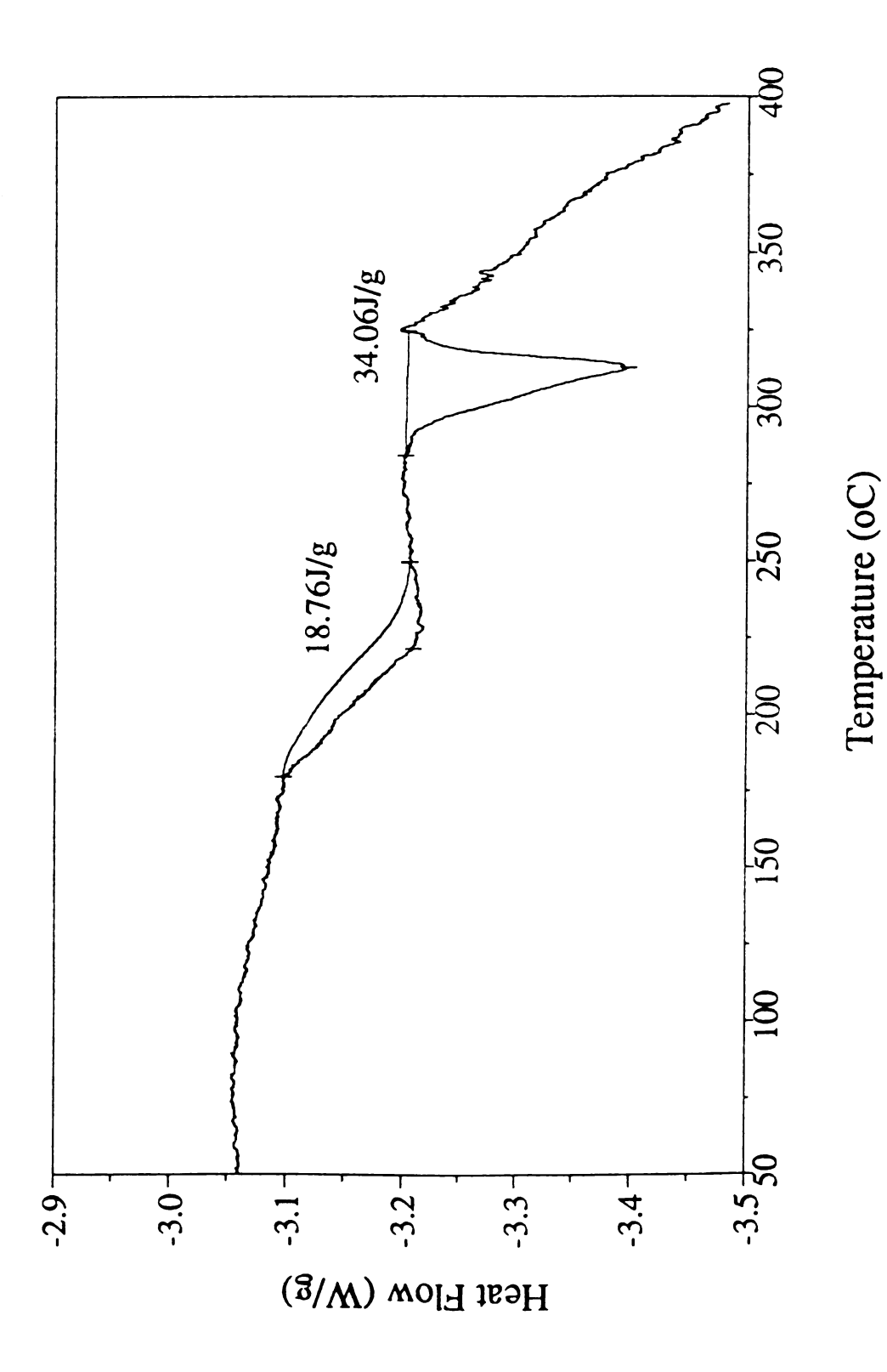


Table III-4. DSC measurement of NKAP-water complex.

Figure III-5. ¹H NMR of Imidazole Titration of AKAP. [AKAP]=

0.00276 M,[Im] in a: 0.0000 M; b: 0.0082 M;

c: 0.0272 M; d: 0.3264 M.

Arrow pointed peak(s) in 0.0-2.5 ppm, protons on Kemp's derivative;

in 3.3-4.4 ppm, -CH₂-N<;

in 6.0-10.4 ppm, proton on anthracene as shown in the

following structure.

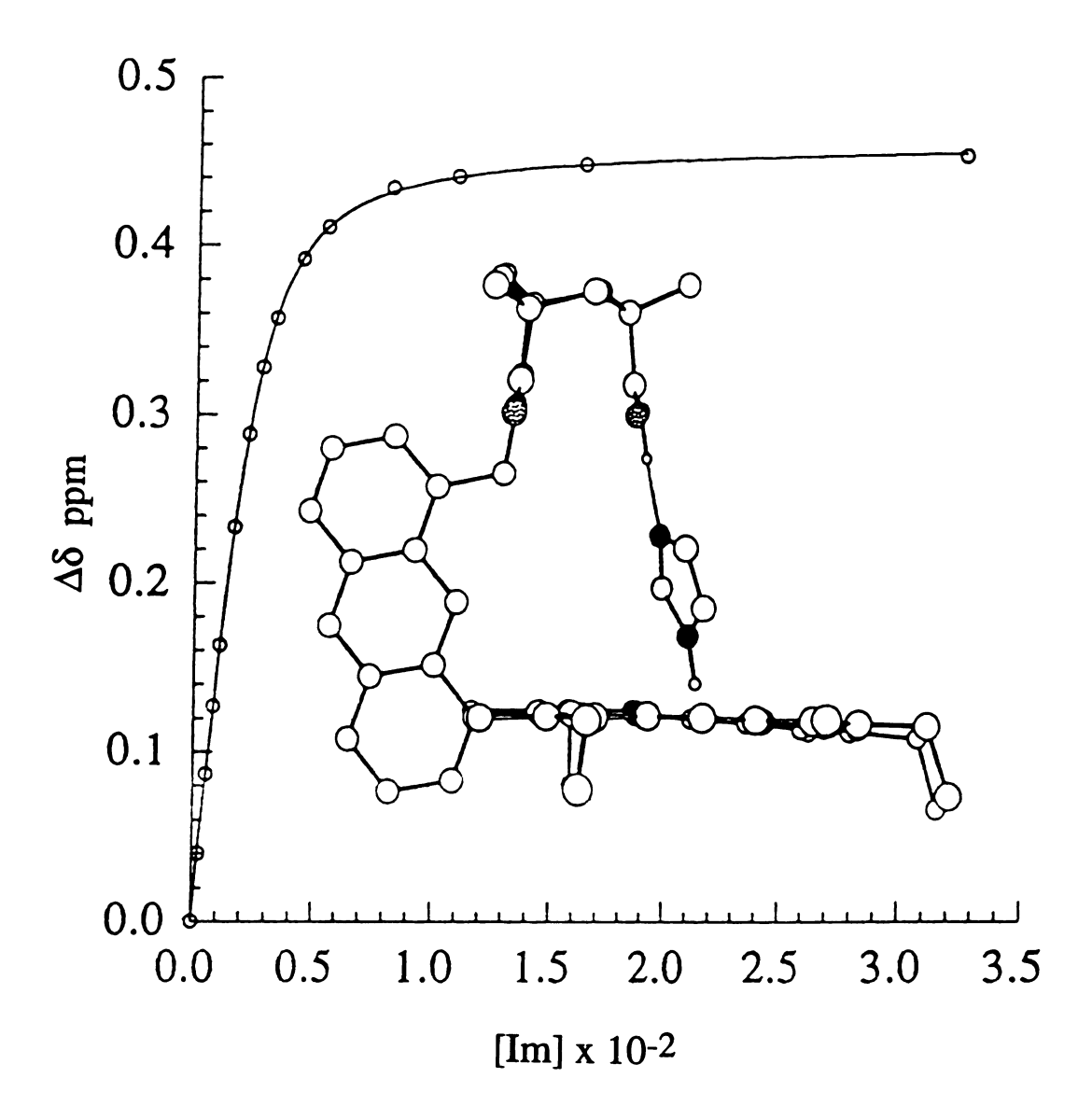


Figure III-6. Schematic structure of AKAP-imidazole and plot of the anthryl methylene protons as a function of concentration of imidazole in CDCl₃.

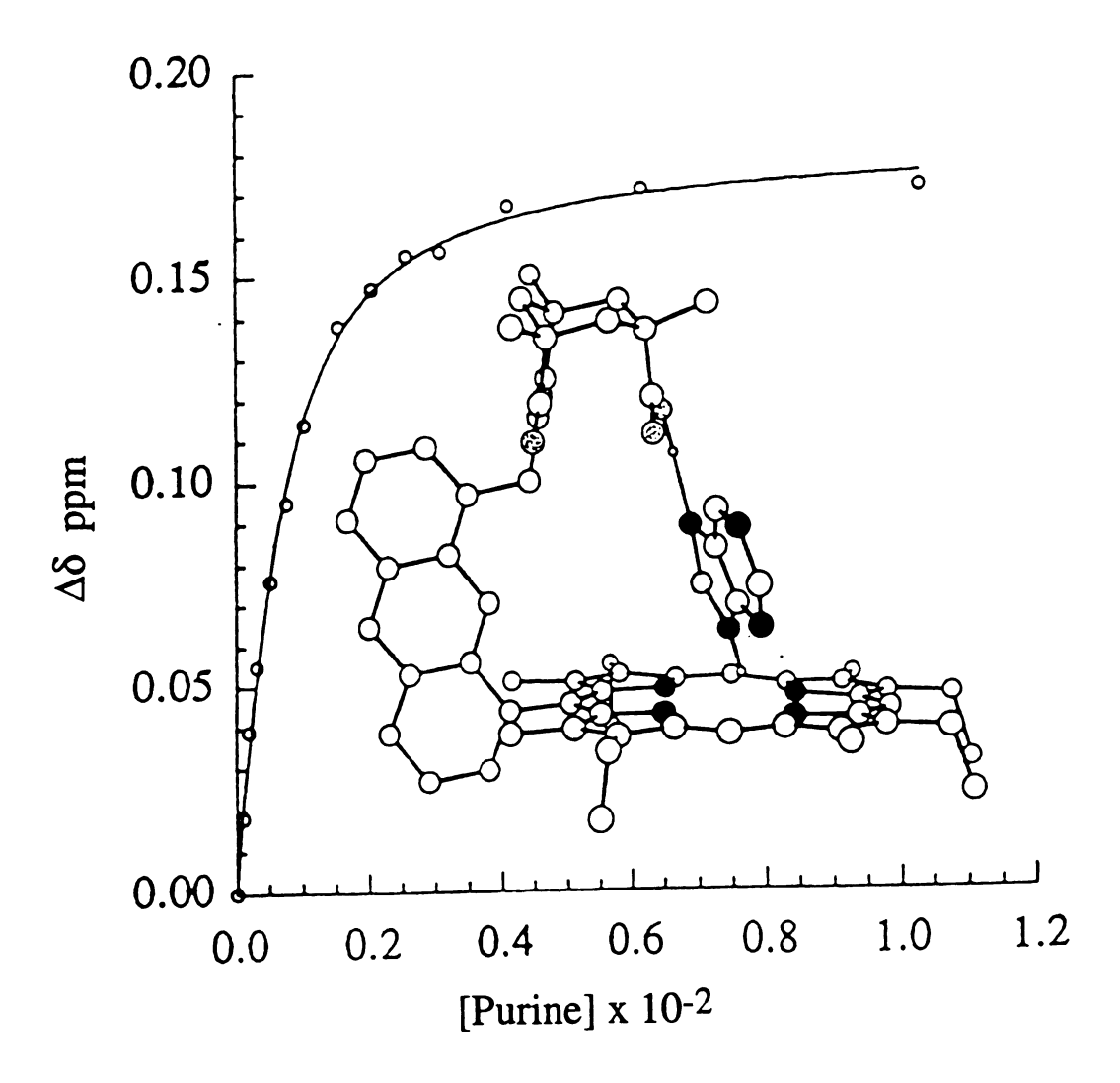


Figure III-7. Schematic structure of AKAP-Purine and plot of the anthryl methylene protons as a function of concentration of purine.

Table III-4. Association Constants for NKAP and AKAP with Substrates.

b) Substrate Binding of Zinc Porphyrins

In order to estimate how much stabilization energy the C-clamp acid group can impart to metalloporphyrin-ligand binding, we examined the zinc porphyrin as a model. The same protocol of ¹H NMR titration as mentioned previously was used for the C-clamp zinc porphyrin systems. A typical NMR titration of ZnNKAP-MeOH is shown in Figure III-8. For the control study using ZnOEP (octaethylporphyrin) whose guest-host interactions cannot be easily followed by ¹H NMR, UV-vis spectroscopy was used to monitor ligand binding. The binding constants of these systems are listed in Table III-5.

Methanol ligation to zinc porphyrin has been well studied.^{3 k} ZnNKAP binds MeOH stronger than the unfunctionalized ZnOEP ($\Delta\Delta G = 3.1 \text{ kJ mole}^{-1}$) due to the additional binding force derived from the H-bonding clearly shown in the crystal structure.

DMF is often employed as solvent for heme model studies and knowledge of DMF binding would be useful. However, DMF titration of ZnNKAP monitored by either ¹H NMR or UV-vis failed to show any evidence for enhanced binding. This may be due to both steric and electronic factors. DMF coordination to metalloporphyrin through the oxygen lone pair would induce the N-methyl groups to bump into the pendant acid group; coordination to zinc also reduces the electron density on the amide oxygen for which H-bonding must compete. The binding constants of ZnOEP and ZnNKAP are practically the same as DMF can bind to zinc from the unhindered side.

Figure III-8. ¹H NMR titration of methanol to ZnNKAP.

[ZnNKAP] = 0.014M and [MeOH] in a: 0.000;

b: 0.013; c: 0.032; d: 0.064; e: 0.132; f: 0.395 M.

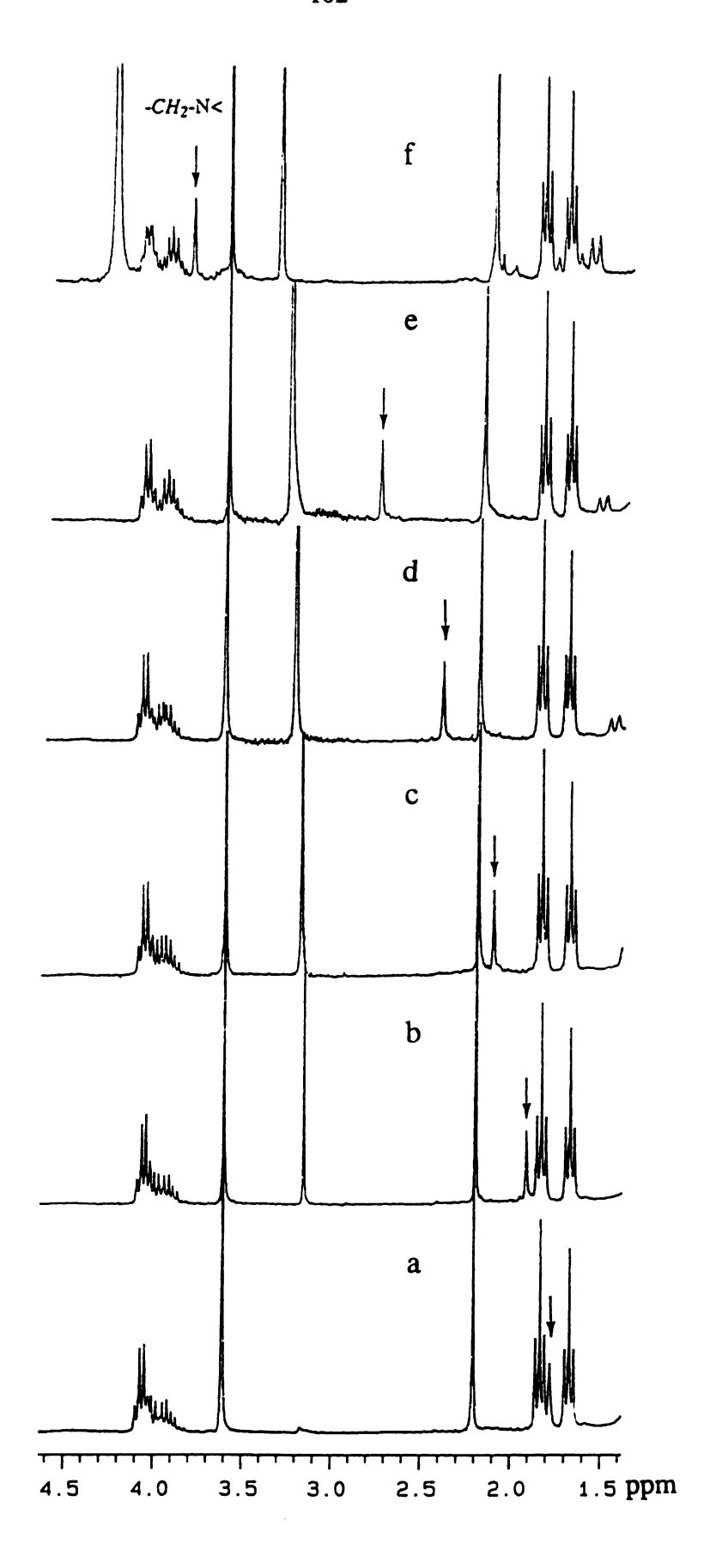


Table III-5. Association Constants of Zn-porphyrins with MeOH and Triazoles.

	-1/2-			
Receptor	Substrate	Basic pKa	$K_a (M^{-1})$	$\Delta\Delta G(KJ \text{ mol-}1)$
ZnOEP	МеОН	ı	7±1	
ZnNKAP	МеОН	1	25±3	3.1(vs ZnOEP)
ZnOEP	DMF		8 ± 1	
ZnNKAP	DMF		5±1	
ZnOEP	1,2,3-triazole	1.2	130 ± 20	
ZnAKAP	ZnAKAP 1,2,3-triazole	1.2	3000 ± 70	7.8 (vs ZnOEP)
ZnOEP	1,2,4-triazole	2.3	390 ± 40	2.7 (vs 1,2,3-triazole)
ZnAKAP	1,2,4-triazole	2.3	21000 ± 1000	9.9 (vs ZnOEP)
				4.8 (vs 1,2,3-triazole)

The most dramatic effect in molecular inclusion has been seen in the case of triazoles. 1,2,4-Triazole, being a weaker base (pKa 2.3)8 than imidazole, is normally not a strong ligand for metalloporphyrins. But ZnAKAP maximizes the binding by a three-point contact as depicted in the schematic structure (Figure III-9). The binding constant is $21,000 \pm 1000$ M⁻¹, with a free energy gain of 9.9 kJ mol⁻¹. ¹H-1,2,3-triazole, capable of only a two-point interaction, displays a significant decrease in binding energy ($\Delta\Delta G$ 4.8 kJ mol⁻¹). The binding of 1,2,4-triazole was conducted by adding aliquots of concentrated CD₃OD solution of the base to the zinc porphyrin dissolved in CDCl₃ due to insolubility of the base in pure CDCl₃. The 1,2,3-triazole study was measured in pure CDCl₃, and the energy gain is 9.4 kJ mol⁻¹, even in the presence of small amount of methanol employed to improve solubility. However, the ¹H-1,2,3-triazole, capable of only a two point interaction, displays a significant decrease in binding energy ($\Delta\Delta G$ 4.5 kJ mol⁻¹). The binding of 1,2,3,-triazole was tested in the condition of dissolve all reagents in CDCl₃, as well as in the condition that very concentrated 1,2,3-triazole in CD₃OD titrated to zinc porphyrin CDCl₃ solution. Both experiments gave the same binding constant within the margin of experimental error. The CD₃OD actually acts more as solvent than binding competitor due to its relative small binding constant. The binding selectivity of ZnAKAP over different triazoles may be a useful way to separate such heterocyclic bases.

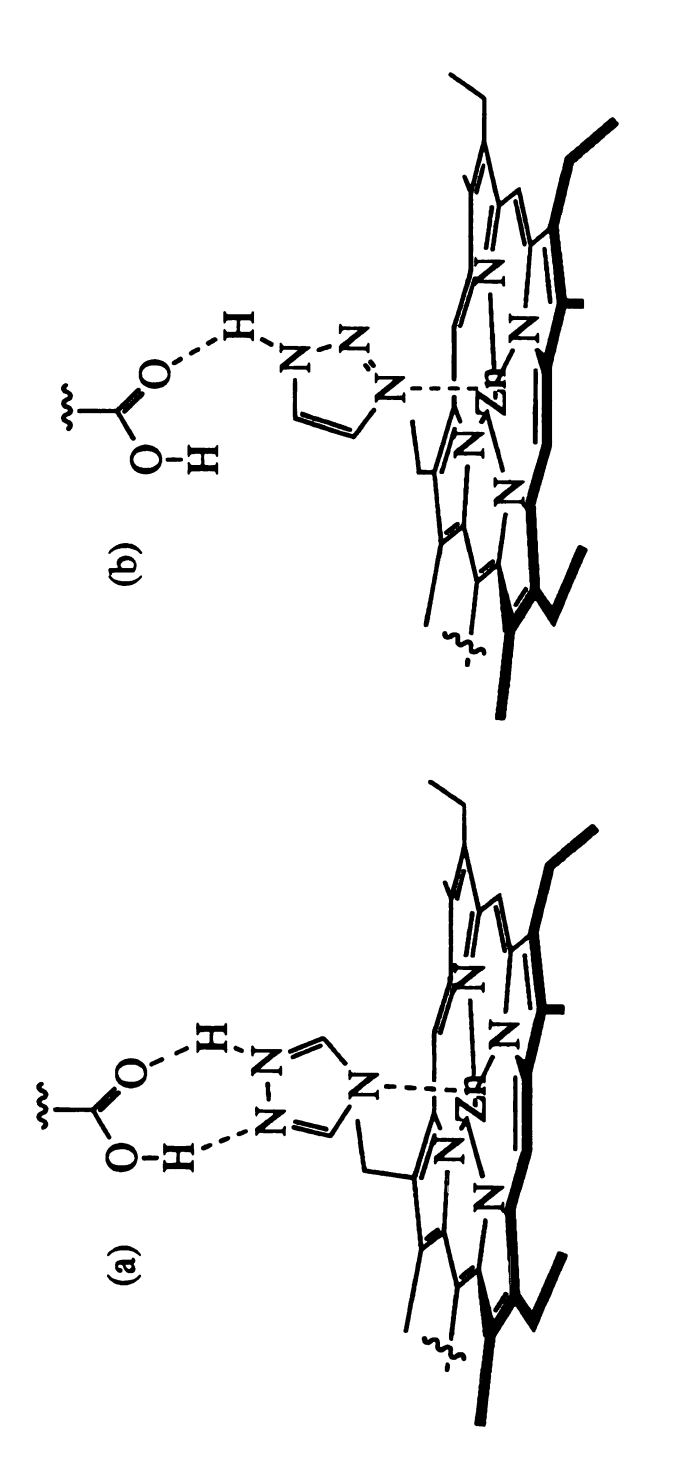


Figure III-9. (a) ZnAKAP-1,2,4-triazole. (b) ZnAKAP-1,2,3-triazole.

3. Discussion

The X-ray structure of the NKAP-H₂O complex allows a rare opportunity to examine the geometry of the acid-H₂O interface. *Ab initio* calculations of benzoic acid monohydrate predict two possible conformations, syn and anti, with the syn being the more stable form. The optimized geometric distances and angles are shown in Figure III-10. The salient feature is that the H-bond COH····O is slightly shorter and less bent than the C=O···H bond. The NKAP-H₂O clearly displays a syn conformation with a slightly shorter and near linear COH····O and a more bent H-bonding for the carbonyl group. The agreement between our structure and the theoretical model seems excellent given the other constraints that the water has to meet within this artificial molecular cleft.

Molecular inclusion in C-clamp porphyrins is brought about by multiple H-bonding. It is always interesting to identify the contribution of each individual hydrogen bond within the overall free energy of complexation. Selective removal of certain H-bonding participants from either the receptor or the substrate has been an important tactic in addressing this question. However, H-bond obliteration studies of this type must be treated with caution since other changes in the molecular properties, such as basicity and conformation, may contribute to the differences in binding energy. A comparison of ZnOEP vs ZnAKAP binding of 1,2,3-triazole provides an estimation of the magnitude of H-bonding strength of acid C=O···H. The energy difference here is 7.8 kJ mol-1. This ΔΔG may be compared to the 3.1 kJ mol-1 observed in MeOH binding to ZnNKAP vs ZnOEP. The difference clearly has something to do with the acidity of the proton (NH vs OH). Another useful comparison

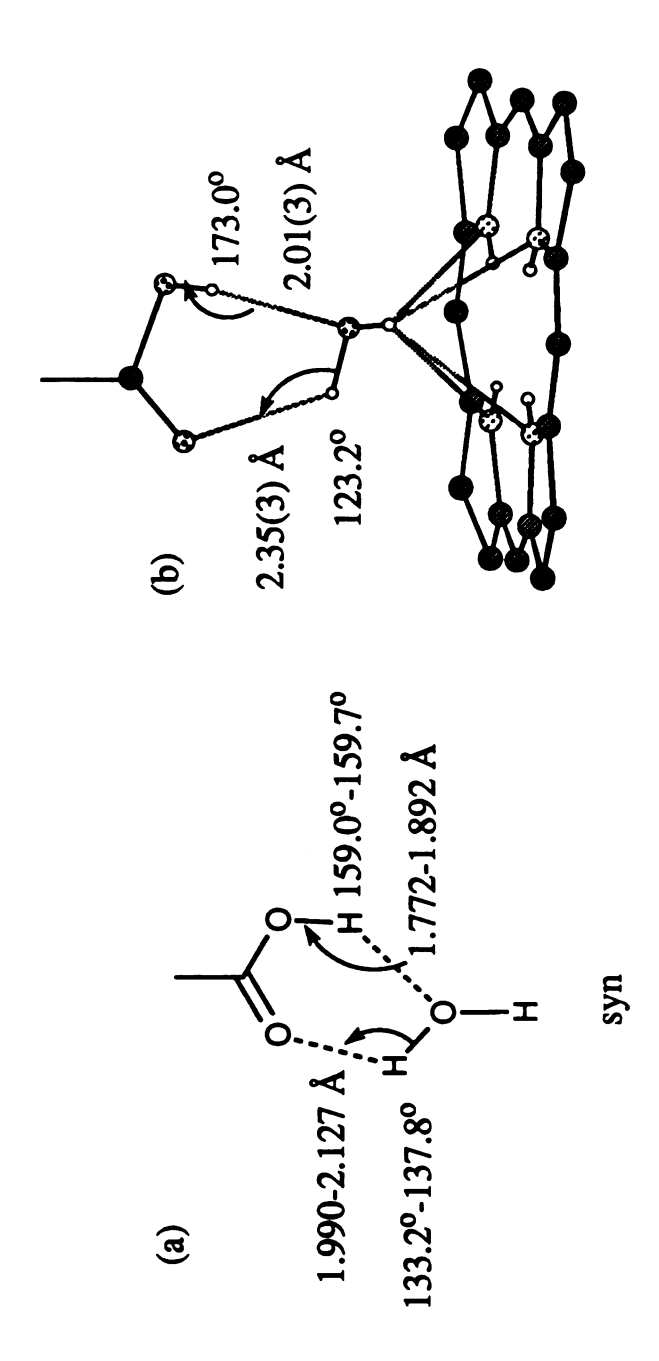


Figure III-10. (a) Calculated structure of syn acid monohydrates. (b) Partial X-ray single crystal structure of NKAP-H₂O.

is the 3-point (1,2,4-triazole) vs 2-point (1,2,3-triazole) contact. The $\Delta\Delta G$ value of 4.8 kJ mol⁻¹ arises from more than just the extra H-bond. The basicity difference of the two triazoles has significantly influenced the Zn-N bond (2.7 kJ mol⁻¹) whereas its effect on the NH···O=C is possibly very small.

D. Conclusion

In conclusion, the functionalized porphyrin receptors, NKAP, AKAP and their zinc complexes, are capable of binding and recognizing various small neutral molecules. The shape and rigidity of the superstructure porphyrin make possible some very effective complexation of substrates through multipoint recognition. The selectivity demonstrated by ZnAKAP suggests possible applications for the separation of heterocyclic bases. It is also possible to further modify the overhanging carboxyl group to effect more sophisticated substrate binding and recognition.

E. References

- 1. Ciba Foundation Symposium, "Host-Guest Molecular Interactions: From Chemistry to Biology", 1991, John Wiley & Sons.
- 2. Momenteau, M.; Reed, C. A. Chem. Rev. 1994, 94, 659-698.
- a) Lindsey, J. S.; Kearney, P. C.; Duff, R. J.; Tjivikua, P. T.; Rebek,
 J., Jr. J. Am. Chem. Soc. 1988, 110, 6575-6577.
 - b) Aoyama, Y.; Yamagishi, A.; Asagawa, M.; Toi, H.; Ogoshi, H. J. Am. Chem. Soc. 1988, 110, 4076-4077.
 - c) Ogoshi, H.; Hatakeyama, H.; Yamamura, K.; Kuroda, Y. Chem. Lett. 1990, 51-54.
 - d) Imai, H.; Nakagawa, S.; Kyuno, E. J. Am. Chem. Soc. 1992, 114, 6719-6723.
 - e) Slobodkin, G.; Fan, E.; Hamilton, A. D. New J. Chem. 1992, 16, 643-645.
 - f) Hayashi, T.; Miyahara, T.; Hashizume, N.; Ogoshi, H. J. Am. Chem. Soc. 1993, 115, 2049-2051.
 - g) Mizutani T.; Ema, T.; Tomita, T.; Kuroda, Y.; Ogoshi, H. J. Am. Chem. Soc. 1994, 116, 4240-4250.
 - h) Kuroda, Y.; Ogoshi, H.; Synlett. 1994, 319-324.
 - i) Kuroda, Y.; Kato, Y.; Ito, M.; Hasegawa, J.; Ogoshi, H. J. Am. Chem. Soc. 1994, 116, 10338-10339.
 - j) Shipps, G., Rebek, J. Tetrahedron Lett. 1994, 35, 6823-6826.
 - k) Bonar-Law, R. P.; Snaders, J. K. M. J. Am. Chem. Soc. 1995, 117, 259-271.

- 4. Chang, C. K., Liang, Y.; Avilés, G.; Peng, S.-M. J. Am. Chem. Soc. 1995, 117, 4191-4192.
- 5. Liang, Y.; Chang, C. K. Tetrahedron Lett. 1995, 36, 3817-3820.
- a) Wilcox, C. S. in "Frontiers in Supramolecular Organic Chemistry and Photochemistry", Schneider, H.-J., Durr, H., Eds.; VCH: Weinheim, Germany, 1990, 122-143.
 b) Wilcox, C. S., Cowart, M. D. Tetrahedron Lett. 1986, 27, 5563-5566.
- 7. Staverman, A. J. Recl. Trav. Chim. 1941, 60, 836-841.
- 8. Albert, A. "Heterocyclic Chemistry", 2nd Ed., Oxford University Press: New York, 1968, 441.
- 9. Nagy, P.; Durant, G. J.; Smith, D. A. in "Modeling the Hydrogen Bond", Smith, D. A., Ed., American Chemical Society, Washington, DC, 1994, 60-79.

Chapter IV

Conformational Control of Intramolecular Hydrogen Bonding in Heme Models: Maximal Co(II)-O₂ Binding in Naphthalene Kemp's Acid Porphyrin

A. Introduction

Hydrogen bonding plays a crucial role in heme protein reactions. In myglobin (Mb) and hemoglobin (Hb), the interaction between the distal histidyl proton and the heme-bound O₂ has been identified as the most significant factor controlling O₂ binding.¹ In catalase and peroxidase, H-bond polarizes the peroxy group to facilitate a heterolytic O-O bond cleavage.² Likewise, in cytochrome a₃, the presence of proton donor is an integral part of O₂ reduction.³ The study of H-bonding effects, therefore, is always a focal point in heme model chemistry. In early times, such studies were mainly confined to intermolecular interactions such as solvent effects, but more recently, synthetic models equipped with intramolecular proton donors have emerged.⁴⁻⁸ While these models clearly established the

positive effect of enhancing O₂ affinity, they did not permit a closer look at how structural and steric perturbations made by the proton donor would influence the heme-substrate reactions. For example, from X-ray⁹ and neutron diffraction¹⁰ data, it has been noted that the H-bonding between the distal histidine and Fe-O₂ in Mb and Hb is an oblique one,⁷ raising possibilities that the proton could interact with both O₁ and O₂. Most model systems available to date, as exemplified by the naphthoic acid porphyrin (NAP),⁵ have the H-bond at O₂ in a stretched-out, coplanar Fe-O₁-O₂···H. Model NAP also has a fatal fault as it undergoes an unusual ring degradation giving rise to an oxaporphyrin.¹¹ In an effort to address the H-bond conformation issue and to sidestep the metabolism of NAP, NKAP and AKAP¹² were designed and synthesized in which the proton donor is overhanging above the heme binding site.

The result of O₂ binding affinity of Co(II)NKAP will be compared with that of Co(II)AKAP and Co(II)NAP in this chapter. Conformational information then can be obtained about H-bonding effect on O₁ or O₂ which affects the O₂ affinity for heme proteins. Additional information from ¹⁵N NMR of Fe(CN)₂ porphyrins provides further support to our conclusion about H-bonding effect.

B. Experimental

(1) Cobalt insertion

The synthesis of the naphthalene Kemp's Acid Porphyrin (NKAP) and its derivatives is described in Chapter II. Cobalt ion was inserted into the porphyrins by heating a methanol solution of cobaltous chloride together with a dichloromethane solution of the free-base porphyrin

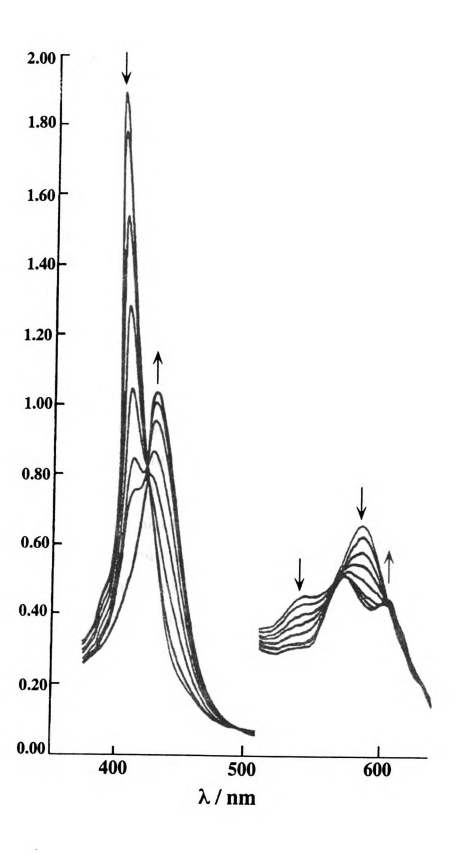
containing a trace amount of sodium acetate. Co(II) complexes were precipitated by graduate evaporation of dichloromethane. Water was added and CH₂Cl₂ was used to extract the cobalt porphyrin. Pure cobalt porphyrin was then obtained after the solvent was removed by rotary evaporation under aspirator vacuum.

(2) O₂ Binding studies

The dioxygen binding experiments were conducted by using fresh inserted Co-complexes. The Co-porphyrins (0.5 mg) were dissolved in CH₂Cl₂ (5 ml) and the solution was degassed by passing argon through it for 30 min. The solution was then transferred to a gas-tight syringe containing a degassed solution of sodium dithionite in water. The reduced Co(II) porphyrins were injected to a 60 ml tonometer and redissolved in freshly distilled DMF (4 ml) The mixture was degassed 3-7 times by freeze-pump-thaw cycles at around 10-5 torr.

Oxygenation was monitored spectrophotometrically at several temperatures. The low temperatures were achieved by immersing the tonometer in a dewar filled with liquid propane (b.p. -42°C), liquid Freon 12 (b.p. -30°C), slush bath of benzyl alcohol (-17°C) or water/crushed ice (0°C). The dioxygen adducts were stable at -42°C but underwent auto oxidation rapidly at room temperature (t_{1/2} at 0°C in most cases were about 4 min). The dioxygen affinities were determined by direct titration of Co(II)porphyrin with pure O₂ or fresh air, using a standard spectrophotometric procedure used by Halpern and coworkers. A typical titration spectrum is shown in Figure IV-1. After each injection of pure oxygen or fresh air, the solutions were allowed to stand for about

Figure IV-1. Typical O₂ titration spectra of Co(II)porphyrins.



2 minutes to reach equilibrium before the spectra were measured. The solubility of O₂ in DMF at low temperature is not determined and all the equilibrium constants are calculated at the standard state of 1 torr. The titration curves typically had correlation coefficients of 0.990 to 0.999 and varied between experiments by less than 15%. The equilibrium constants shown in Table IV-1 are the average of 2-4 runs. Since the UV-vis spectrum of the oxygenated complexes is very similar with that of the oxidized Co(III) complex, the solution of O₂ complex was pumped again after the titration in order to obtain the original spectrum of Co(II) porphyrin. This process also proved that no oxidation had taken place during the O₂ titration.

(3) Iron insertion

The typical ferrous sulfate method was used for Fe(III) insertion. ¹⁴ Free base porphyrin (10 mg) was dissolved in 30 ml mixed solvent of acetic acid: pyridine (20:1). This porphyrin solution was placed in a pear-shaped flask with a gas inlet tube. Argon was passed through the gas inlet to the solution and the mixture was heated on a steam bath to 80°C. A saturated aqueous solution of ferrous sulfate was added by a syringe into the reaction system through the gas outlet side arm. The temperature was then raised to 90°C for half an hour. The argon flow was terminated and the mixture was allowed to cool down to room temperature. A stream of air was introduced upon the cooling to allow the auto oxidation of the unstable Fe(II) porphyrin complex. Water was added and the porphyrin was extracted by CH₂Cl₂. Purification from column gave the μ-oxo dimer which was then washed with 5% HCl solution to generate Fe(III) porphyrin chloride.

(4) ¹⁵N NMR studies

The ¹⁵N NMR measurement was performed by dissolving 3-5 mM high-spin ferric porphyrins in 0.75 ml DMSO-d₆. A 10-fold excess of KC¹⁵N (98%, Icon Inc.) was added to this porphyrin DMSO solution and color change was observed instantly. The ¹⁵N NMR was collected on a Varian VXR 500 spectrometer. The sweepwidth for a normal ¹⁵N spectrum is 100 MHz. A 200 µs delay prior to acquisition serves to diminish acoustic probe ringing. At room temperature, spectra of Fe(CN)₂ porphyrins usually require 30,000 to 80,000 scans. The chemical shift of the Fe bound C¹⁵N was recorded with excess KC¹⁵N as the reference peak set at -100 ppm.

C. Results and Discussion

1. Oxygen Binding

To measure O_2 binding, both Co(II) and Fe(II) have been tested, but Fe(II)NKAP proves to be too labile even at -42°C. The O_2 adduct of Co(II)NKAP is much more stable with DMF serving as solvent and weak trans-ligand. Appreciable auto oxidation does not occur below -20°C and $t_{1/2}$ at 0°C is about 4 minutes. Reversible O_2 binding of Co(II)NKAP was studied spectrosphotometrically in a tonometer at several temperatures (-42°C, -30°C, -17°C and 0°C). Thermodynamic parameters (ΔH and ΔS) were then derived from the van't Hoff plot (Figure IV-2). Table IV-1 summarizes the O_2 binding parameters of several relevant models, including NKAP, AKAP, NAP and equine myoglobin. 18

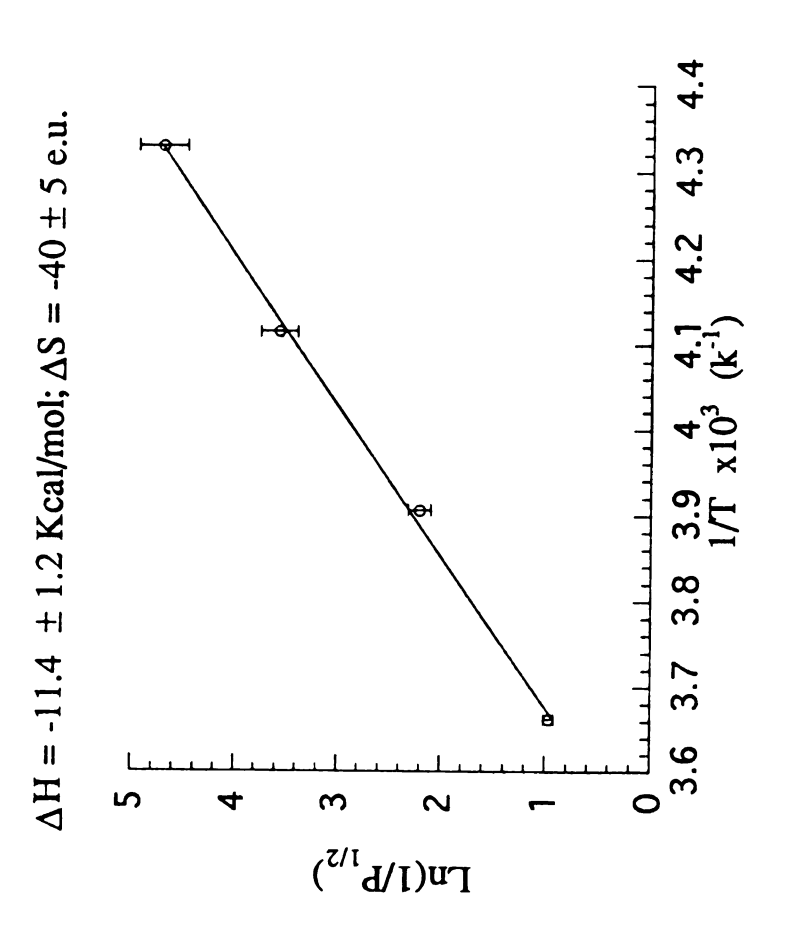


Figure IV-2. Van't Hoff plot of 1/T vs Ln(1/P_{1/2}).

Table IV-1. O₂ Binding Parameters to Co(II)porphyrins.

0 400 6 -30 -30 -30 -30 -30 -30 -30 -30 -30 -30	0.009 ± 0.001 0.028 ± 0.005 0.11 ± 0.02 0.38 ± 0.10 2.3)	-11.4 ± 1.2	-40±5
0 # 13 	0.028 ± 0.005 0.11 ± 0.02 0.38 ± 0.10 2.3	-11.4±1.2	-40±5
	0.11 ± 0.02 0.38 ± 0.10 2.3	-11.4 ± 1.2	-40±5
	0.38 ± 0.10 2.3)		
(25)	2.3)		
<i>I</i> ,			
\$ \$ \$ \$ \$ \$ \$ \$ \$ \$ \$ \$ \$ \$ \$ \$ \$ \$ \$	2.4 ± 0.3		
О.Н	0.028		
11-	0.24	-14.3	-56
	5.00		
Me Ester of NKAP & AKAP 42	>200		
CoMb (Equine) 18 25	57	-11.3	46

The O_2 affinity was evaluated by $P_{1/2}$. As shown in Figure IV-3, for the equilibrium of the O_2 binding, the binding constant is described in equation I. When half of the Co(II) porphyrin is coordinated, the pressure of O_2 added is termed as $P_{1/2}$. The binding constant is then derived as reversely proportional to $P_{1/2}$. The lower the $P_{1/2}$ is, the higher the O_2 affinity will be.

The $P_{1/2}$ obtained at -42°C from Co(II)NKAP is an all-time record for Co(II) porphyrin models. It is at least three times better than that of Co(II)NAP reported previously.⁵ The $5x10^4$ -fold enhancement from the ester to acid is truly dramatic. The affinity is even higher if a stronger trans ligand is present.¹⁶ In the anthracene case, the enhancement is less impressive. The increase from ester to acid is only about 10^2 , demonstrating the importance of the distance and geometry of the proton donor. This difference may be due to a mismatch of the geometry and/or increased motion of the pendent group. The difference between the Co(II)NKAP and Co(II)NAP at first seems hard to reconcile. Even if the previous $P_{1/2}$ of Co(II)NAP at O°C is given a tenfold reduction,¹⁷ the adjusted ΔH and ΔS are still much more negative than Co(II)NKAP. We believe that the disparity is caused by the mode of H-bonding. In Co(II)NAP, the coplanar and inflexibile Fe-O-O···H has the highest gain in ΔH but suffers the highest loss in ΔS .

As already discussed in Chapter III, the C-clamp NKAP is ideal for biting a monoatomic ligand. Therefore, in Co(II)NKAP, the H-bond would aim at O_1 , which may not be good for best gain in ΔH but is conformationally less restrictive for the chelated O_2 . Thus, the smaller

CoPorphyrin +
$$O_2 \stackrel{K}{=} Co(O_2)$$
Porphyrin

$$K = \frac{[Co(O_2)Porphyrin]}{[CoPorphyrin] P_{O_2}}$$
(I)

When half of the CoPorphyrin coordinated

[Co(O₂)Porphyrin] = [CoPorphyrin]; $\begin{bmatrix} K_{-} & 1 \end{bmatrix}$

Figure IV-3. The equation of reversible O₂ binding and the definition of P_{1/2}.

loss in ΔS is apparently more than enough to compensate for the enthalpic loss to afford large binding constants throughout the temperature range.^{4a}

2. Further information from ¹⁵N NMR

To lend further support to our contention that NKAP disfavors the open end of diatomic ligands, ¹⁵N-NMR was used to probe the ligand environment.¹⁹ H-bonding is known to cause a large upfield shift of the 15N signal for (C15N)₂Fe^{III} porphyrins, due to reduced spin transfer from iron to cyanide.²⁰ The ¹⁵N chemical shift of the iron cyano porphyrins is tabulated in Table IV-2. Typical porphyrin complexes such as OEPhemin (Table IV-2), in DMSO containing tenfold excess of KC¹⁵N, exhibit one single peaks around δ 720. With the anthracene AKAP, which should clamp down a C=N well if the acid group is in place, biscyano-FeAKAP has two peaks at δ 622 and 490. When the -CO₂H is reduced to -CH₂OH, the corresponding peaks become δ 701 and 657. The more upfield signal is due to the H-bonded CN which weakens the axial ligand field and simultaneously shifts the trans ligand signal. The spread between the two signals becomes smaller as the H-bond becomes weaker. With NKAP, the (C¹⁵N)₂FeNKAP shows two peaks at d 715 and 670, suggesting a quite ineffective H-bond to this cyano nitrogen. Using Figure IV-4 as a model, an iron-bound CN would place the N at X - a very awkward position to align with the proton. Replacing the linear CN by a bent O=O would not give a better O2···H-O alignment without first requiring severely twisting the acid group off center (estimated C43-N5 rotation of at least 40° for an optimum H-bond). While such rotation may still happen, the more likely H-bond in our model is an oblique interaction toward the π -bond or both

Table IV-2. ¹⁵N NMR chemical shift of Fe(CN)₂porphyrins

FePorphyrin		δ (ppm)
N C N C N C N C N N		720
O L FO X N Fe N C N N Fe N	X=COOH X=CH ₂ OH	622, 490 701, 657
O LO OH N N C N Fe N N N N N N N N N N N N N N N N N		715, 670

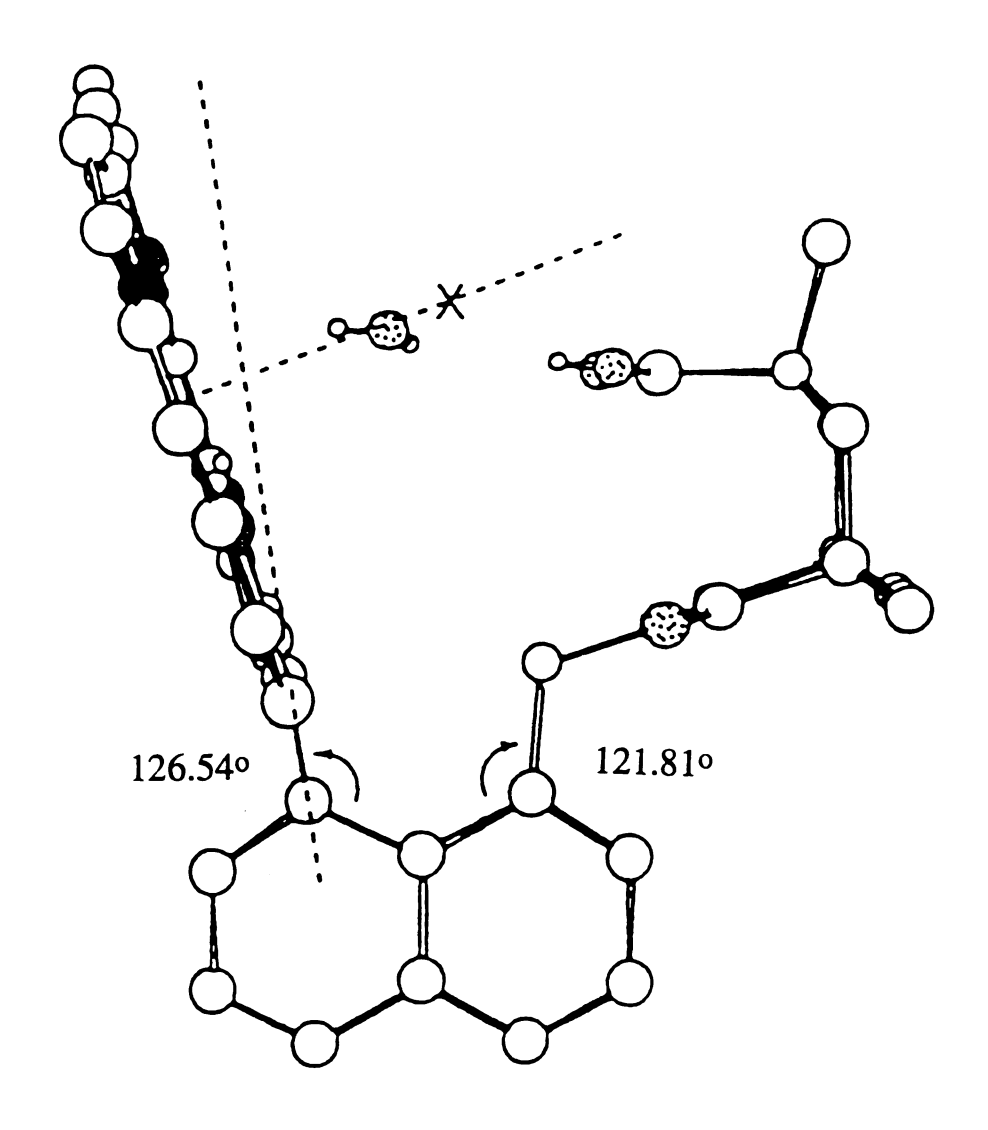


Figure IV-4. Side-view of NKAP-H₂O complex.

O1 and O2, if the X-ray structure is any indication.

D. Conclusion

This study demonstrates conformational control of the distal H-bonding effect in the heme-O₂ reaction; it highlights the fact that due to the entropic factor, a high O₂ binding constant is not necessarily the result of an ideal Fe-O-O···H interaction. Rather, the binding is always enhanced with less restrictive H-bond(s). The CoNKAP is an attractive electrocatalyst for O₂ reduction. The preferential H-bonding with monoatomic ligand also makes NKAP an excellent model for studying ferryl heme intermediates. These results will be discussed in Chapter V.

E. References

- (a) Mims, M. P.; Porras, A. G.; Olson, J. S.; Noble, R. W.; Peterson,
 J. A. J. Biol. Chem. 1983, 258, 14219-14232.
 - (b) Rohlfs, R. J.; Mathews, A. J.; Carvert, T. E.; Olson, J. S.; Springer, B. A.; Egeberg, K. D.; Sligar, S. G. J. Biol. Chem. 1990, 265, 3168-3176.
- 2. Poulos, T. L.; Kraut, J. J. Biol. Chem. 1980, 255, 8199-8205.
- 3. Babcock, G. T.; Wikström, M. Nature, 1992, 356, 301-309.
- 4. (a) Momenteau, M.; Reed, C. A. Chem. Rev. 1994, 94, 659-698 and references therein.
 - (b) Jameson, G. B.; Ibers, J. A. Comments Inorg. Chem. 1983, 2, 97-126.
- (a) Chang, C. K.; Traylor, T. G. Proc. Natl. Acad. Sci. U.S.A. 1975, 72, 1166-1170.
 - (b) Chang, C. K.; Ward, B.; Young, Y.; Kondylis, M. P. J. Macromol. Sci.-Chem. 1988, A25, 1307-1312.
 - (c) Chang, C. K.; Kondylis, M. P. J. Chem. Soc. Chem. Commun. 1986, 316-318.
- 6. Momenteau, M.; Mispelter, J.; Loock, B.; Lhoste, J.-M. J. Chem. Soc. Perkin Trans. I 1985, 61-69 and 221-231.
- 7. Wuenschell, G. E.; Tetreau, C.; Lavalette, D.; Reed, C. A. J. Am. Chem. Soc. 1992, 114, 3346-3355.

- 8. Collman, J. P.; Zhang, X.; Wong, K.; Brauman, J. I. J. Am. Chem. Soc. 1994, 116, 6245-6251.
- 9. (a) Shaanan, B. Nature(London) 1982, 296, 683-684.
 (b) Condon, P. J.; Royer, W. E. J. Biol. Chem. 1994, 269, 25259-25267.
- 10. Phillips, S. E. V.; Schoenborn, B. P. Nature(London) 1981, 292, 81-82.
- 11. Chang, C. K.; Avilés, G.; Bag, N. J. Am. Chem. Soc. 1995, 116, 12127-12128.
- 12. Avilés, G. "Interaction of Intermoleculaar Carboxylic Acid with Heme-O₂ Complex", Ph.D. Dissertation, Michigan State University, 1991.
- 13. Marzilli, G. L.; Marzilli, P. A.; Halpern, J. J. Am. Chem. Soc. 1971, 93, 1374-1378.
- 14. Chang, C. K.; DiNello, R. K.; Dolphin, D. *Inorg. Chem.* 1980, 20, 147-155.
- 15. Brinigar, W. S.; Chang, C. K. J. Am. Chem. Soc. 1974, 96, 5595-5597.
- 16. Due to complications involving 6-coordinate competition and technical problems in measuring such small P_{1/2} (requiring proportionally larger tonometer) at low temperature, only the DMF results are presented.

- 17. The O₂ affinity of Co(II)NAP at 0°C is subject to a high degree of uncertainty due to additional complications brought about by the catabolic reaction. ¹¹ During re-examination, the P_{1/2} at 0°C could be as low as 5-10 torr which is included in Table IV-1.
- 18. Spilburg, C. A.; Hoffman, B. M.; Petering, D. H. J. Biol. Chem. 1972, 247, 4219-4223.
- 19. Avilés, G.; Chang, C. K. J. Chem. Soc. Chem. Commun. 1992, 31-32.
- 20. (a) Behere, D. V.; Gonzalez-Vergara, E.; Goff, H. M. *Biochim. Biophys. Acta* 1985, 832, 319-323.
 - (b) Morishima, I.; Inubushi, T. J. Am. Chem. Soc. 1978, 100, 3568-3574.

CHAPTER V

Structural and Vibrational Character of H-bonded Vanadyl Porphyrins. Models of H-Bonded Ferryl Heme

A. Introduction

Ferryl heme, or oxoiron(IV) porphyrin, is an important intermediate in the enzymatic cycles of dioxygen activation and reduction. The Fe(IV)=O species is known as Compound II of catalases and peroxidases¹. Its presence has also been demonstrated in cytochrome P₄₅₀ and related oxygen transfer process² as well as in cytochrome c oxidase³ and cytochrome d.⁴ Extensive studies have been devoted to understanding the nature of the iron-oxo bond in proteins as well as in model compounds. In particular, resonance Raman studies on peroxidase Compound II⁵, ferryl myoglobin⁶, and heme model complexes⁷ have given much insight on how the Fe-O bond is influenced by ligand and polarization effects. The reported Fe-O stretching frequency falls in the range between 750-810 cm⁻¹ for proteins and 807-852 cm⁻¹ for various 5-

or 6-coordinate porphyrin models. One dominating factor that tends to reduce v_{Fe-O} comes from the trans-ligand which competes with the oxo group for metal d orbitals.^{7a} Another often suggested factor that may lower v_{Fe-O} is hydrogen-bonding, although the importance or the magnitude of this effect in various heme proteins remains largely a subject of speculation.^{3,4,5}

In the course of studying the properties of oxoiron(IV) porphyrins, other oxometalloporphyrin complexes of the third row transition metals, including titanium⁸, vanadium⁹, chromium¹⁰, and manganese¹¹ have been reported. Vanadyl porphyrins with a stable VO bond, can serve as a convenient model for the more reactive ferryl porphyrins.

Even though vanadium has not been shown to be present in mammalian systems, they do occur as natural products. ¹² To date, the best evidence for a biological role of vanadium is from bacteria (nitrogen fixation in Azotobacter species) and from plants (haloperoxidases in marine algae). Significant amounts of vanadium in a biological system were first discovered in 1911 by the German physiologist M. Henze in the blood of the ascidian *Phallusia mammillate*. ¹³ The ascidians have a striking physiological feature in accumulating vanadium effectively from the surrounding seawater. A two step reduction process is proposed from V(V) to V(III) with V(IV) as intermediate. ¹⁴ Most of the peroxidases have been reported to be heme-containing enzymes and divided into three families: plant peroxidases, animal peroxidases and catalases. ¹⁵ However, peroxidases isolated from brown algae belonging to *Fucales* and *Laminariales* are vanadium-dependent haloperoxidases. ¹⁶ Additionally, the degradation of chlorophyll and other biologically active porphyrins is

thought to be the source of vanadyl porphyrins in petroleum.¹⁷ Therefore, vanadium chemistry has always been interesting and useful in understanding biological systems.

In the study of vanadyl porphyrins, ¹⁸ Spiro and coworkers have examined solvent effects, including H-bonding, axial ligand interactions and radical cation formation on the stretching frequency of the V-O bond by resonance Raman spectroscopy. They have shown a linear correlation between v_{V-O} and the solvent acceptor number. ¹⁹ Although H-bonding was implied, ¹⁸ no direct spectroscopic evidence has been reported.

Our success in synthesizing the C-Clamp porphyrins, especially the Naphthalene Kemp's Acid Porphyrin (NKAP) and its amide derivative NKAmideP,²⁰ has provided us the opportunity to probe intramolecular H-bonding effect on oxo species.

B. Experimental

1. Reagents

All reagents used in this work were purchased from Aldrich Chemical Co. except as noted below. HOAc (glacial) was from EM Science and NaOAc (anhydrous) was purchased from J. T. Baker. CH₂Cl₂ was freshly distilled over CaH₂ before use. NKAP, NKAmideP and NAP were synthesized by previously discussed methods in Chapter II.²⁰

2. VO Insertion

a) NKAP(VO). NKAP 10 mg (0.01 mmol), acetic acid 15ml, sodium acetate 450 mg and VO(acac)₂ 100 mg were placed in a round-bottom

flask fitted with a ground glass joint connected to a reflux condenser. The mixture was refluxed under argon and the progress of the reaction was monitored by UV-vis spectroscopy (Figure V-1). When a sample, withdrawn with a pipette, indicated that no more complex was being formed (>95% conversion), the reaction was quenched by adding 15 ml of water. The mixture was allowed to stand overnight to crystalize. The product was collected by filtration and washed with water until the filtrate was colorless. The crude compound was purified by running it over a short column of silica gel with methylene chloride as solvent to give the pure red solid product. Yield: 9.9 mg (92%). FABMS: m/e, 920. UV-vis: λ_{max} nm (relative intensity): 417.0 (10.4), 540.0 (1.0), 578.0 (1.2). The IR spectra showed a strong absorption band at 978 cm⁻¹ characteristic of a vanadyl vibration.

b) NKAmideP(VO), NAP(VO) and OEP(VO). These were prepared by similar protocol to that for NKAP(VO). The purification of the crude products from the vanadyl Naphthalene Kemp's Amide Porphyrin, NKAmideP(VO), and vanadyl Naphthoic Acid Porphyrin, NAP(VO), gave two compounds, one as major product and another as a minor portion.

3. Instrumentation

a) Spectroscopy

UV-vis spectral measurements were carried out on a Cary 219 or a Shimadzu 160 spectrophotometer, with samples dissolved in CH₂Cl₂ or 1-MeIm. Infrared spectra were obtained by either layering the vanadyl porphyrin complex on a NaCl plate or by placing the CH₂Cl₂ solution of

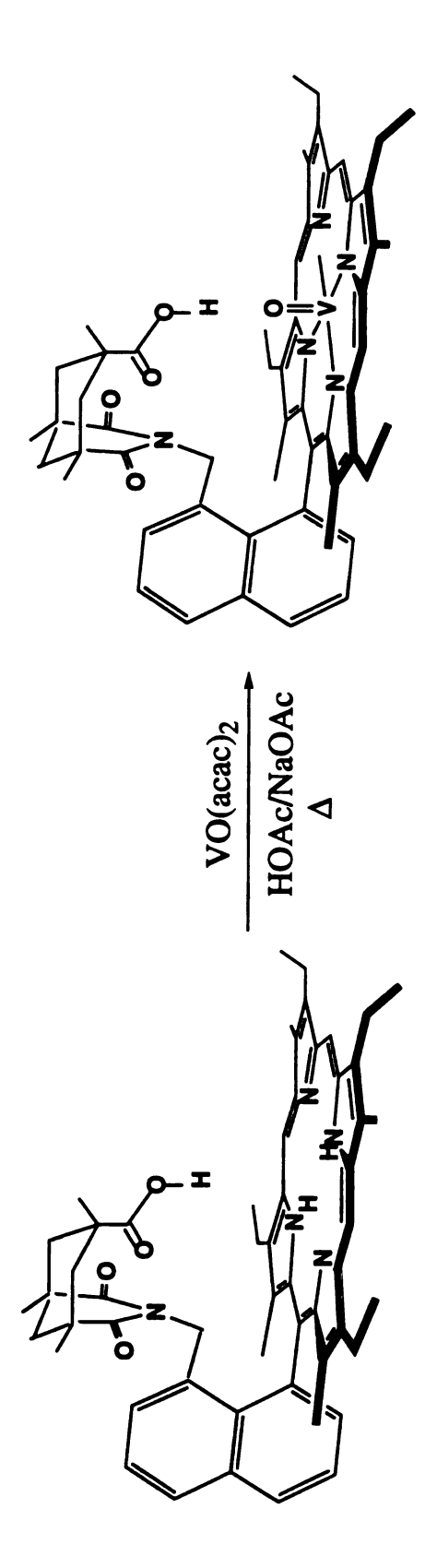


Figure V-1. Vanadyl insertion to NKAP.

the VO porphyrins in a liquid cell; spectra were then recorded on a Nicolet IR/42 spectrometer. FABMS (fast atom bombardment mass spectra) were recorded on a JEOL HX-110 HF double focusing spectrometer operating in the positive ion detection mode. Resonance Raman (RR) studies were carried out by Dr. Einhard Schmidt.²¹

b) X-Ray Determination

Crystals of NKAmideP(VO) and NAP(VO) suitable for singlecrystal X-ray diffractometry were obtained by diffusion of methanol into a sample solution in CH₂Cl₂ followed by slow evaporation. Data collection was performed on a Nonius CAD4 diffractometer at room temperature using graphite-monochromated Mo K_{α} radiation. The crystal used for analysis were of approximate dimensions 0.30 x 0.40 x 0.40 mm for NKAmideP(VO) and 0.05 x 0.10 x 0.20 mm for NAP(VO). The unit cell parameters were determined by a least squares fit of 25 machinecentered reflections having 20 values in the ranges of 41.62-57.14° for NKAmideP(VO) and 12.00-17.70° for NAP(VO). The intensity data were reduced and corrected for Lorentz and polarization factors using the applied programs. The crystal structures were solved by direct methods using the NRCVAX program package. All non-hydrogen atoms were refined anistropically. The protons on N6 were located from a difference Fourier map and positionally refined. All the rest of the hydrogen atoms were placed at calculated positions with fixed isotropic thermal parameters. Other crystallographic parameters are listed in Table V-1.

Table V-1. Crystallographic Data for NKAmideP(VO) and NAP(VO)

	NKAmideP(VO)	NAP(VO)
Formula	C55N6O4H60V	C43N4O3H42V
fw	928.05	713.76
cryst syst	Monoclinic	Triclinic
space group	C 2/c	pΤ
a, Å	19.729(22)	11.367(9)
b, Å	12.0219(16)	13.369(7)
c, Å	41.280(5)	14.579(7)
α, deg	90	106.97(5)
β, deg	101.307(10)	100.56(7)
γ, deg	90	113.70(6)
V, Å3	9600.3(20)	1822.5(20)
Z	8	2
Q(calc), gcm ⁻³	1.284	1.301
μ, cm ⁻¹	21.318	0.031
scan speed, deg min-1	2.06-8.04	1.37-8.24
scan width, deg	$2(0.65 + 0.35 \tan \theta)$	$2(0.65+0.35\tan\theta)$
no. of measd reflns	6064	4766
no. of obsd reflns	4246 ($I > 2\sigma(I)$)	$1979(I > 2\sigma(I))$
no. of refined params	606	461
R _f , R _w	0.055, 0.055	0.047, 0.048
Gof	2.33	1.35

Note: $R_f = \sum |F_o - F_c| / \sum |F_o|$

 $R_{\rm W} = (\sum (w(F_{\rm o}\text{-}F_{\rm c}))^2/\sum (wF_{\rm o}^2))^{1/2}$

Gof = $(\sum (w(F_0-F_c))^2/(\# \text{ refins-}\# \text{ params}))^{1/2}$

C. Results and Discussion

Four vanadyl compounds have been studied in this work. They are NKAP(VO), NKAmideP(VO), NAP(VO) and vanadyl octaethyl porphyrin, OEP(VO). Among these four systems, OEP(VO) is used basically as a reference. In all other systems, the VO moiety potentially has two possible orientations, one toward the acid or amide (as "cis"); and the other has the opposite orientation (as "trans" isomer).

1. H-Bonding for 5-Ligated VO-porphyrins

IR spectroscopy studies were recorded for all the four vanadyl systems. The results are listed in Table V-2. Previous studies of vanadyl porphyrins have established that the VO stretching frequency is in the 1000 cm⁻¹ region, therefore we assigned the peak at 991cm⁻¹ observed in IR spectrum of OEP(VO) as the stretching of the VO bond. 18 In the spectra of NKAP(VO), a peak at 971 cm⁻¹ was detected instead (Figure V-2). The 20 cm⁻¹ shift to lower energy is due to the intramolecular Hbonding provided by the carboxylic acid proton. In order to prove that this shift is exclusively caused by H-bonding, further resonance Raman (RR) studies were carried out. After deprotonation with a bulky base, 1,5-diazabicyclo[4.3.0]non-5-ene (DBN), the VO absorption band of NKAP(VO) shifted to 991cm⁻¹. The porphyrin core vibrations were not affected during this process. DBN could not coordinate to the vanadium as a sixth ligand as OEP(VO) vibrations were also unaffected by DBN. Thus, the 20 cm⁻¹ vibrational shift is solely caused by intramolecular Hbonding.

Table V-2. IR Data of Vanadyl Porphyrins

Porphyrins	υν=0 (5-coordinated), cm ⁻¹	υ _{V=O} (6-coordinated), cm ⁻¹
OEP(VO)	991	958
NKAP(VO)	971	•
NKAmP(VO) major pdt	286	954
NAP(VO) major pdt	991	•

Figure V-2. IR Spectrum of NKAP(VO).

The sample was layered on NaCl plate.

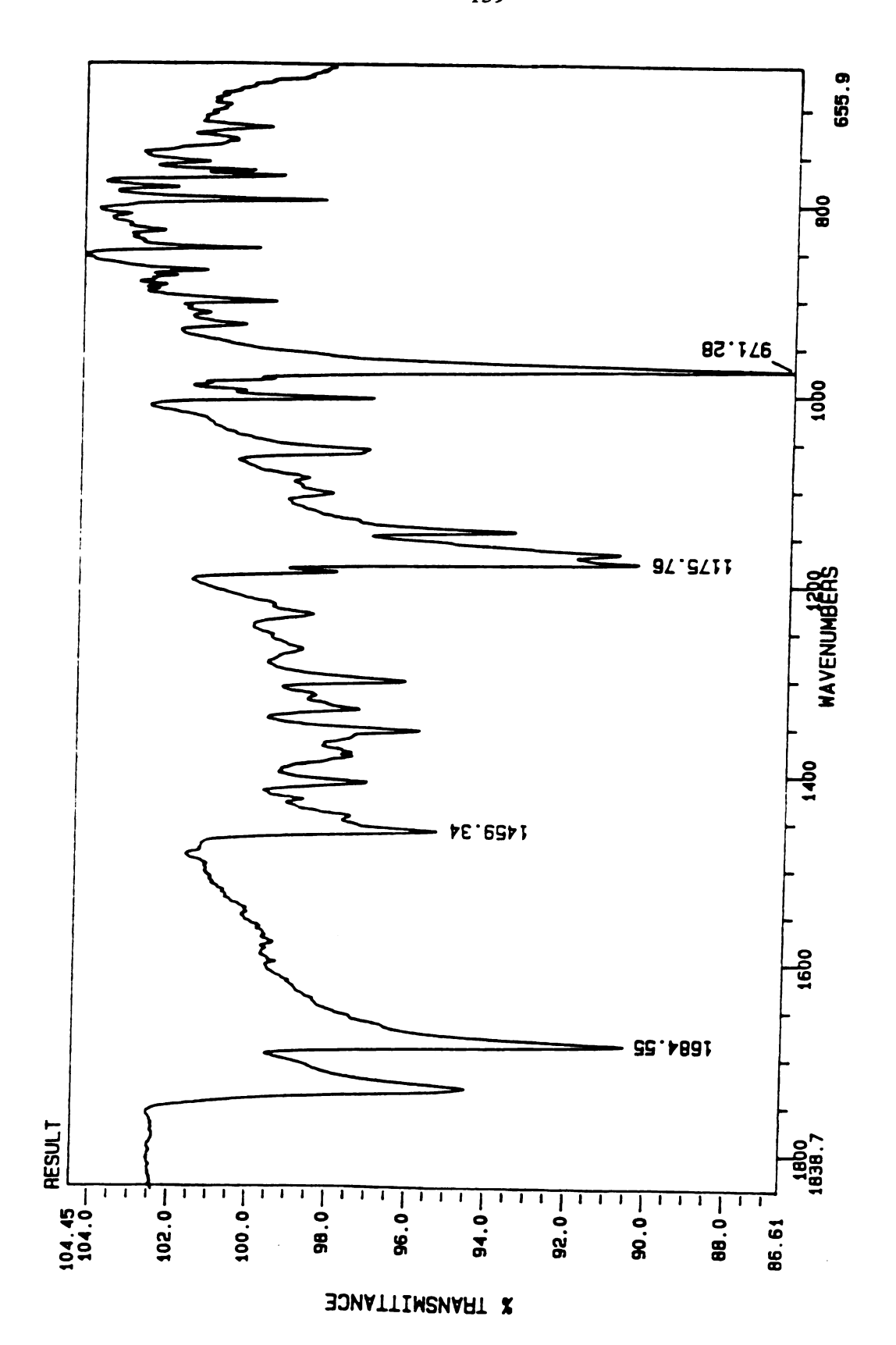


Figure V-3 shows the IR spectra of the major and minor products of NKAmideP(VO). The major product has a 987 cm⁻¹ absorption, a 4 cm⁻¹ shift to lower wavenumber. This implies a relatively weak intramolecular H-bonding from the amide proton to the vanadyl oxygen. The minor product of NKAmideP(VO) displayed a 991 cm⁻¹ vibration, with no H-bonding effect and thus corresponding to a "trans" isomer with reference to the IR of OEP(VO).

However, the major product of NAP(VO) showed a 991 cm⁻¹ vibration while the minor compound had the vibration at 972 cm⁻¹. This implies the major product is a "trans" isomer and the minor is a "cis" isomer.

2. H-Bonding for 6-Ligated VO-porphyrins

The amide of NKAmideP(VO) cannot be deprotonated by nitrogen base, such as pyridine or 1-methylimidazole(1-MeIm), thus allowing the opportunity to detect the H-bonding effect for 6-coordinated vanadyl porphyrins. However, 6-ligated species cannot be fully achieved even in pure 1-MeIm (Figure V-4). Two Soret peaks at 436 nm and 418 nm indicated a mixture of 5- and 6-coordinated species (Table V-3). This phenomenon can be explained by the strong electron donation from the oxo ligand which reduces the effective positive charges on the V(IV) center. The out of plane geometry of VO is another contributing factor.²²

IR studies of OEP(VO) in pure 1-MeIm showed two absorption bands; one at 987 cm⁻¹ is from the remaining 5-coordinated species while the other is shifted to 958 cm⁻¹, reflecting the 6-coordinated complex. The Δv is 28 cm⁻¹. As for NKAmideP(VO), we detected a peak at 954 cm⁻¹.

Figure V-3. IR Spectrum of NKAmideP(VO).

- a) Major product;
- b) Minor product.

The samples were layered on NaCl plates.

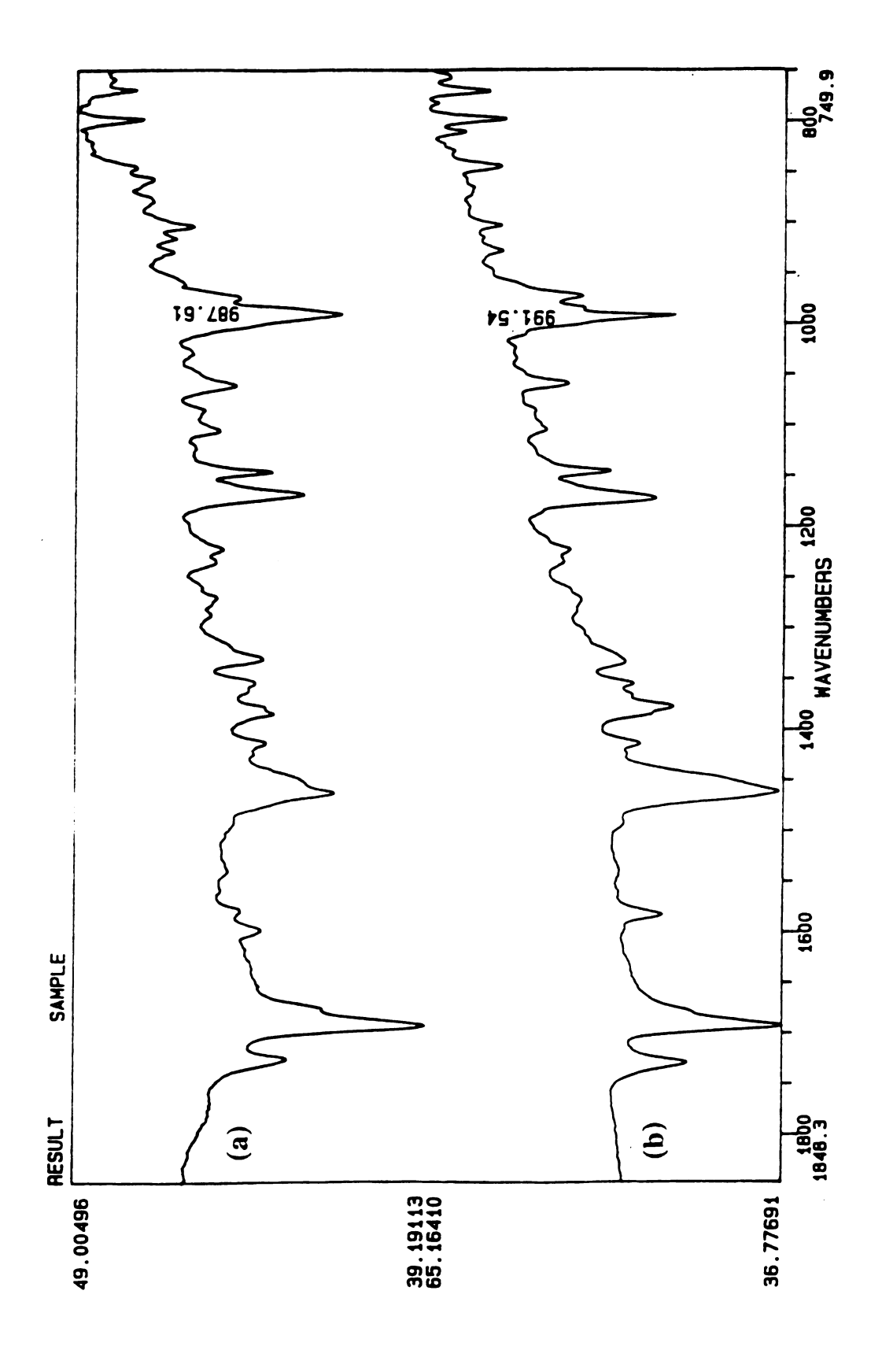
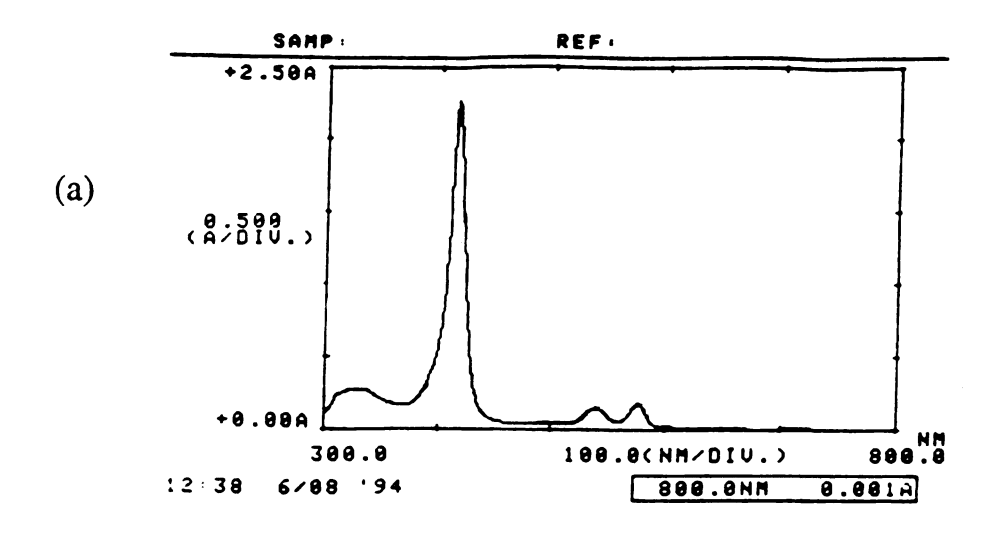
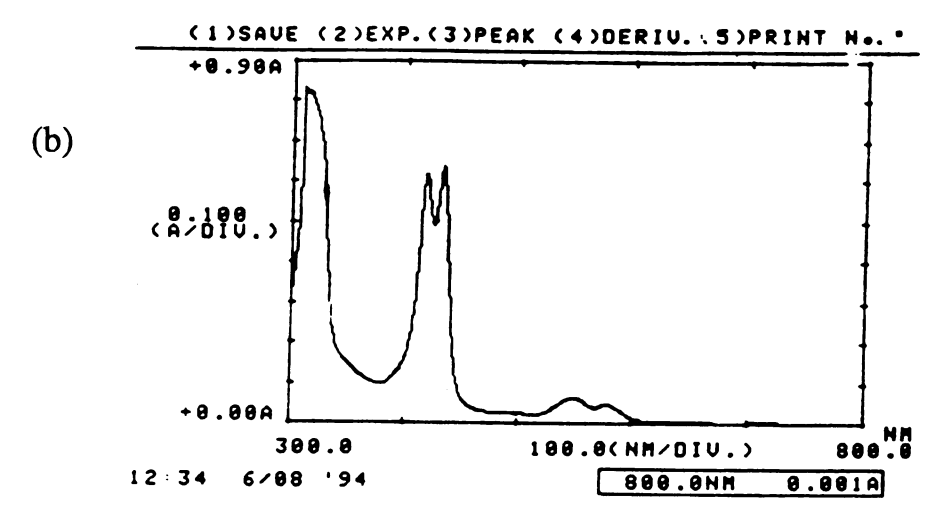


Figure V-4. The optical spectra of NKAmideP(VO) in a) CH₂Cl₂; b) pyridine; c) 1-MeIm





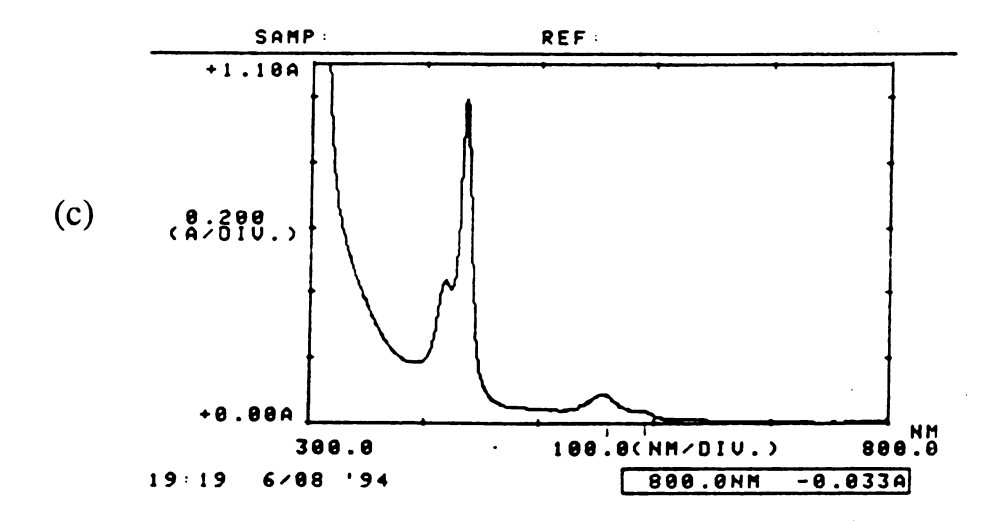


Table V-3. The Optical Absorption Spectral Data of Several Vanadyl Porphyrins.

Compound	Solvent	5-/6- Coord.	Soret, $\lambda(nm)$ (rel. int.)	visible, λ(nm) (rel. int.)
NKAP(VO)	CH ₂ Cl ₂	5	417.0 (10.4)	540.0 (1.0); 578.0 (1.2)
NKAmideP(VO)	CH ₂ Cl ₂	ς,	414.0(18.2)	538.0 (1.0); 575.5 (1.1)
NKAmideP(VO)	pyridine	both	418.0 (11.2); 436.0 (25.5)	556.0 (2.3); 594.0 (1.0)
NKAmideP(VO) 1-Me-Imidaz	-Me-Imidazole	both	418.0 (12.9); 433.0 (13.3)	547.5 (1.3); 578.5 (1.0)
OEP(VO)	CH2Cl2	S	406.5 (19.5)	532.5 (1.0); 570.0 (1.9)
OEP(VO) 1	1-Me-Imidazole	both	407.5 (6.4); 427.0 (14.8)	549.0 (1.3); 583.5 (1.0)
	-Me-Imidazole	both	407.5	(6.4); 427.0 (14.8)

The hydrogen bonding effect brought 4 cm⁻¹ red shift for VO stretching mode which is of the same magnitude of the 5-ligated complex.

3. X-Ray Single Crystal Structure of NKAP(VO) and NAP(VO)

Attempts to grow crystals of NKAP(VO) were unsuccessful due to its poor solubility. Crystals for NKAmideP(VO) and NAP(VO) were grown from the major product of the vanadyl insertion. Table V-4 lists the atomic coordinates of non-hydrogen atoms of NAP(VO), and Table V-5 lists the atomic coordinates of non-hydrogen atoms and the two protons on N6 of NKAmideP(VO). A listing of selected bond distance and angles for both compounds is given in Table V-6.

For NKAmideP(VO), the crystal was monoclinic and its ORTEP structure is shown in Figure V-5a. The oxo ligand is in the expected orientation towards the amide, a "cis" structure, as predicted by RR and IR. The four porphyrin nitrogens are coplanar within the standard error. H-bonding distance is 2.04(5) Å from the amide proton to the vanadyl oxygen. The angle of the N(6)-HN(6)-O1 is 161(4)°. The average V-N bond distance is 2.067 Å and the V-O bond length is 1.590(3) Å. A side view of this structure (Figure V-5b) shows that the naphthalene ring plane is tilted from the 90° angle to the porphyrin mean plane in order to bring the amide proton to the best alignment to the vanadyl oxygen. This torsion also brings the amide proton closer to the vanadyl oxygen since the vertical distance of the naphthalene ring is shortened along the tilting.

The crystal obtained from the major isomer of NAP(VO), contrary to what we got for NKAmideP(VO), has the oxo pointing on the opposite

Table V-4. Atomic Parameters x, y, z and B_{iso}. for NAP(VO) with E. S. Ds. refer to the last digit printed.

	X	y	Z	Biso
<u></u>	0.73087(12)	0.14775(11)	0.26545(9)	2.47(7)
Nl	0.9403 (5)	0.2400 (5)	0.3392 (4)	2.6 (3)
N2	0.7645 (5)	0.2131 (5)	0.1550 (4)	2.7 (3)
N3	0.5401 (5)	0.1357 (5)	0.2202 (4)	2.4 (3)
N4	0.7214 (5)	0.1803 (5)	0.4109 (4)	2.7 (3)
C1	1.0074 (7)	0.2369 (6)	0.4267 (5)	2.8 (4)
C2	1.1452 (7)	0.2609 (6)	0.4280 (5)	3.0 (4)
C 3	1.1627 (7)	0.2922 (6)	0.3489 (5)	3.0 (4)
C 4	1.0330 (7)	0.2772 (6)	0.2920 (5)	2.8 (5)
C5	1.0110 (7)	0.2929 (7)	0.2040 (5)	3.4 (5)
C 6	0.8877 (7)	0.2661 (6)	0.1387 (5)	3.0 (5)
C 7	0.8636 (7)	0.2774 (7)	0.0436 (5)	3.4 (5)
C 8	0.7279 (7)	0.2292 (7)	-0.012 (5)	3.4 (5)
C 9	0.6658 (7)	0.1897 (6)	0.0677 (5)	3.0 (4)
C10	0.5276 (7)	0.1383 (6)	0.0521 (5)	3.2 (5)
C11	0.4665 (7)	0.1129 (6)	0.1229 (5)	2.8 (4)
C12	0.3224 (7)	0.0674 (6)	0.1093 (5)	3.0 (5)
C13	0.3101 (7)	0.0642 (6)	0.1986 (5)	2.7 (4)
C14	0.4453 (7)	0.1088 (6)	0.2685 (5)	3.0 (5)
C15	0.4794 (7)	0.1321 (7)	0.3702 (5)	3.3 (5)
C16	0.6076(7)	0.1721 (7)	0.4386 (5)	3.4 (5)
C17	0.6402 (7)	0.2040 (7)	0.5462 (5)	3.6 (5)
C18	0.7697 (7)	0.2244 (7)	0.5835 (5)	3.7 (5)
C19	0.8203 (7)	0.2086 (6)	0.4987 (5)	2.9 (5)
C20	0.9511 (6)	0.2234 (6)	0.5023 (5)	2.6 (4)

Table V-4 (cont'd)

C21	1.2524 (7)	0.2550 (7)	0.4992 (6)	4.0 (6)
C22	1.2925 (7)	0.3417 (8)	0.3252 (6)	4.4 (6)
C23	1.3654 (10)	0.4751 (9)	0.3682 (9)	9.1 (9)
C24	0.9759 (8)	0.3328 (9)	0.0043 (7)	5.7 (7)
C25	0.6495 (8)	0.2198 (8)	-0.1007(6)	4.7 (6)
C26	0.6255 (11)	0.3221 (10)	-0.0911(7)	7.5 (8)
C27	0.2153 (7)	0.0357 (7)	0.0126 (5)	3.7 (5)
C28	0.1999 (9)	0.1415 (9)	0.0075 (7)	6.5 (7)
C29	0.1820 (7)	0.0228 (7)	0.2241 (6)	4.3 (5)
C 30	0.5477 (7)	0.2225 (8)	0.6057 (6)	4.6 (6)
C31	0.4581 (10)	0.1114 (9)	0.6090 (8)	7.4 (8)
C32	0.8454 (8)	0.2669 (9)	0.6941(6)	5.5 (7)
C33	1.0380 (7)	0.2289 (6)	0.5965 (5)	3.0 (5)
C34	1.0094 (8)	0.1231 (7)	0.6045 (6)	4.6 (5)
C35	1.0905 (9)	0.1149 (8)	0.6826(7)	5.3 (6)
C36	1.2025 (9)	0.2126 (8)	0.7553 (6)	5.2 (6)
C37	1.2385 (8)	0.3274 (7)	0.7531 (6)	4.4 (6)
C38	1.3598 (9)	0.4299 (8)	0.8237 (6)	5.9 (6)
C39	1.3980 (9)	0.5387 (8)	0.8191 (7)	6.8 (6)
C40	1.3164 (9)	0.5482 (7)	0.7428 (7)	6.3 (6)
C41	1.1977 (7)	0.4537 (6)	0.6727 (5)	3.6 (5)
C42	1.1545 (7)	0.3369 (7)	0.6727 (5)	3.3 (5)
C43	1.1119 (8)	0.4804 (6)	0.6018 (6)	3.8 (5)
O 1	0.7006 (5)	0.0137 (4)	0.2166 (4)	3.4 (3)
O2	0.9991 (5)	0.4676 (5)	0.6031 (4)	4.7 (4)
O3	1.1712 (5)	0.5225 (5)	0.5432 (4)	5.2 (4)

Biso is the Mean of the Principal Axes of the Thermal Ellipsoid.

Table V-5. Atomic Parameters x, y, z and Beq for NKAmideP(VO) with E.S.Ds. refer to the last digit printed.

	X	у	Z	B_{eq}
<u></u>	0.56932(4)	0.41684(7)	0.087358(21)	2.75(4)
N1	0.56751(19)	0.4745 (3)	0.13440 (9)	2.86(19)
N2	0.47465(18)	0.4921(3)	0.07188(9)	2.70(18)
N3	0.53869(18)	0.3102(3)	0.04801(9)	2.67(19)
N4	0.62916(18)	0.2885(3)	0.11131(9)	2.69(18)
N5	0.85156(19)	0.5428(3)	0.15519(10)	3.13(20)
N6	0.74863(22)	0.6254(4)	0.08617(12)	5.3 (3)
C1	0.61567(24)	0.4551(4)	0.16312(12)	2.94(23)
C2	0.6049(3)	0.5368(4)	0.18832(12)	3.6 (3)
C3	0.5508(3)	0.6019(4)	0.17429(12)	3.5 (3)
C4	0.52783(25)	0.5636(4)	0.14107(12)	3.4 (3)
C5	0.4722(3)	0.6092(4)	0.11967(12)	3.6 (3)
C6	0.44646(24)	0.5759(4)	0.08760(12)	3.2(3)
C 7	0.3889(3)	0.6271(4)	0.06590(13)	3.6(3)
C8	0.38224(24)	0.5756(4)	0.03616(12)	3.06(24)
C9	0.43545(23)	0.4915(4)	0.03974(12)	3.98(15)
C10	0.44645(24)	0.4201(4)	0.01519(12)	3.02(24)
C11	0.49383(24)	0.3355(4)	0.01911(12)	2.94(24)
C12	0.5001(3)	0.2555(4)	-0.00666(12)	3.15(25)
C13	0.5491(3)	0.1808(4)	0.00723(12)	3.4(3)
C14	0.57335(24)	0.2163(4)	0.04149(12)	3.04(24)
C15	0.6233(3)	0.1631(4)	0.06369(12)	3.4(3)
C16	0.64876(24)	0.1946(4)	0.09619(12)	3.3(3)
C17	0.7007(3)	0.1346(4)	0.11858(13)	3.6(3)
C18	0.7132(3)	0.1910(4)	0.14772(12)	3.4(3)

Table V-5 (cont'd)

C19	0.66811(24)	0.2880(4)	0.14333(12)	3.03(24)
C20	0.66289(24)	0.3669(4)	0.16727(12)	2.95(24)
C21	0.6458(3)	0.5553(5)	0.22254(14)	5.2(3)
C22	0.5167(3)	0.6921(5)	0.18995(14)	5.0 (3)
C23	0.4566(4)	0.6537(7)	0.20348(17)	8.3(5)
C24	0.3469(3)	0.7222(5)	0.07522(14)	5.2(3)
C25	0.3293(3)	0.5964(5)	0.00536(13)	4.6(3)
C26	0.2687(3)	0.5209(8)	0.00321(17)	8.8(5)
C27	0.4579(3)	0.2551(5)	-0.04105(13)	4.5(3)
C28	0.3884(4)	0.1992(6)	-0.04347(16)	7.7(4)
C29	0.5754(3)	0.0846(5)	-0.00912(13)	5.1(3)
C30	0.7323(3)	0.0260(5)	0.11129(14)	5.0(3)
C31	0.7012(3)	-0.0734(6)	0.12645(17)	6.9(4)
C32	0.7654(3)	0.1542(5)	0.17702(16)	6.2(4)
C33	0.69999(25)	0.3447(4)	0.20238(12)	3.17(24)
C34	0.6618(3)	0.2835(5)	0.22008(13)	4.7 (3)
C35	0.6840(3)	0.2595(6)	0.25347(14)	5.8(4)
C36	0.7452(3)	0.3015(5)	0.26942(13)	5.3(3)
C37	0.7879(3)	0.3636(5)	0.25285(13)	4.0(3)
C38	0.8511(3)	0.4019(5)	0.26997(13)	5.1(3)
C39	0.8952(3)	0.4578(6)	0.25507(14)	5.4(3)
C40	0.8760(3)	0.4794(5)	0.22112(13)	4.5(3)
C41	0.81412(24)	0.4459(4)	0.20247(12)	3.20(24)
C42	0.76635(24)	0.3854(4)	0.21798(12)	3.09(24)
C43	0.79791(24)	0.4731(4)	0.16563(12)	3.3(3)
C44	0.8431(3)	0.6580(4)	0.15649(12)	3.7(3)
C45	0.8974(3)	0.7311(5)	0.14514(13)	4.1(3)
C46	0.9661(3)	0.6692(5)	0.15131(14)	5.2(3)
C47	0.9603(3)	0.5598(5)	0.13262(14)	4.5(3)
C48	0.9068(3)	0.4886(5)	0.14476(13)	3.9(3)

Table V-5 (cont'd)

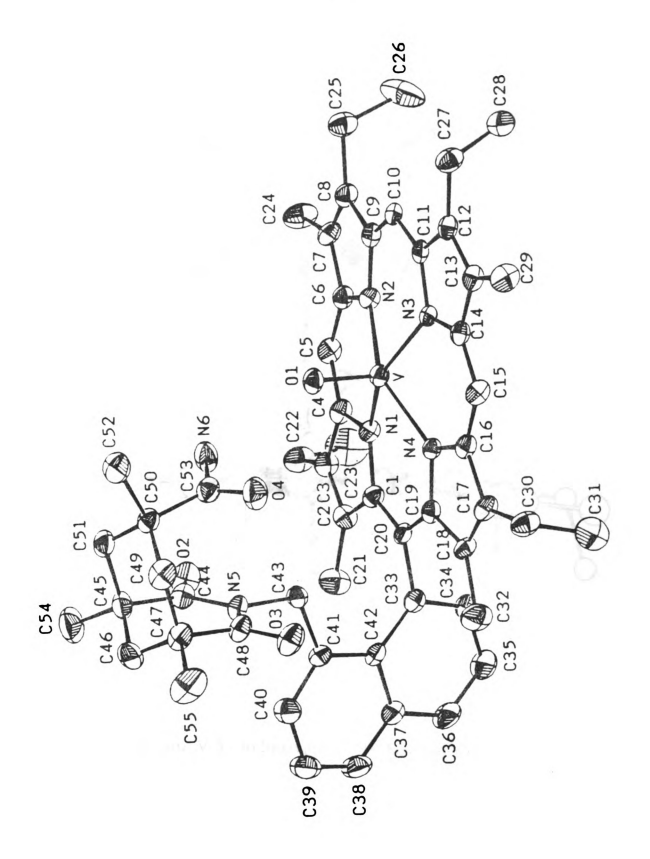
3) 4.7(3)
2) 3.7(3)
4) 4.2(3)
4) 5.7(3)
2) 3.9(3)
6) 6.8(4)
9) 8.1(5)
3.62(17)
5.13(21)
0) 5.41(22)
0) 5.80(25)
6.6(14)
6.3(14)

Beq is the Mean of the Principal Axes of the Thermal Ellipsoid.

Table V-6. Selected Bond Distances (Å) and Angles (deg) and Their Estimated Standard Deviations for NKAmideP(VO) and NAP(VO).

	NKAmideP(VO)		NAP(VO)
	Distances	ral	
V-O(1)	1.590(3)	V-O(1)	1.583(5)
V-N(1)	2.069(4)	V-N(1)	2.066(6)
V-N(2)	2.061(4)	V-N(2)	2.069(6)
V-N(3)	2.064(4)	V-N(3)	2.073((6)
V-N(4)	2.073(4)	V-N(4)	2.068(6)
O(1)-HN(6)	2.04(5)		
	Angles	ral	
N(6)-HN(6)-O(1)	161(4)		
N(1)-V-O(1)	104.34(17)	N(1)-V-O(1)	102.61(24)
N(2)-V-O(1)	103.73(16)	N(2)-V-O(1)	105.32(24)
N(3)-V-O(1)	102.75(17)	N(3)-V-O(1)	103.79(24)
N(4)-V-O(1)	105.62(16)	N(4)-V-O(1)	106.91(25)
N(1)-V-N(2)	87.85(15)	N(1)-V-N(2)	87.82(22)
N(1)-V-N(3)	152,9115)	N(1)-V-N(3)	153.60(22)
N(1)-V-N(4)	85.10(15)	N(1)-V-N(4)	84.70(22)
N(2)-V-N(3)	85.47(15)	N(2)-V-N(3)	84.94(22)
N(2)-V-N(4)	150.65(15)	N(2)-V-N(4)	147.76(23)
N(3)-V-N(4)	87.97(15)	N(3)-V-N(4)	87.99(22)

Figure V-5. (a) ORTEP structure of NKAmideP(VO).



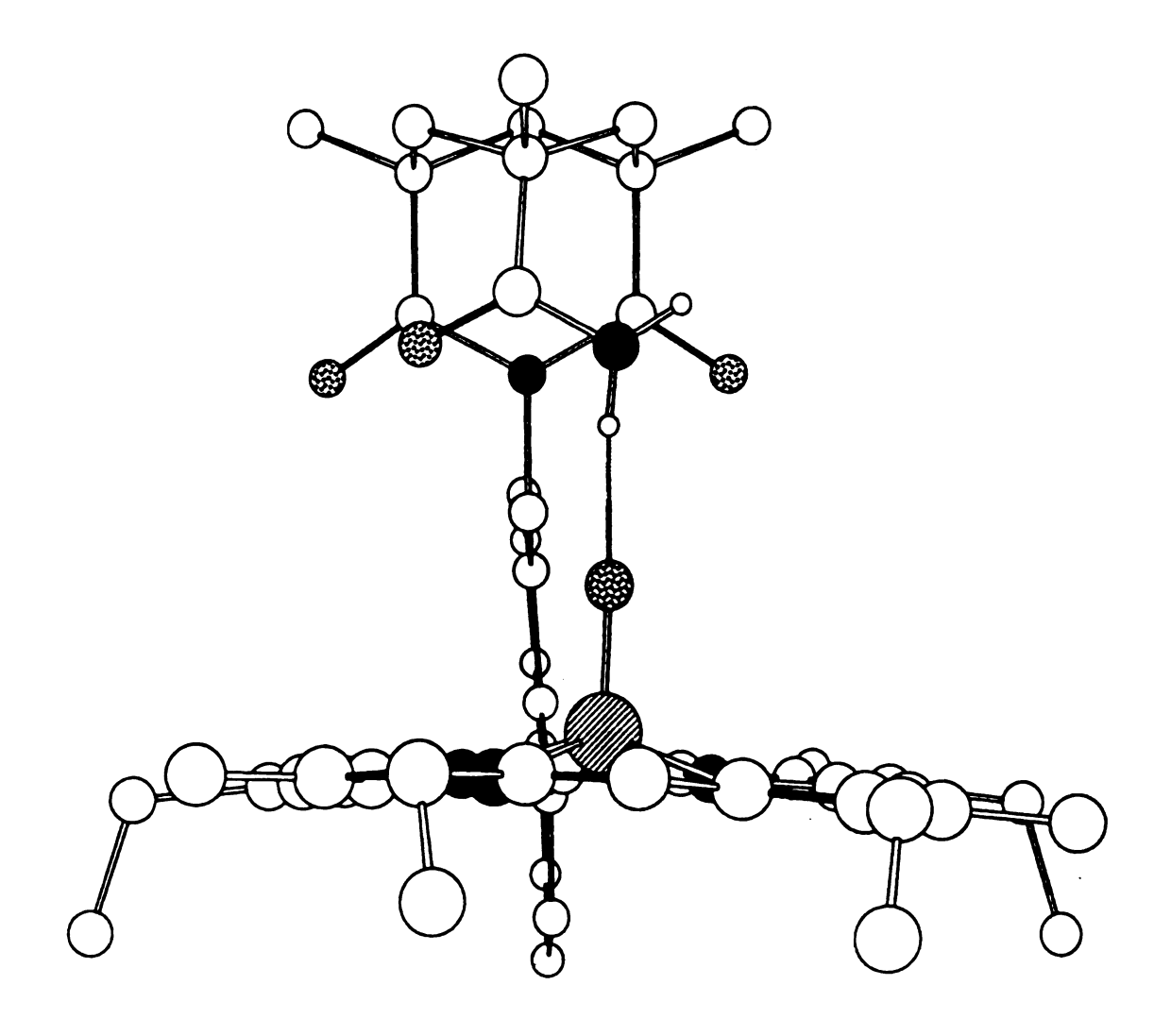


Figure V-5. (b) Sideview of NKAmideP(VO).

porphyrin side of the carboxylic acid, a "trans" isomer in agreement with the IR results (Figure V-6). The average V-N bond length is 2.069 Å and the V-O bond distance is 1.583(5) Å. From the unit cell structure (Figure V-6b), we observe dimer formation of NAP(VO). Two molecules of NAP(VO) come together through two intermolecular hydrogen bonds between the two carboxylic acids. The "trans" configuration is most likely the result of such acid pairing, blocking the "cis" site.

4. Orientation of the VO Directed by H-Bonding

From the results of X-ray determination and IR studies, we conclude that the oxo orientation is determined by hydrogen bonding. The strong hydrogen bonding present in NKAP(VO) induces a single "cis" isomer either by formation of COOH···O=V(acac)₂ prior to the metal insertion; or by equilibrium of the two isomers after the V=O insertion.

For NKAmideP(VO), since the amide group constitutes a weaker hydrogen bond than the acid, most of the oxo goes to the amide side ("cis") and only a minor proportion goes to the opposite side to form the "trans" isomer. As for NAP(VO), due to the dimer formation, the acid proton is unavailable for hydrogen bonding. The oxo rather picks the less sterically hindered side of the porphyrin to give mostly the "trans" isomer.

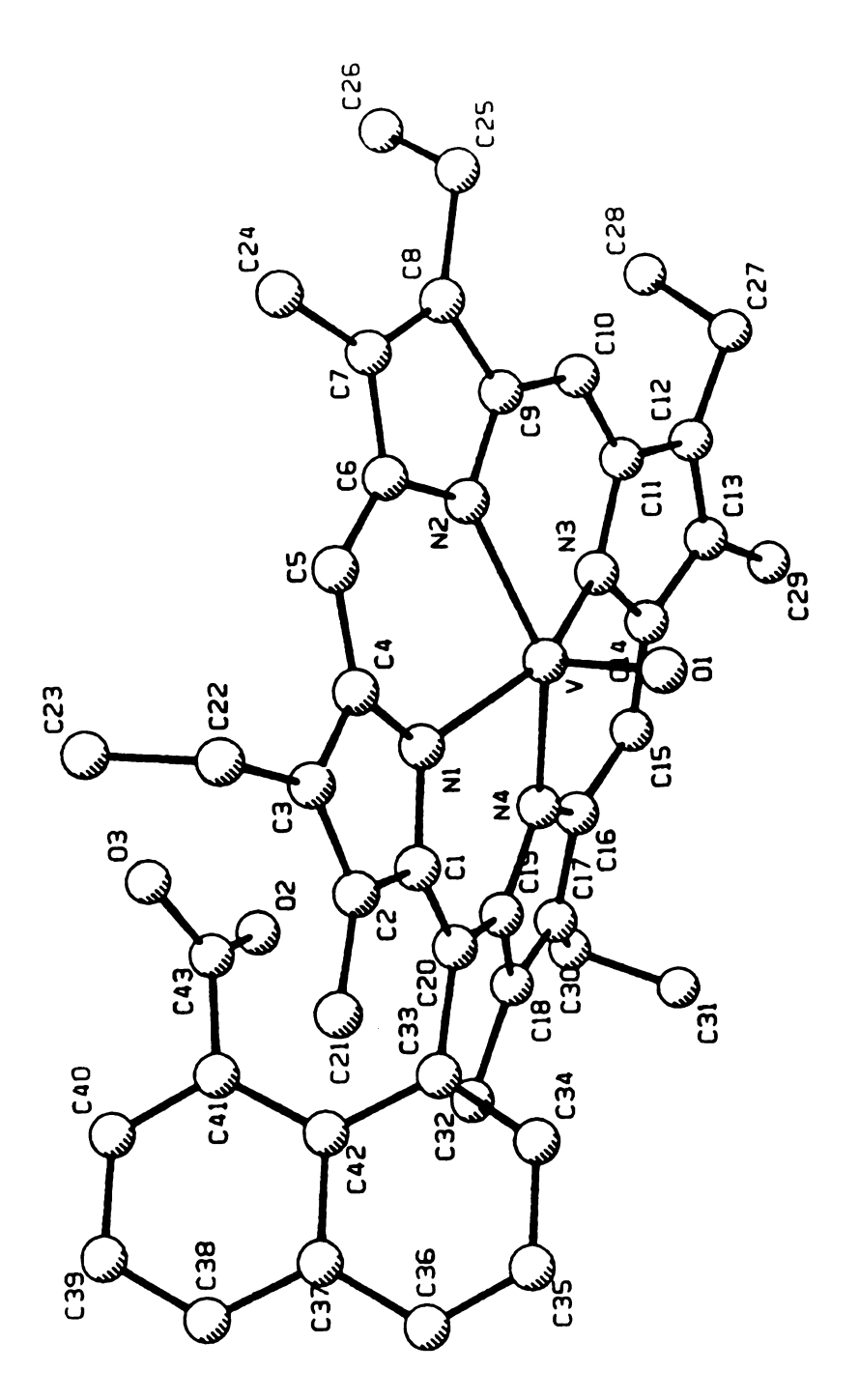


Figure V-6. (a) X-Ray crystal structure of NAP(VO).

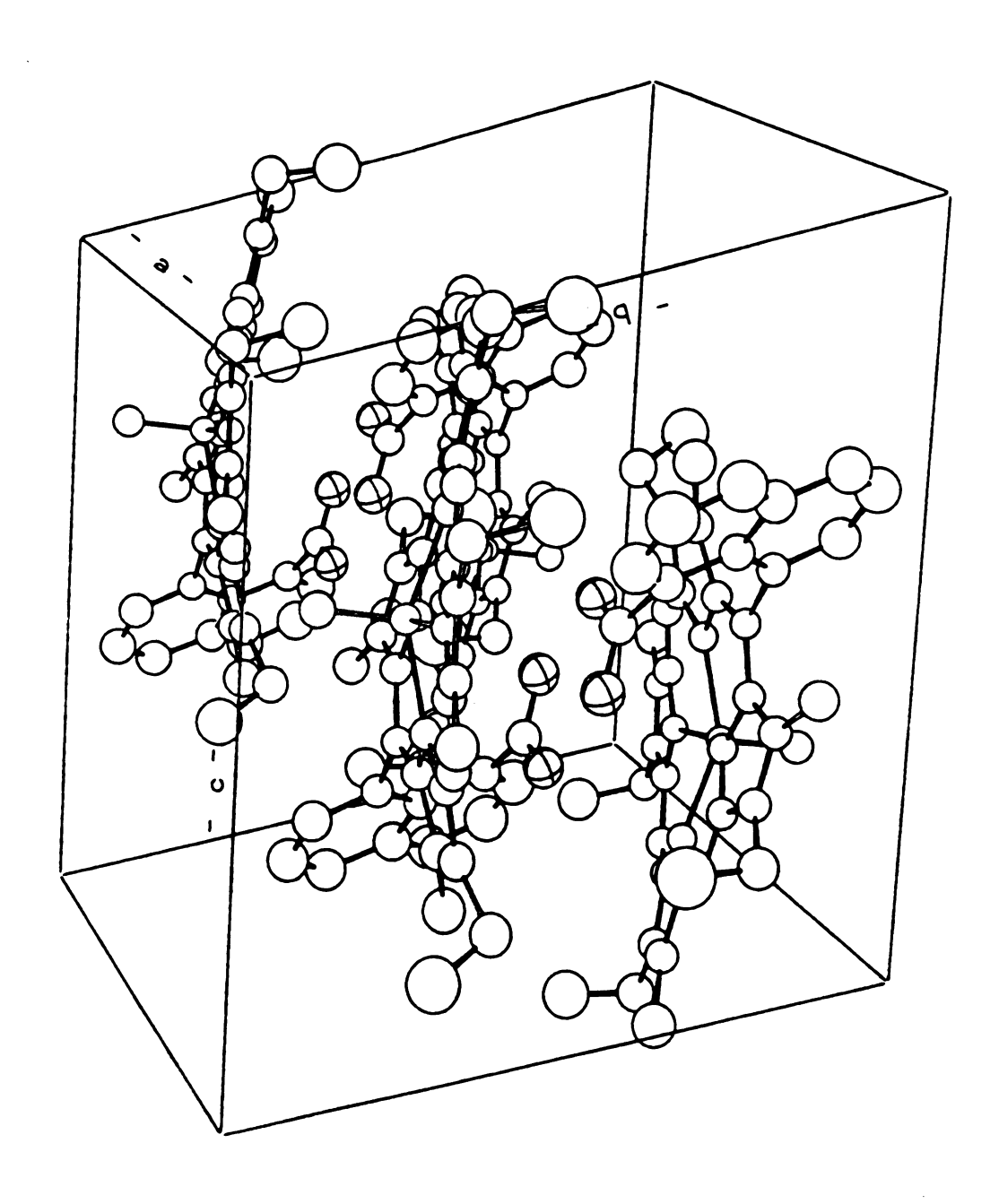


Figure V-6. (b) Unit cell structure of NAP(VO).

D. Conclusion

The hydrogen bonding effect on the 5- and 6-coordinated vanadyl porphyrin as observed in NKAP(VO) and NKAmideP(VO) gives a $\Delta v_{V=O}$ of 4 cm⁻¹ to 20 cm⁻¹ depending on the relative strength of their hydrogen bonds. In comparison, the magnitude of the hydrogen bonding strength of HRP II is almost a 10 cm⁻¹ shift to lower energy.^{5a} This H-bond presumably plays a central role in HRP II activity. In cytochrome c peroxidase, there is proposed strong H-bonding from distal arginine (Arg 48) and trytophan (Trp 51) to the ferryl heme causing the Fe^{IV}=O shift to 753 cm⁻¹, a very low frequency in the 750-810 cm⁻¹ range for proteins.

H-Bonding to V=O and Fe=O reduces the oxygen to metal π interactions and shift the M=O vibration to lower energy. The lower energy absorption indicates a weaker VO bond and sometimes longer bond length. Table V-7 shows some crystal structures of vanadyl porphyrins. The relative longer VO bond of (cis)NKAmideP(VO) [1.590(3)] vs (trans)NAP(VO) [1.583(5)] observed by X-ray analysis could be the result of hydrogen bonding. It is comparable with the intermolecular hydrogen bonding brought about by quinol adducts or by water molecules in the solid state. Even though when comparing NKAP(VO) with OEP(VO)²³ and etioPorphyrin(VO) [ETP(VO)], the latter two compounds have longer V=O bond length than the H-bonded NKAmideP(VO). We suspect that the C-clamp porphyrin may clamp down on the oxo group and in effect push the V=O toward the porphyrin plane.

With the soret electronic excitation, the vanadyl VO stretching mode is strongly enhanced in resonance. H-bonding weakens the VO bond

Table V-7. Structural Data of Several Vanadyl Compounds

punoduoo	V=0, Å	V=O, Å V-out of plane, Å average V-N, Å Reference	average V-N, Å	Reference
NKAmideP(VO)	1.590(3)	0.504(2)	2.067	this
NAP(VO)	1.583(5)	0.522(3)	2.069	work
OEP(VO)	1.620(2)	0.543	2.102	24a
DPEP(VO)	1.619(7)	0.48	2.078	24b
TPP(VO)	1.625(16)	0.53	2.080	25
ETP(VO)	1.599(6)	0.49(1)	2.058	25
[ETP(VO)] ₂ -[H ₂ Q]	1.614(9)	0.51(1)	2.070	25

(H₂Q: abbreviation of 1,4-dihydroxybenzene)

due to reduced oxygen to V(IV) electron donation. Removal of this H-bond allows the electron density to localize to the VO moiety. The stronger the H-bonding to vanadyl, the lower the stretching energy of VO will be. This has been proven by intramolecular H-bonding studies of both NKAP(VO) and NKAmideP(VO) systems. The coordination by a sixth ligand causes the vibration energy to drop more than 30 cm⁻¹ due to electron donation from the sixth ligand to vanadium.

The 20 cm⁻¹ vV=O shift observed due to H-bonding provides a benchmark for H-bonded M=O species. Any shift greater than 25 cm⁻¹ cannot be accounted for by H-bonding alone, in which case trans-ligand coordination probably also plays a role.

E. References

- a) Hewson, W. O.; Hager, L. P. in *The Porphyrins*; Dolphin, D.,
 Ed.; Acdemic: New York, 1979; Vol VII, Chapter 6.
 b) Reczek, C. M.; Sitter, A. J.; Turner, J. J. Mol. Struct. 1989, 214, 27-35.
- 2. a) Watanabe, Y.; Groves, J. T. in *The Enzymes*, Sigman, D. S. Ed.; Academic: New York, 1992; Vol XX, Chapter 9 and references therein.
 - b) There is another proposed intermediate which is isoelectronic to the Fe=O species but in the form of Fe(III)porphyrin N-oxide, see Weber, L.; Hommel, R.; Behling, J.; Haufe, G.; Hennig, H. J. Am. Chem. Soc. 1994, 116, 2400-2408.
- a) Varotsis, C.; Babcock, G. T. Biochem. 1990, 29, 7357-7362.
 b) Ogura, T.; Takahashi, S.; Hirota, S.; Shinzawa-Itoh, K.;
 Yoshikawa, S.; Appelman, E. H.; Kitagawa, T. J. Am. Chem. Soc. 1993, 115, 8527-8536.
- 4. a) Kahlow, M. A.; Zuberi, T. M.; Gennis, R. B.; Loehr, T. M. *Biochem.* 1991, 30, 11485-11489.
 - b) Ozawa, S.; Watanabe, Y.; Nakashima, S.; Kitagawa, T.; Morishima, I. J. Am. Chem. Soc. 1994, 116, 634-641.
- 5. a) Sitter, A. J.; Reczek, C. M.; Terner, J. J. Biol. Chem. 1985, 260, 7515-7522.
 - b) Hashimoto, S.; Tatsuno, Y.; Kitagawa, T. *Proc. Natl. Acad. Sci. U.S.A.* 1986, 83, 2417-2421.

- c) Hashimoto, S.; Teraoka, J.; Inubushi, T.; Kitagawa, T. J. Biol. Chem. 1986, 261, 11110-11118.
- 6. a) Sitter, A. J.; Reczek, C. M.; Terner, J. Biochim. Biophys. Acta 1985, 828, 229-232.
 - b) Fenwick, C.; Marmor, S.; Govindaraju, K.; English, A. M.; Wishart, J. F.; Sun, J. J. Am. Chem. Soc. 1994, 116, 3169-3170.
- 7. a) Kean, R. T.; Oertling, W. A.; Babcock, G. T. J. Am. Chem. Soc. 1987, 109, 2185-2187.
 - b) Oertling, W. A.; Kean, R. T.; Babcock, G. T. *Inorg. Chem.* 1990, 29, 2633-2645.
- 8. a) Latour, J. M.; Gallunb, B.; Marchon, J.-L. J. Chem. Soc. Chem. Commun. 1979, 570-571.
 - b) Woo, L. K.; Hays, J. A.; Goll, J. G. *Inorg. Chem.* 1990, 29, 3916-3917.
- 9. a) Pettersen, R. C.; Alexander, L. E. J. Am. Chem. Soc. 1968, 90, 3873-3876.
 - b) Buchler, J. W.; Puppe, L.; Rohbock, K.; Schneehage, H. M. Ann N. Y. Acad. Sci. 1973, 206, 116-121.
 - c) Macor, K. A.; Czernuszewicz, R. S.; Spiro, T. G. *Inorg. Chem.* 1990, 29, 1996-2000.
 - d) Lin, M.; Lee, M.; Yue, K. T.; Marzilli, L. G. *Inorg. Chem.* 1993, 32, 3217-3226.
- 10. a) Nill, K. H.; Wasgestian, F.; Pfell, A. *Inorg. Chem.* 1979, 18, 564-567.

- b) Groves, J. T.; Kruper, W. J.; Jr.; Haushalter, R. C.; Butler, W. M. *Inorg. Chem.* 1982, 21, 1363-1368.
- c) Penner-Hahn, J. E.; Benfatto, M.; Hedman, B.; Takahash, T.; Sebastian, D.; Groves, J. T.; Hodgson, K. O. *Inorg. Chem.* 1986, 25, 2255-2259.
- 11. Stern, M. K.; Groves, J. T. in "Manganese Redox Enzymes", V. L. Pecoraro, Ed.; VCH, 1992, Chap. 11 and references therein.
- 12. Vanadium and its Role in Life, in "Metal Ions in Biological Systems", Vol. 31. Sigel, H. and Sigel, A., Ed.; Marcel Dekker, New York, 1995.
- 13. Henze, M. Hoppe-Seyler's Z. Physiol. Chem., 1911, 72, 494-496.
- 14. Michibata, H. Adv. Biophys. 1993, 29, 105-109.
- 15. Welinder, K. G. in *Molecular and Physiological Aspects of Plant Peroxidases*, University of Geneva, 1986, 1.
- 16. Vilter, H.; Glombitza, K.-W.; Grawe, A. Bot. Mar. 1983, 26, 331-337.
- 17. a) Nagy., B. Chemistry 1966, 39, 9-14.
 b) Rosscup, R. J.; Pohlman, H. P. Polym. Prep., Am. Chem. Soc., Div. Petrol. Chem., 1967, 12, A-103-104.
- 18. Su, Y. O.; Czernuszewicz, R. S.; Miller, L. A.; Spiro, T. G. J. Am. Chem. Soc. 1988, 110, 4150-4157.

- 19. a) Mayer, U.; Gutmann, V.; Gerger, W. Monatash. Chem. 1975, 106, 1235--1239.
 - b) Gutmann, V. Electrochem. Acta. 1976, 21, 661-672.
 - c) Gutmann, V. The donor-Acceptor Approach to Molecular Interactions, Plenum: New York, 1978.
- a) Chang, C. K.; Kondylis, M. P. J. Chem. Soc. Chem. Commun.
 1986, 316-318.
 - b) Liang, Y.; Peng, S.-M.; Chang, C. K. J. Molecular Recognition in press.
- 21. Schmidt, E. "Ligand Binding Properties of Metalloporphyrins, Factors That Influence Their Chemical Properties and Relationships to Biological Proteins", Ph.D. Dissertation, Michigan State University, 1995.
- 22. Ozawa, T.; Hanaki, A. Inorg. Chim. Acta. 1988, 141, 49-51.
- 23. Poulos, T. L.; Finzel, B. C. Pept. Protein Rev. 1984, 4, 115-118.
- 24. a) Molinaro, F. S., Ibers, J. A. Inorg. Chem. 1976, 15, 2278-2283.
 - b) Pettersen, R. C. Acta Crystallogr., Sect. B, 1969, 25, 2527-2539.
- 25. Drew, M. G. B.; Mitchell, P. C. H.; Scott, C. E. *Inorg. Chim. Acta.* 1984, 82, 63-68.

Chapter VI

Structural and Vibrational Properties of RuCO and FeCO C-Clamp Porphyrin and Derivative

A. Introduction

The binding of small substrates to porphyrins that model the heme active site has drawn considerable attention of bioinorganic chemists. In order to provide insights into structure/function relationships, factors like steric interaction, substituent effects on porphyrin and trans ligand effects have been studied for O₂, CO and NO binding.¹ CO binding, in particular, has been studied in exploring the nature of the heme binding site and in evaluating cis and trans ligand effects.² Crystallographic studies of carbon monoxy hemoglobins and myoglobins³ have shown that the CO ligand exhibits a bent or tilted configuration with respect to the heme plane. This stereochemical feature of the hemeproteins is associated with nonbonding interactions of the axial ligand with nearby amino acid residues in the

ligand-binding pocket. These interactions are thought to lower the CO affinities in the proteins and protect the organisms from CO poisoning.⁴ However, for non-constrained heme derivatives, the bonded CO appears in near linear geometry. There are many factors affecting CO bonding and they are usually hard to evaluate practically with high degree of reliability. Generally, ligands capable of influencing the $d\pi$ orbitals and hence the $\pi(Fe)$ - $\pi^*(CO)$ back-bonding are predicted to affect the CO bonding as well as the CO stretching frequency. Goedken has reported several examples to illustrate the sensitivity of Fe(II)-CO bonding.⁵

In comparing properties of oxy and carboxy heme, the Fe-CO overlap density is greater than the Fe-O₂ overlap density, according to theoretical calculations.¹ This is in agreement with the greater affinity of CO. One influence caused by this stronger overlap is that the CO bonding is more sensitive to the ligand field strength of the trans ligand on Fe(II).¹ Iron monocarbonyl heme models with different trans ligands, such as THF,⁶ pyridine⁷ and mercaptan,⁸ have provided strong evidence of this kind of sensitivity. Here, we have conducted research to show how a fine-tuned trans ligand environment can shift the CO vibration in the C-clamp porphyrin NKAP and its derivative NKAmideP.

B. Experimental

1. Preparation of RuCOporphyrins

Ru₃(CO)₁₂ was allowed to react with free base porphyrin under the conditions reported by Collen and coworkers.⁹ 11.6 mg of NKAP in freshly distilled toluene was heated on an oil bath under argon. A small amount (3 mg) of triruthurium dodecacarbonyl [Ru₃(CO)₁₂] was added.

After each additional 8 hours, a small amount (3 mg) of Ru₃(CO)₁₂ was added. The reaction was monitored by UV-Vis and by TLC. When the metal insertion was completed (~ 48 h), the reaction was stopped by adding 1 ml of methanol.

The product was purified on the TLC plate using methylene chloride as the eluent. The first band was yellowish brown, and proved to be $Ru_3(CO)_{12}$ by mass spectrometry and UV-Vis. The second band was orange colored showing the properties of ruthenium inserted porphyrin. The UV-vis spectrum of the product was consistent with formation of RuCO-porphyrin. The product is a monocarbonyl complex as identified by Ibers.⁹ For RuCONKAP: MS, m/e (relative intensity) 983 (M+, 1.0); IR CO vibration at 1931 cm⁻¹; UV-Vis λ_{max} nm (relative intensity) 397.5 nm (12.8); 521.0 (1.0); 533.0 (1.1). For RuCONKAmideP: MS, m/e (relative intensity) 982 (M+, 2.0); IR: CO vibration at 1927 cm⁻¹; UV-Vis λ_{max} nm (relative intensity) 399.5 nm (12.7); 522.0 (1.0); 553.5 (1.1).

2. Preparation of FeCOporphyrins

A solution of sodium dithionite was introduced to a methylene chloride solution of Fe(III) porphyrin under argon. CO gas was then added to this Fe(II)porphyrin solution and the color of the solution changed instantaneously. An IR cell was first flushed with argon to eliminate air and the methylene chloride solution of Fe(II)COporphyrin was introduced to this liquid IR cell through a cannula; IR measurement was then conducted.

3. Instrumentation

a) Spectroscopy

UV-vis spectral measurements were carried out on a Shimadzu 160 spectrophotometer, with samples dissolved in methylene chloride. Infrared spectra were obtained by either layering the RuCOporphyrin complex on a NaCl plate or by measurement of the CH₂Cl₂ solution of FeCOporphyrin in a liquid IR cell. Spectra were recorded on a Nicolet IR/42 spectrometer at a resolution of 1 cm⁻¹. Mass spectra were measured from a benchtop VG Troi-1 mass spectrometer using the DCI (Desorption Chemical Ionization) probe for sample inlet.

b) X-Ray Structure Determination

Crystals of RuCONAKP(MeOH) and RuCONKAmideP(MeOH) suitable for single-crystal X-ray diffractometry were obtained by diffusion of methanol into the sample solution in CH₂Cl₂ followed by slow evaporation. Crystallographic data are listed in Table VI-1. Data collection was performed on a Nonius diffractometer at room temperature using graphite-monochromated Mo K_{α} radiation. The crystals used for analysis were of approximate dimensions 0.05 x 0.22 x 0.25 mm for RuCONKAP(MeOH) and 0.40 x 0.40 x 0.50 mm for RuCONKAmideP (MeOH). The unit cell parameters were determined by a least squares fit of 25 machine-centered reflections having 20 values in the ranges of 9.40-20.22° for RuCONKAP(MeOH) and 15.48-23.66° for RuCONKAmideP (MeOH). The intensity data were reduced and corrected for Lorentz and polarization factors using the applied programs. The crystal structures were solved by direct methods using the NRCVAX program package. All

Table VI-1. Crystallographic Data of RuCONKAP(MeOH) and RuCONKAmideP(MeOH)

	RuCONKAP	RuCONKAmideP
Formula	RuC57N5O6H63	RuC57N6O5H64
fw	1015.21	1014.23
cryst syst	monoclinic	monoclinic
space group	p 2 _{1/c}	p 2 _{1/c}
a, Å	10.706(3)	10.650(3)
b, Å	25.999(3)	26.071(8)
c, Å	18.760(3)	18.842(8)
β, deg	103.002(22)	103.13(3)
v, Å ³	5087.7(17)	5095(3)
Z	4	4
Q(calc), gcm ⁻³	1.325	1.322
μ, cm ⁻¹	3.515	3.525
transm coeff	0.967-1.000	0.926-1.000
scan speed, deg min-1	2.06-8.24	2.06-8.24
scan width, deg	$2(0.60 + 0.35 \tan \theta)$	$2(0.60+0.35\tan\theta)$
no. of measd reflns	6639	6648
no. of obsd reflns	2639 (I>2σ(I))	4516(I>2σ(I))
no. of refined params	6639	6648
R_f, R_w	0.0045, 0.044	0.042, 0.041
Gof	1.13	2.12

Note: $R_f = \sum |F_0 - F_c| / \sum |F_0|$

 $R_{\rm W} = (\sum (w(F_{\rm o}-F_{\rm c}))^2/\sum (wF_{\rm o}^2))^{1/2}$

Gof = $(\sum (w(F_0-F_c))^2/(\# \text{ refins-}\# \text{ params}))^{1/2}$

non-hydrogen atoms were refined anisotropically. All the hydrogen atoms were placed at calculated positions with fixed isotropic thermal parameters. The highest difference Fourier peaks were 0.320 eÅ-3 for RuCONKAP(MeOH) and 0.420 eÅ-3 RuCONKAmideP(MeOH), respectively.

C. Results and Discussion

1. X-Ray Single Crystal Structures of RuCONKAP(MeOH) and RuCONKAmideP(MeOH)

The orange colored crystals obtained were in the shape of long needles. Table VI-2 lists the atomic coordinates of non-hydrogen atoms of RuCONKAP(MeOH) and Table VI-3 lists that of RuCONKamideP(MeOH). A listing of selected bond distance and angles for both compounds is given in Table VI-4.

For RuCONKAP(MeOH), the crystal is monoclinic and its ORTEP structure is shown in Figure VI-1. The CO is on the opposite side from the Kemp's acid with one molecule of solvent methanol bound trans. Just like the methanol inclusion in ZnNKAP, the methanol hydroxy proton is H-bonded with the Kemp's acid carbonyl oxygen. The methanol oxygen is coordinated to ruthenium as an axial ligand with an Ru-O distance of 2.202(6). In RuCONKAmideP(MeOH) (Figure VI-2), the Ru-O(MeOH) distance is 2.205(4) and the methanol hydroxy proton is H-bonded with Kemp's amide carbonyl oxygen. In both crystal structures, the CO appears in almost linear geometry with Ru-C-O angles 177.5(8)° for RuCONAKP

Table VI-2. Atomic Parameters x, y, z and B_{iso} for RuCONKAP(MeOH) with E.S.Ds. refer to the last digit printed.

	x	у	Z	Biso
Ru	0.33672(8)	0.13948(3)	0.15460(4)	2.50(3)
C	0.2763 (9)	0.1960 (3)	0.1887 (5)	3.1 (5)
Ο	0.2338 (7)	0.2330 (3)	0.2084 (4)	5.5 (4)
O 1	0.4061 (6)	0.07065 (23)	0.1070 (3)	3.8 (3)
O2	0.2069 (7)	-0.1106 (3)	0.1494 (4)	5.4 (4)
О3	0.4443 (7)	-0.0707 (3)	0.3728 (4)	5.8 (4)
O 4	0.4539 (8)	-0.0286 (3)	0.1497 (4)	7.3 (5)
O5	0.5843 (8)	-0.0135 (3)	0.2545 (5)	8.0 (6)
Nl	0.1644(6)	0.1023 (3)	0.1421 (3)	2.6 (4)
N2	0.2877(6)	0.1678(3)	0.0501(4)	2.4(4)
N3	0.5173(6)	0.1691(3)	0.1630(4)	2.7(3)
N4	0.3915(6)	0.1043(3)	0.2546(4)	2.3 (3)
N5	0.3324(7)	-0.0890(3)	0.2585(4)	3.3 (4)
C1	0.1165(8)	0.0761(3)	0.1947(5)	2.8 (5)
C2	-0.0160(9)	0.0611 (4)	0.1623(5)	3.6 (5)
C3	-0.0426(8)	0.0787 (4)	0.0918(5)	3.4 (5)
C4	0.0694(8)	0.1046(3)	0.0803(5)	2.7 (4)
C5	0.0739(8)	0.1305 (4)	0.0157(4)	3.5 (5)
C 6	0.1718(8)	0.1610 (3)	0.0027(5)	2.9 (5)
C 7	0.1691(9)	0.1908 (4)	-0.0635(5)	3.5(5)
C8	0.2830(8)	0.2153 (3)	-0.0547(5)	3.0(5)
C9	0.3605(9)	0.2012 (3)	0.0178 (5)	3.1(5)

Table VI-2 (cont'd)

C10	0.4837(8)	0.2152 (4)	0.0468 (5)	3.1 (5)
C11	0.5579(8)	0.2002 (3)	0.1136 (5)	3.0 (5)
C12	0.6907(9)	0.2125 (4)	0.1411 (5)	4.2 (5)
C13	0.7309(9)	0.1889 (4)	0.2057(5)	4.1 (6)
C14	0.6222(8)	0.1612 (3)	0.2190 (5)	3.0 (4)
C15	0.6136(8)	0.1332 (4)	0.2810(5)	3.5(5)
C16	0.5124(8)	0.1080 (3)	0.2991(4)	2.6 (4)
C17	0.5145(8)	0.0841 (3)	0.3684(4)	2.6 (4)
C18	0.3928(8)	0.0678 (3)	0.3677(4)	2.5 (4)
C19	0.3150(8)	0.0799 (3)	0.2952(5)	2.5 (5)
C20	0.1877(9)	0.0644 (3)	0.2651(5)	2.9 (5)
C21	-0.1102(10)	0.0329 (5)	0.1949(6)	6.3 (7)
C22	-0.1636(10)	0.0715 (4)	0.0353(6)	5.3 (6)
C23	-0.1727(14)	0.0238 (5)	-0.0053(8)	10.8 (10)
C24	0.0579(10)	0.1924 (5)	-0.1280(6)	5.9 (7)
C25	0.3224(10)	0.2537 (4)	-0.1051(5)	4.5 (6)
C26	0.2666(13)	0.3062 (5)	-0.1002(7)	8.1 (9)
C27	0.7718(11)	0.2510 (5)	0.1091(6)	6.6 (7)
C28	0.8554 (16)	0.2244 (7)	0.0728 (8)	11.6(12)
C29	0.8615(10)	0.1889 (5)	0.2573(6)	6.0 (7)
C30	0.6309(9)	0.0812 (4)	0.4299(5)	4.7(6)
C31	0.6577(11)	0.1294 (6)	0.4752(6)	8.6(9)
C32	0.3559(9)	0.0434 (4)	0.4315(5)	3.9(5)
C33	0.1120(8)	0.0448 (4)	0.3189(4)	2.9(5)

Table VI-2 (cont'd)

		·		
C34	0.0562(9)	0.0813 (4)	0.3538(5)	3.6 (5)
C35	-0.0247(10)	0.0691 (4)	0.4008(6)	4.7 (6)
C36	-0.0507(9)	0.0198 (4)	0.4106(5)	4.6 (6)
C37	0.0039(9)	-0.0209(4)	0.3781(5)	3.2 (5)
C38	-0.0318(9)	-0.0725 (4)	0.3859(6)	4.5 (6)
C39	0.0216(10)	-0.1109 (4)	0.3570(6)	5.4 (6)
C40	0.1106(10)	-0.0999 (4)	0.3145(5)	5.1 (6)
C41	0.1488(9)	-0.0509 (4)	0.3027(5)	3.9 (5)
C42	0.0897(8)	-0.0088 (3)	0.3313(5)	2.8 (5)
C43	0.2537(9)	-0.0439 (4)	0.2610(5)	3.5 (5)
C44	0.3036(9)	-0.1187 (4)	0.1952(5)	3.8 (5)
C45	0.3984(9)	-0.1592 (4)	0.1866(5)	4.3 (6)
C46	0.4603(10)	-0.1815 (4)	0.2616(6)	4.9 (7)
C47	0.5262(9)	-0.1407 (4)	0.3122(5)	4.3 (5)
C48	0.4340(9)	-0.0970 (4)	0.3182(5)	3.8 (5)
C49	0.6342(9)	-0.1181 (4)	0.2799(6)	4.7 (6)
C50	0.5944(9)	-0.0964 (4)	0.2020(5)	3.8 (5)
C51	0.5035(9)	-0.1352 (4)	0.1539(5)	5.0 (6)
C52	0.7150(11)	-0.0899 (4)	0.1716(7)	7.1 (8)
C53	0.5356(10)	-0.0427 (4)	0.1985(6)	5.5 (7)
C54	0.3305(12)	-0.2018 (4)	0.1350(6)	6.6 (7)
C55	0.5852(12)	-0.1621 (4)	0.3880(6)	7.0 (7)
C56	0.4742(13)	0.0702 (5)	0.0529(7)	7.8(9)

Biso is the Mean of the Principal Axes of the Thermal Ellipsoid.

Table VI-3. Atomic Parameters x, y, z and B_{iso} for RuCONKAmideP(MeOH) with E.S.Ds. refer to the last digit printed.

	x	у	Z	Biso
Ru	0.33981(4)	0.140072(18)	0.15862(3)	2.615(20)
C	0.2778 (5)	0.19604 (22)	0.1925 (3)	3.5 (3)
0	0.2346 (4)	0.23267 (17)	0.21175(24)	5.9 (3)
O 1	0.4131 (4)	0.07161 (14)	0.11243(20)	3.91(21)
O2	0.1978 (4)	-0.10710(17)	0.14887(24)	6.0 (3)
O3	0.4524 (5)	-0.07125(17)	0.36910(23)	6.2 (3)
O4	0.4447 (5)	-0.02750(16)	0.1474 (3)	6.6 (3)
N1	0.1670 (4)	0.10256 (17)	0.14508(22)	2.81(21)
N2	0.2931(4)	0.16825(16)	0.05388(22)	2.75(21)
N3	0.5211(4)	0.17013(17)	0.16766(23)	3.06(22)
N4	0.3927(4)	0.10596(16)	0.25927(23)	2.72(21)
N5	0.3284(5)	-0.08760(18)	0.2571(3)	4.0 (3)
N6	0.5838(6)	-0.00936(21)	0.2490(3)	6.8 (4)
C1	0.1181 (5)	0.07708(22)	0.1969(3)	3.2 (3)
C2	-0.0161(5)	0.06255(23)	0.1639(3)	4.0 (3)
C 3	-0.0411(5)	0.07893 (23)	0.0942(3)	4.1 (3)
C4	0.0707(5)	0.10431(21)	0.0824(3)	3.2 (3)
C5	0.0787(5)	0.12996(22)	0.0191(3)	3.5 (3)
C6	0.1773(5)	0.16062(21)	0.0055(3)	3.2 (3)
C 7	0.1754(5)	0.18932(22)	-0.0602(3)	3.4 (3)
C8	0.2891(5)	0.21465(22)	-0.0508(3)	3.4(3)
C 9	0.3635(5)	0.20053(21)	0.0214 (3)	3.0(3)

Table VI-3 (cont'd)

C10	0.4897(5)	0.21510(21)	0.0518 (3)	3.5 (3)
C11	0.5641(5)	0.20060(22)	0.1187 (3)	3.4 (3)
C12	0.6973(5)	0.21431(23)	0.1477 (3)	4.0 (3)
C13	0.7343(5)	0.19071(23)	0.2131(3)	3.9 (3)
C14	0.6228(5)	0.16390(21)	0.2260 (3)	3.3 (3)
C15	0.6171(5)	0.13605(23)	0.2874(3)	3.5(3)
C16	0.5139(5)	0.11115(21)	0.3048(3)	2.9 (3)
C17	0.5145(5)	0.08685(21)	0.3731(3)	3.0 (3)
C18	0.3941(5)	0.06879(20)	0.3711(3)	2.8 (3)
C19	0.3167(5)	0.08081(20)	0.2980(3)	2.8 (3)
C20	0.1873(5)	0.06718(20)	0.2688(3)	2.7 (3)
C21	-0.1114(6)	0.0361 (3)	0.1986(4)	6.9 (4)
C22	-0.1637(6)	0.0721 (3)	0.0376(4)	6.3 (4)
C23	-0.1750(9)	0.0229 (4)	-0.0006(5)	11.8 (6)
C24	0.0643(6)	0.1910 (3)	-0.1250(3)	5.5 (4)
C25	0.3287(6)	0.2514 (3)	-0.1011(3)	4.5 (3)
C26	0.2753(8)	0.3039 (3)	-0.0970(4)	7.4 (5)
C27	0.7779(6)	0.2500 (3)	0.1127(4)	6.1 (4)
C28	0.8639(10)	0.2245 (4)	0.0795(5)	11.5(8)
C29	0.8654(6)	0.1921 (3)	0.2649(4)	6.4 (4)
C30	0.6306(6)	0.0848(3)	0.4365(3)	4.5 (3)
C31	0.6519(7)	0.1343 (4)	0.4808(4)	8.7 (5)
C32	0.3557(9)	0.04255(24)	0.4330(3)	4.2(3)
C33	0.1118(5)	0.04631(21)	0.3206(3)	3.0(3)

Table VI-3 (cont'd)

C34	0.0569(5)	0.08251(23)	0.3564(3)	3.9 (3)
C35	-0.0234(6)	0.0707 (3)	0.4027(4)	4.9 (4)
C36	-0.0534(6)	0.0206 (3)	0.4110(3)	5.0 (4)
C37	0.0005(5)	-0.01872(23)	0.3777(3)	3.9 (3)
C38	-0.0332(6)	-0.0709 (3)	0.3869(4)	5.3 (4)
C39	0.0171(7)	-0.1092 (3)	0.3552(4)	6.1 (4)
C40	0.1083(7)	-0.09885(4)	0.3146(4)	5.5 (4)
C41	0.1463(6)	-0.04994(23)	0.3033(3)	3.8 (3)
C42	0.0888(5)	-0.00747(22)	0.3328(3)	3.2 (3)
C43	0.2509(6)	-0.04177(22)	0.2624(3)	4.2 (3)
C44	0.2981(6)	-0.11602(23)	0.1927(3)	4.2 (3)
C45	0.3923(6)	-0.15685(22)	0.1819(3)	4.0 (3)
C46	0.4525(6)	-0.18093(23)	0.2534(4)	4.9 (4)
C47	0.5256(6)	-0.14075(25)	0.3061(3)	4.6 (3)
C48	0.4338(6)	-0.09777(23)	0.3156(3)	4.5 (4)
C49	0.6333(6)	-0.11908(24)	0.2723(4)	5.1 (3)
C50	0.5909(6)	-0.09476(22)	0.1972(3)	4.1 (3)
C51	0.4959(6)	-0.13189(24)	0.1485(3)	4.6 (3)
C52	0.7071(7)	-0.0885 (3)	0.1638(4)	6.7 (5)
C53	0.5333(6)	-0.04175(24)	0.1979(3)	4.7 (4)
C54	0.3193(7)	-0.1976 (3)	0.1285(4)	6.4 (4)
C55	0.5854(8)	-0.1643 (3)	0.3793(4)	7.3 (5)
C56	0.4775(8)	0.0712 (3)	0.0577(4)	7.6(5)

Biso is the Mean of the Principal Axes of the Thermal Ellipsoid.

Table VI-4. Selected Bond Distance (Å) and Angle (deg) and Their Estimated Standard Deviations for RuCONKAP(MeOH) and RuCONKAmideP(MeOH).

RuCONI	KAP	RuCONKAn	nideP
	Distanc	ce (Å)	
Ru-N1 2	2.050(7)	Ru-N1	2.049(4)
Ru-N2 2	2.050(7)	Ru-N2	2.058(4)
Ru-N3 2	2.054(7)	Ru-N3	2.055(4)
Ru-N4 2	2.051(6)	Ru-N4	2.054(4)
Ru-C 1	.781(9)	Ru-C	1.779(6)
C-O 1	.160(11)	C-O	1.154(7)
Ru-O(MeOH) 2	2.202(6)	Ru-O(MeOH)	2.205(4)
	Angle ((deg)	
Ru-C-O	177.5(8)	Ru-C-O	177.3(6)
O(MeOH)-Ru-C	177.1(3)	O(MeOH)-Ru-C	177.83(20)
N1-Ru-C(O)	92.3(4)	N1-Ru-C(O)	92.30(22)
N2-Ru-C(O)	90.6(3)	N2-Ru-C(O)	91.29(22)
N3-Ru-C(O)	94.3(4)	N3-Ru-C(O)	94.34(22)
N4-Ru-C(O)	95.3(3)	N4-Ru-C(O)	94.03(22)
O(MeOH)-Ru-N1	87.0(3)	O(MeOH)-Ru-N1	87.30(16)
O(MeOH)-Ru-N2	86.65(24)	O(MeOH)-Ru-N2	86.59(16)
O(MeOH)-Ru-N3	86.5(3)	O(MeOH)-Ru-N3	86.07(16)
O(MeOH)-Ru-N4	87.47(24)	O(MeOH)-Ru-N4	88.08(16)
N1-Ru-N2	91.7(3)	N1-Ru-N2	92.08(16)
N1-Ru-N3	173.4(3)	N1-Ru-N3	173.36(18)
N1-Ru-N4	87.7(3)	N1-Ru-N4	87.62(16)
N2-Ru-N3	88.4(3)	N2-Ru-N3	87.78(17)
N2-Ru-N4	174.1(3)	N2-Ru-N4	174.67(17)
N3-Ru-N4	91.5(3)	N3-Ru-N4	91.90(16)

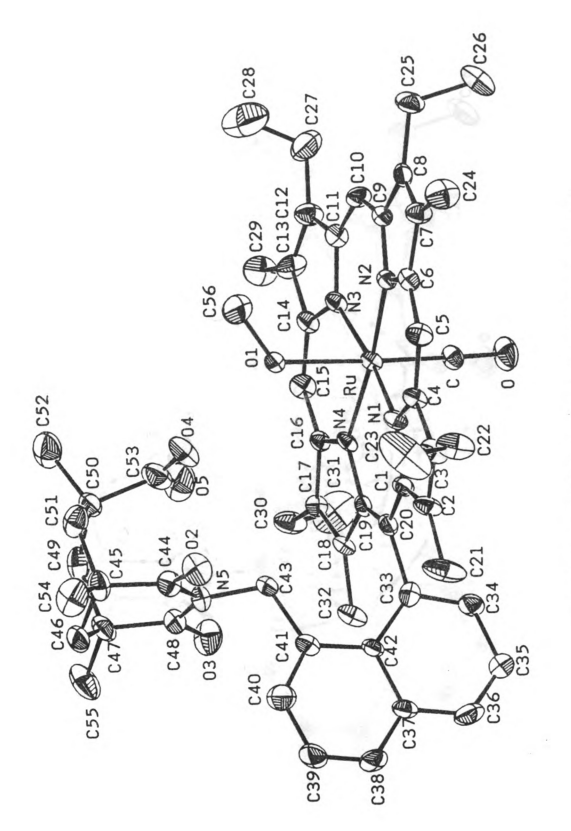


Figure VI-1. ORTEP structure of RuCONKAP(MeOH).

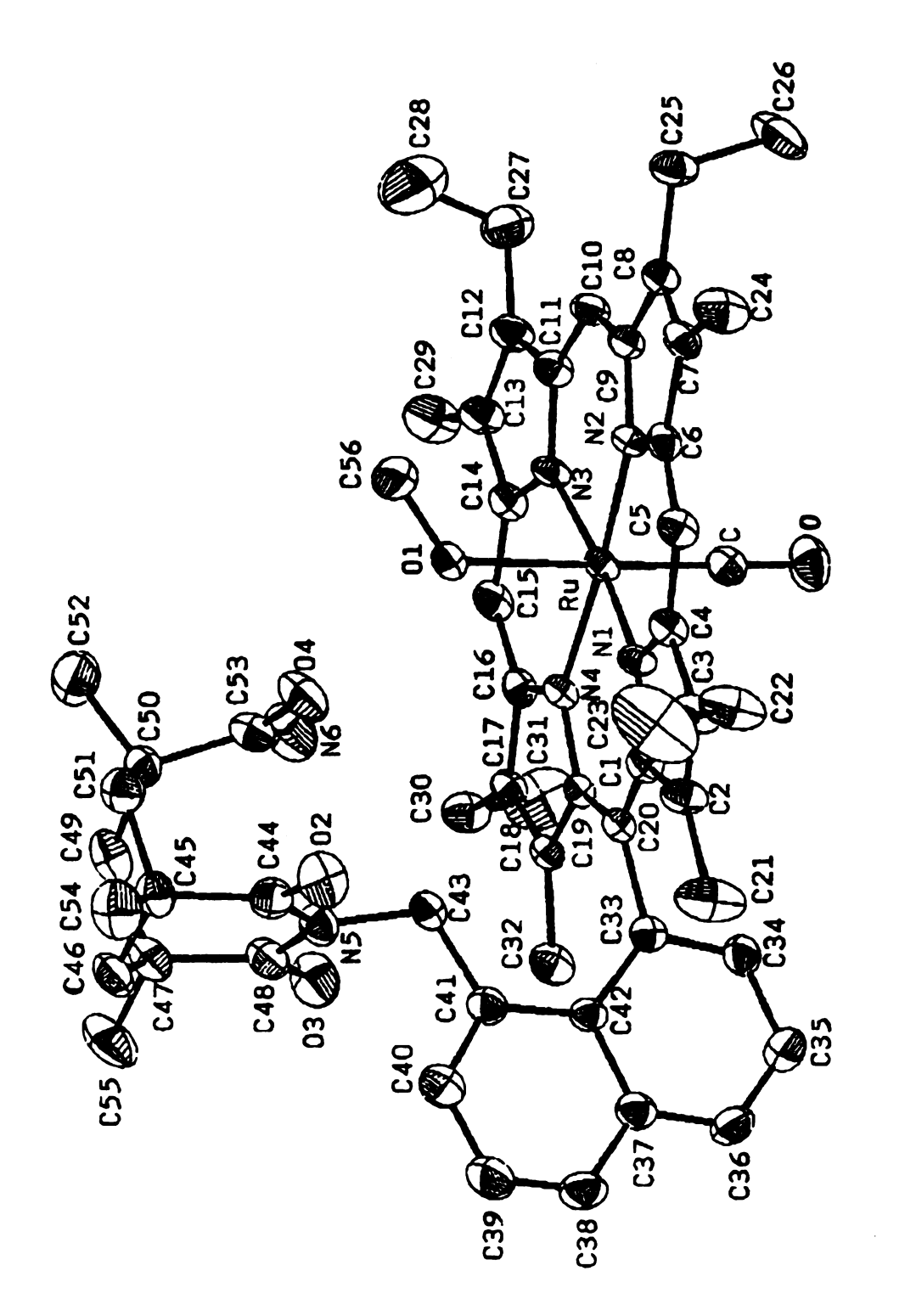


Figure VI-2. ORTEP structure of RuCONKAmideP(MeOH).

and 177.3(5)° for RuCONKAmideP, which agree with those found in other RuCO or FeCO porphyrins (Table VI-5).

The average Ru-N(porphyrin) distances of RuCONKAP(MeOH) and RuCONKAmideP(MeOH) are 2.054(4) and 2.051(7), respectively. These results agree within experimental error with those found for other RuCOporphyrins (Table VI-5). The deviations from planarity of the porphyrin mean plane are 0.2Å, comparable with those found in other metalloporphyrins.

2. IR studies of RuCOporphyrins

Table VI-6 lists the results of infrared spectroscopic studies of the C-O vibration of RuCOporphyrins. Literature results from RuCOporphyrins having various trans ligands are included in Table VI-6 as well. According to the reported υ_{CO} range of 1920-1960 cm⁻¹, the CO vibration for RuCONKAP is characterized at 1931 cm⁻¹ and for RuCONKAmideP, at 1927 cm⁻¹. Both RuCOporphyrins exhibit a very strong and sharp CO vibration. Since in both compounds methanol is a trans ligand, the difference must be brought about by H-bonding on methanol, perturbing the electron density on methanol oxygen and causing the shift in C-O vibration.

3. IR Studies of FeCOporphyrins

Table VI-7 lists the C-O vibrations of FeCOporphyrins. In analogy to the ruthenium system, the FeCO complexes of NKAP and NKAmideP most likely have a water molecule (from aqueous dithionite solution) trapped between the metal and the Kemp's acid and acting as the sixth

Table VI-5. Bond Distance (Å) and Angle (deg) Comparison of Selected Carbonylated Metalloporphyrins.

compounds	av M-N(Å) M-C (Å)	M-C (Å)	C-0(Å)	Fe-C-O(deg)	M-L(Å)	M-L(Å) Mout of plane (Å)
RuCONKAmideP(MeOH)	2.054(4)	1.779(6)	1.154(7)	177.3(6)	2.205(4)	
RuCONKAP(MeOH)	2.051(7)	1.781(9)	1.160(11)	177.5(8)	2.202(6)	
Ru(CO) _{out} (β-PocPivP)(H ₂ O) _{in}	2.034(4)	1.813(3)	1.149(4)	178.7(3)	2.198(2)	0.20
RuCOTPP(EtOH) ¹⁰	2.049(5)	1.77(2)	1.16(3)	176(2)	2.21(2)	0
RuCOTPP(py) ¹²	2.052(9)	1.838(9)	1.141(10)	178.4(7)	2.193(4)	0.079
Ru(CO) _{out} (OCCOPor)(H ₂ O) _{in}	2.054(5)	1.794(5)	1.157(6)	178.1(4)	2.187(4)	0.26
FeCO(deutP)(THF) ⁶	1.98(3)	1.706(5)	1.144(5)	178.3(14)	2.127(4)	0.10
$\{[FeCOTTP(SC_2H_5)]^{-}\}^{8}$	1.993(4)	1.78(1)	1.17(1)		2.352(2)	0.04
FeCOTPP(py) ^{7a}	2.02(3)	1.77(2)	1.12(2)	179(2)	2.10(1)	0.02

Tabe VI-6. C-O Vibrations for RuCOporphyrins

compounds	v _{CO} cm ⁻¹	Reference
RuCONKAmideP(MeOH)	1927	this work
RuCONKAP(MeOH)	1931	this work
RuCO(PorpIX)(Imidazole)	1930	13
RuCO(OEP)(t-Bu(py))	1935	14
RuCO(TPP)	1945	15

Tabe VI-7. C-O Vibrations for FeCOporphyrins

spunodwoo	v _{CO} cm ⁻¹	Reference
FeCONK AmideP(H ₂ O)	1952	this work
FeCONKAP(H ₂ O)	1956	this work
FeCO(deutP)(THF)	1955	9
FeCO(deutP)(py)	1973	7b
FeCO(TPP)(py)	1980	7a

ligand to iron. The result of such H-bonding would cause a increase in electron density on the water oxygen, and therefore make it a stronger ligand comparing to a non-bonded water molecule.

4. Trans Ligand Effect in Affecting CO Vibration in M-COporphyrins

CO bonding has been recognized as being highly sensitive to its trans ligand strength. 5-8,10-15 The existence of trans ligand shifts the CO stretching frequency to lower energy (Table VI-6); RuCOTPP has CO vibration at 1945 cm⁻¹ without any trans ligand. As shown in Table VI-5 of selected carbonylated metalloporphyrins, the geometry of carbonylmetalloporphyrins varies due to different trans ligands. In the case of RuCOporphyrins, as ethanol being a weaker ligand than pyridine, a longer C-O bond and a shorter Ru-C distance in RuCOTPP(EtOH) are observed as compared to RuCOTPP(py). Similar correlation exists in FeCOporphyrins. For the RuCONKAP(MeOH) and RuCONKAmideP (MeOH), there are slight differences between them. RuCONKAP(MeOH) has a shorter Ru-O(MeOH), longer Ru-C and longer C-O distance as well. CO vibration from IR studies displayed that CO is 4 cm⁻¹ stronger in RuCONKAP(MeOH). The same magnitude of CO frequency shift has been observed for FeCONKAP(H₂O) comparing to FeCONKAmideP(H₂O), as shown in Table VI-7. The higher v_{CO} detected for the NKAP complexes suggests a higher bond order for the coordinated CO ligand and hence, a weaker trans ligand effect. Since the difference affecting the trans ligand field comes solely from the H-bonding between the methanolic proton and the carbonyl oxygen of the Kemp's acid versus amide, it is good evidence that amide C=O is a better electron donor than the acid C=O.

D. Conclusion

The FeCO and RuCO complexes of NKAP and NKAmideP have been synthesized and investigated by X-ray crystallography and IR spectroscopy. The CO ligand in the ruthenium complexes is located at the site opposite from the Kemp's acid or the amide cap with a metal-bound methanol serving as the trans ligands to CO. The CO stretching vibration is found to be 4-5 cm⁻¹ stronger in the NKAP complex comparing to that of NKAmideP. The same magnitude is also detected for the FeNKAP versus FeNKAmideP, arguing strongly that a H₂O molecule, instead of MeOH, is present as the trans ligand in the iron systems. The fact that CO prefers the opposite coordination site from the proton donor indicates that there is little stabilization of the CO ligand by H-bonding in the Fe- and Ru-porphyrin complexes.

E. Reference

- 1. "Iron porphyrin" Part I. Eds.: Lever, A. B. P. and Gray, H. B.; Addison-Wesley, London, 1982.
- (a) Caughey, W. S.; Barlow, C. H.; O'Keeffe, D. H.; O'Tode, M. C. Ann. N. Y. Acad. Sci. 1972, 206, 296-309.
 - (b) Buchler, J. W.; Kokisch, W. E.; Smith, P. D. Struc. Bonding (Berlin) 1978, 34, 79-134.
- 3. (a) Huber, R.; Epp, O.; Formanek, K. J. Mol. Biol. 1970, 52, 349-354.
 - (b) Heidner, E. J.; Ladner, R. C.; Perutz, M. F. J. Mol. Biol. 1976, 104, 707-712.
 - (c) Norvell, J. C.; Nunes, A. C.; Schoenborn, B. P. Science 1975, 190, 568-570.
 - (d) Tucker, P. W.; Phillips, S. E. V.; Perutz, M. F.; Houtchens, R. A.; Caughey, W. S. Proc. Natl. Acad. Sci. USA 1978, 75, 1076-1080.
 - (e) Steigemann, W.; Weber, E. J. Mol. Biol. 1979, 127, 309-338.
 - (f) Baldwin, J. M. J. Mol. Biol. 1980, 136, 103-128.
- 4. Collman, J. P. Acc. Chem. Res. 1977, 10, 265-172.
- 5. Goedken, V. L.; Peng, S.-M.; Molin-Norris, J.; Park, Y. J. Am. Chem. Soc. 1976, 98, 8391-8400.
- 6. Scheidt, W. R.; Haller, K. J.; Fons, M.; Mashiko, T.; Reed, C. A. *Biochem.* 1981, 20, 3653-3657.
- 7. (a) Peng, S.-M.; Ibers, J. A. J. Am. Chem. Soc. 1976, 98, 8032-8036.

- (b) Alben, J. O.; Caughey, W. S. Biochem. 1968, 7, 175-183.
- 8. Caron, C.; Mitschler, A.; Riviére, G.; Ricard, L.; Schappacher, M.; Weiss, R. J. Am. Chem. Soc. 1979, 101, 7401-7402.
- 9. Collen, D.; Jun, E. M. J. Chem. Soc. Chem. Commun. 1972, 584-585.
- 10. Bonnet, J. J.; Eaton, S. S.; Eaton, G. R.; Holm, R. H.; Ibers, J. A. J. Am. Chem. Soc. 1973, 95. 2141-2149.
- 11. Slebodnick, C.; Kim, K.; Ibers, J. A. *Inorg. Chem.* **1993**, *32*, 5338-5342.
- 12. Little, R. G.; Ibers, J. A. J. Am. Chem. Soc. 1973, 95, 8583-8590.
- 13. Tsutsui, M.; Ostfeld, D.; Francis, J. N. J. Coord. Chem. 1971, 1, 115-119.
- 14. Eaton, G. R.; Eaton, S. S. J. Am. Chem. Soc. 1975, 97, 235-236.
- 15. Chow, B. C.; Cohen, I. A. Bioinorg. Chem. 1971, 1, 57-63.

